

# Encapsulation of Nanoparticles within Poly(ethylene oxide) Shell

**Dissertation**

submitted to the

Faculty of Chemistry, University of Hamburg

for the degree

Doctor of Natural Sciences

by

Marija Nikolić

from Smederevo (Serbia)

Hamburg, 2007.

The work described in this thesis was carried out at the Institute of Physical Chemistry,  
University of Hamburg in the group of Prof. Dr. Horst Weller

1. Referee: Prof. Dr. Horst Weller
2. Referee: Prof. Dr. Stephan Förster

To my parents

Мојим родитељима



## Acknowledgements

I would like to express my sincere gratitude to Prof. Dr. Horst Weller for giving me the opportunity to discover the nano-world in his laboratories, and for all his help, support and encouragement during my work, and for very helpful discussions and suggestions.

I am very grateful to Prof. Dr. Stephan Foerster for very valuable discussions, constant interest in my work and for his positive attitude, which was sometime more than necessary.

To Prof. Dr. Dieter Rether I want to thank for accepting to be a member of the dissertation committee and for all the affairs dealing with Graduate School GK611.

To Prof. Dr. Ivanka Popovic I am very thankful for all the support in all respects, at the beginning in Belgrade, but also at the end for reading this text.

Lynne I would like to thank very much for her perfect corrections, which brought the text into this form.

My special thanks go to Rosemarie Pakula who was always willing to help and could deal with my fear of bureaucratic matters very patiently.

Many thanks go to the people from the NMR service at TMC. For the beautiful TEM pictures, I am very grateful to Andreas Kornowski and Sylvia Bartholdi-Nawrath. For the help with GPC measurements, I would like to thank Michael Stolzenburg. I would also like to thank Stephan Hauschild for all his help too. Anja Rank is acknowledged for the cryo-TEM images.

During the work in the lab, I had from time to time help from very hardworking students: Cristina Arbelo Román, Van-Huong Tran and Irena Korbel.

Without Mona's, Ulli's and Andrea's help there was danger that the people would have to read the Zusammenfassung written by me. I believe that all of them are very grateful, as I am, that it didn't come to that. For Mona's all support and help I know that simple "thank you" is not enough... For all the help and very nice atmosphere in the lab I am very thankful to Alexey, Andrea, Sergei, Hauke, Kirsten,... My office would not have been half so interesting a place to be at without Jan.

Without the constant support and encouragement, I might not be here writing this thesis. For that I want to thank my parents who are always there for me. Not only for the help with nice ideas for this work, but also for all his support, patience and love, I want to thank my Srba.



## Content

|   |           |
|---|-----------|
| 1. Introduction   | 1         |
| 2. Background   | 3         |
| <b>2.1 Size quantisation effect</b>   | <b>3</b>  |
| <b>2.2 Synthesis of narrow size distribution semiconductor colloids</b>                                 | <b>5</b>  |
| <b>2.3 Water solubility</b>   | <b>7</b>  |
| 2.3.1 Solubilisation by ligand exchange   | 9         |
| 2.3.2 Encapsulation of the nanoparticles in micelle-like structures                                     | 11        |
| 2.3.3 Magnetic nanoparticles  | 12        |
| <b>2.4 Properties of water-soluble nanoparticles</b>  | <b>13</b> |
| 3. Results and Discussion   | 15        |
| <b>3.1 Synthesis and characterisation of CdSe/CdS and CdSe/CdS/ZnS nanocrystals</b>                     | <b>15</b> |
| 3.1.1 Core/shell, CdSe/CdS, nanoparticles   | 16        |
| 3.1.2 Core/shell/shell, CdSe/CdS/ZnS, nanoparticles   | 22        |
| <b>3.2 Synthesis and characterisation of poly(ethylene oxide)-based ligands</b>                         | <b>26</b> |
| 3.2.1 Poly(ethylene oxide)- <i>b</i> -(ethylene imine) synthesised via cationic polymerization          | 26        |
| 3.2.2 Functionalisation of poly(ethylene oxide) via the diisocyanate coupling reaction                  | 31        |
| 3.2.3 Poly(ethylene oxide) with SH end groups obtained via esterification with mercaptopropionic acid   | 38        |
| 3.2.4 Poly(ethylene oxide) with SH end groups obtained via the Michael type addition reaction           | 41        |
| <b>3.3 Ligand exchange with amino-functionalised poly(ethylene oxide)s</b>                              | <b>46</b> |
| 3.3.1 Ligand exchange with mono-amino poly(ethylene oxide), PEO-NH <sub>2</sub>                         | 46        |
| 3.3.2 Ligand exchange with poly(ethylene oxide)- <i>b</i> -(ethylene imine), PEO- <i>b</i> -PEI         | 48        |
| 3.3.3 Changes in the luminescence efficiency due to ligand exchange and change of the medium            | 52        |
| 3.3.4 Ligand exchange with amino-functionalised PEOs with different architectures of the binding blocks | 60        |
| <i>Influence of pH and increased ionic strength</i>   | 63        |
| <i>Application of amino-functionalised PEOs for other types of nanoparticles</i>                        | 66        |
| <i>Size of nanoparticle-PEO conjugates and self-organisation</i>  | 69        |

|   |            |
|---|------------|
| <i>Crosslinking of the organic stabilising shell</i>  | 83         |
| <b>3.4 Ligand exchange with mercapto-functionalised poly(ethylene oxide)s</b>                       | <b>90</b>  |
| 3.4.1 Ligand exchange with linear mercapto-functionalised poly(ethylene oxide)                      | 90         |
| 3.4.2 Ligand exchange with branched mercapto-functionalised poly(ethylene oxide)                    | 102        |
| 4. Conclusion   | 111        |
| 5. Zusammenfassung  | 115        |
| 6. Experimental part  | 119        |
| <b>6.1 Synthesis procedures and methods</b>   | <b>119</b> |
| 6.1.1 Synthesis of CdSe/CdS nanoparticles   | 119        |
| 6.1.2 Synthesis of CdSe/CdS/ZnS nanoparticles   | 120        |
| 6.1.3 Synthesis of poly(ethylene oxide)- <i>b</i> -(ethylene imine) block copolymers                | 121        |
| 6.1.4 Synthesis of amino-functionalised poly(ethylene oxide) via the diisocyanate coupling reaction | 121        |
| 6.1.5 Synthesis of poly(ethylene oxide)s with a mercapto end group                                  | 123        |
| 6.1.6 Ligand exchange procedures  | 123        |
| 6.1.7 Crosslinking of PEO2000-PEI-branched shell  | 125        |
| 6.1.8 Photochemical investigations  | 125        |
| <b>6.2 Characterisation</b>   | <b>126</b> |
| 6.2.1 Nuclear Magnetic Resonance Spectroscopy (NMR)   | 126        |
| 6.2.2 Size Exclusion Chromatography (SEC)   | 126        |
| 6.2.3 Fourier Transformed Infrared Spectroscopy (FTIR)  | 126        |
| 6.2.4 Optical Characterisation  | 127        |
| 6.2.5 Transmission electron microscopy (TEM)  | 127        |
| 6.2.6 Cryo-Transmission electron microscopy (Cryo-TEM)  | 127        |
| 6.2.7 Powder X-ray diffraction measurements (XRD)   | 128        |
| 6.2.8 Dynamic light scattering  | 128        |
| 7. Literature   | 129        |
| 8. Appendix   | 137        |
| <b>Appendix 1</b>   |            |
| Calculation of the number of different amino groups in the branched poly(ethylene imine)            | 137        |

## *Content*

---

|   |            |
|---|------------|
| <b>Appendix 2</b>   |            |
| Calculation of the number of polymer chains per nanoparticle<br>from the average distance between the nanoparticles on a TEM grid | 139        |
| <b>Appendix 3</b>   |            |
| Used chemicals and their safety precaution information  | 143        |
| <b>CV</b>   | <b>149</b> |
| <b>Declaration</b>  | <b>151</b> |



## **1. Introduction**

Materials in the nanometre size regime possess properties which are distinctly different from their corresponding bulk properties. The properties are also size dependant, which means that they are controllable by synthetic means. With the developments of colloidal synthetic approaches to produce almost perfect nanoparticles, with respect to size distribution, shape and crystal structure, intense interest in the application of these materials has arisen. Special interest exists in the area of biomedical applications. Semiconductor nanoparticles with size tuneable luminescence are perfect candidates for fluorescent labelling, which is a common way to study the interactions of biomolecules on the cellular and the integrative level. Since the dimensions of nanoparticles are smaller or comparable to those of cells, viruses or genes, magnetic nanoparticles can be directed close to the biological entity of interest and still be manipulated with an external field, thus offering new possibilities for application in biomedicine.

Synthesized by wet chemical approaches, the obtained nanometre-sized materials can be handled as easily as ordinary liquids, but are limited to solvents which are compatible with the stabilising organic shell, which is determined by synthetic demands. The organic shell is an integral part of a colloidal nanoparticle system, which provides colloidal and overall stability in solution and, being a shield to the environment, determines the chemical behaviour of the colloid. Since the shell is loosely bonded to the inorganic nanoparticle core, it can be manipulated with, even completely exchanged, giving the possibility of tailoring the properties of the nanoparticles.

Replacement of the organic shell, so-called ligand exchange, is a very frequently employed method to achieve the phase transfer of nanoparticles from organic, non-polar solvents to aqueous ones. The molecules used for building a new ligand shell should possess a functionality through which a connection with the nanoparticle can be achieved, as well as a suitable water-soluble part. The choice of molecules which can build a ligand shell and stabilise nanoparticles in solution is very broad, however, it is always necessary

to look one step further and choose the most suitable one for the intended application. When biomedical applications are involved, besides water-soluble, the use of a biocompatible and non-toxic organic shell is the natural choice. Poly(ethylene oxide), in addition to its good water-solubility, is known to be a well-suited material for biomedical applications, and is thus a highly desirable material for use as a stabilising organic shell for nanoparticles. Poly(ethylene oxide) alone cannot bind to nanoparticles and must first be functionalised in order to be used as a stabilising ligand.

Within the frame of this study, poly(ethylene oxide) ligands for the stabilisation of aqueous colloidal solutions of nanoparticles will be prepared. The main aim in the design of suitable poly(ethylene oxide)-based ligands is to introduce functional groups, preferably at the end of the polymer chain, which can make a connection to the nanoparticles. Once the poly(ethylene oxide)-based ligands are connected to the nanoparticle, the solubility properties will be determined by this new water-soluble organic shell. A method to achieve ligand exchange and phase transfer to water will be developed. Properties, such as colloidal stability under different conditions and photostability of the water-soluble nanoparticles important for future application, will be investigated. In a case where multidendate ligands were used, the possibility of crosslinking the organic shell around the inorganic core, in order to further stabilise a polymer-nanoparticle complex, will be investigated.

The nanoparticle-polymer conjugates obtained in this way do not only have desirable solubility properties, but can also be thought of as new hybrid materials, consisting of an inorganic hydrophobic core and an organic hydrophilic part, both of which can be designed separately. Amphiphilic block copolymers, which consist of hydrophilic and hydrophobic parts, are prone to spontaneous organisation (self-assembly) in aqueous solutions into structures that can be predicted and controlled by knowing the balance of the constituents of the molecule. Similarly, as in the case of a block copolymer, the possibility of controlling the organisation of nanoparticle-polymer conjugates in an aqueous solution, by the choice of each of the inorganic and organic constituents, as well as by the ratio of both, will be explored.

## **2. Background**

### **2.1 Size quantisation effect**

Nanoparticles are small crystals of a few hundred to a few thousand atoms with dimensions on the nanometre scale. Due to their small size, their properties differ significantly from those of the corresponding bulk material.<sup>1,2</sup> First, the large surface to volume ratio, where a large fraction of the atoms of such a crystal are situated at the surface, contributes to their different properties to those of larger crystals, in which these atoms do not play a major role in the overall behaviour of the material. Second, the electronic structure in this size regime is also influenced by size (size quantization effect), whereby semiconductor nanocrystals, with which this work is mostly concerned, are the most illustrative examples with which to explain this phenomenon. For semiconductor materials, the energy difference between the highest occupied and the lowest unoccupied electron energy state (conduction and valence band, respectively) is a material constant called the band gap,  $E_g$ . When excited to the valence band, an electron forms a bound state with the positive hole, which remains in the conduction band, through Coulomb interactions, a so-called Wannier exciton. Imagined as a hydrogen atom, an exciton can be described by the Bohr radius. Values of the Bohr radius of some semiconductors, such as CdSe, are between 1 and 50 nm. When the size of the crystal approaches the value of the Bohr radius of the exciton, the energy of the exciton is increased due to the confinement of the electron and a hole within the crystal. The final result is that with decreasing size of the nanocrystal, the band gap is increased. This phenomenon is known as quantum confinement or size quantization effect. Using the effective mass approximation,<sup>3</sup> the increase in the band gap with decreasing radius of a nanoparticle is quantitatively expressed by the following relationship:

$$E = E_g + \frac{h^2}{8m_e R^2} \left( \frac{1}{m_e^*} + \frac{1}{m_h^*} \right) - \frac{1.8e^2}{4\pi\epsilon\epsilon_0 R}$$

where,  $E_g$  is the band gap of the bulk material. The positive contribution of the confinement energy is described by the second term with a  $1/R^2$  dependence, where  $h$  is the Planck constant,  $m_e^*$  and  $m_h^*$  the effective mass of the electron and the hole, respectively, and  $m_e$  the mass of an electron at rest. The third term describes the contribution of the Coulomb attraction, which varies as a function of  $1/R$ ;  $\epsilon$  is the dielectric constant of the semiconductor and  $\epsilon_0$  the dielectric constant of vacuum. For small values of  $R$ , the confinement term is dominant, making  $E$  greater than  $E_g$ . For large values of  $R$ , the value of  $E$  approaches that of  $E_g$ .

The size quantization effect can be explained using the linear combination of atomic orbitals (LCAO) theory.<sup>4</sup> By combination of the atomic orbitals, an equal number of molecular orbitals (MO) are formed (Figure 2.1.1). With increasing number of atoms, the number of MO increases, and the MO merge into bands for an infinite number of atoms (bulk).

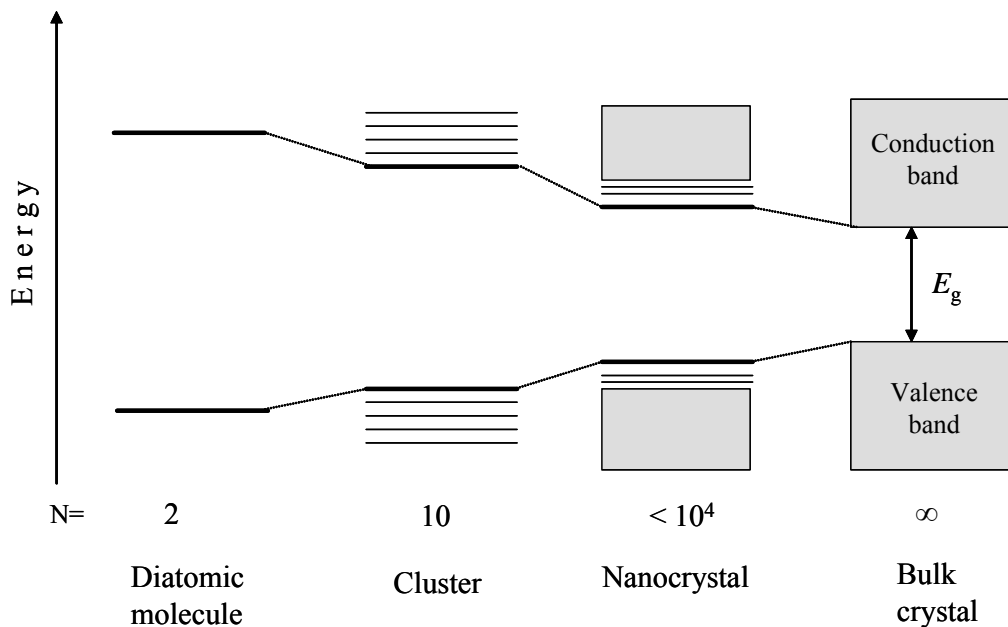


Figure 2.1.1. Evolution of molecular orbitals into bands  
(N represents the number of atoms)

Nanocrystals lie between molecules and infinite crystals with increasing distance between the highest occupied molecular orbital and the lowest unoccupied molecular orbital as the number of building atoms (the size) of the nanocrystal decreases.

Macroscopic manifestations of the changes of the band gap are the shifts in absorption onset and the luminescence peak position with changing size of the semiconductor nanocrystal. Thus, by changing the size, different spectral colours of the emission from semiconductor fluorophores can be chosen. By changing the material from ZnS and ZnSe over CdSe and CdTe to PbS and PbSe, the whole spectrum from UV to infrared can be covered in narrow peaks. Apart from fundamental interest in nanometre-sized materials, such properties offer great possibilities for various applications where their luminescence response to light excitation can be utilised.

Since the properties of nanometre-sized materials are size dependant, it is obvious that a great necessity exists in both fundamental investigations as well as in the development of applications for a synthetic approach to be chosen which results in samples with a narrow size distribution.

## **2.2 Synthesis of narrow size distribution semiconductor colloids**

To obtain nanoparticles nearly free from structural defects and with a good size distribution, the high temperature organic approaches are still unrivalled. This type of synthesis was first described for CdX (X = S, Se, Te) in 1993<sup>5</sup> and since then a number of improvements have resulted, however, the principles have remained the same. The synthesis consists in the pyrolytic decomposition of precursor molecules in the presence of surfactant molecules (so-called ligands) such as tri-*n*-octylphosphine oxide (TOPO), which was employed in the first described synthesis of CdSe by this method. In addition to TOPO, a number of other surfactants, such as alkylamines, phosphonic or fatty acids, can be used. With the use of carefully chosen high boiling organic surfactants and the proper precursor molecules, other types of nanoparticles, such as CoPt<sub>3</sub> and Fe<sub>3</sub>O<sub>4</sub>, with very good size distribution and high crystallinity can also be prepared by this method.<sup>6,7</sup> In a typical synthesis, the surfactant molecules are heated to high temperatures, around

300 °C, and then precursor molecules are injected, whereby nucleation occurs. The role of the surfactant molecules during the synthesis is to form a complex with the atoms on the surface of the nanoparticles as well as with the precursor atoms, thus preventing uncontrollable growth of the nanoparticles. The reaction only occurs at elevated temperatures and, hence, the growth of the nanoparticles can be stopped once the desired size is attained by decreasing the temperature. For semiconductor nanoparticles, the growth can easily be followed by means of optical spectroscopy.

In semiconductor nanoparticles, the surface atoms can give rise to states with a high electron affinity (surface traps), which can lower the luminescence efficiency by acting as centres for non-radiative processes. To reduce the non-radiative processes, the nanoparticles are usually coated with a higher band gap material by the same reaction approach. The precursor for the shell growth is slowly added to the unpurified reaction mixture and a temperature is chosen at which the nucleation of the shell precursor does not occur. The reaction conditions chosen can also allow the growth to be preferentially epitaxial. Thus core/shell nanoparticles are obtained which exhibit higher luminescence efficiencies and improved photochemical stability compared to the bare core nanoparticles.

As the same surfactant molecules are used for the growth of the shell, as were employed for the synthesis of the core, the nanoparticles are covered with a layer of these organic molecules (ligands) which have a functional group through which they bind to the surface atoms of the nanoparticles. These ligands provide solubility and colloidal stability of the nanoparticles, preventing them to agglomerate, which allows for the easy handling of these inorganic crystals as with ordinary liquids. The solubility characteristics of the surfactant molecules will in this way determine the final solubility properties of the nanoparticles. However, the conclusion that the solubility of a ligand in a certain solvent means that the nanoparticle can be dissolved in the same solvent is not given. At this stage, the nanoparticles are not soluble in highly polar solvents, such as methanol, although TOPO alone is soluble in such solvents. Upon the addition of methanol, the polar group of the loosely bound TOPO molecules forms strong bonds with the methanol molecules, thus allowing agglomeration of the nanoparticles. The usual way of purifying the nanoparticles is, thus, through precipitation with methanol. The precipitate, still

containing some, more strongly bonded TOPO molecules, can be re-dispersed in chloroform. In each purification step, some of the more loosely bonded ligands are lost, leading eventually to irreversible agglomeration of the nanoparticles. While the surfactant molecule is attached to the nanoparticle through its polar head group, which does not contribute to the solubility characteristic of the nanoparticles, the hydrophobic aliphatic chain of the surfactant molecule determines the solubility and allows the nanoparticles to be dispersed in solvents such as chloroform, toluene and hexane. Thus, the nanoparticles synthesized through this advanced synthetic approach are non-polar and insoluble not only in polar organic solvents but also in water, which is the ultimate goal.

### **2.3 Water solubility**

Fluorescence imaging is one of the strongly emerging fields in biology and medicine, and semiconductor nanoparticles are certainly finding a very representative place among the fluorophores which can be employed.<sup>8-10</sup> In the first published application of semiconductor nanoparticles in biolabelling experiments, where the water solubilisation strategy was simultaneously proposed, their advantages over organic fluorophores were convincingly presented.<sup>11,12</sup> Unlike organic dye molecules, these inorganic nanocrystals are less sensitive to environmental changes and have lower rates of photodegradation, allowing long-term experiments.

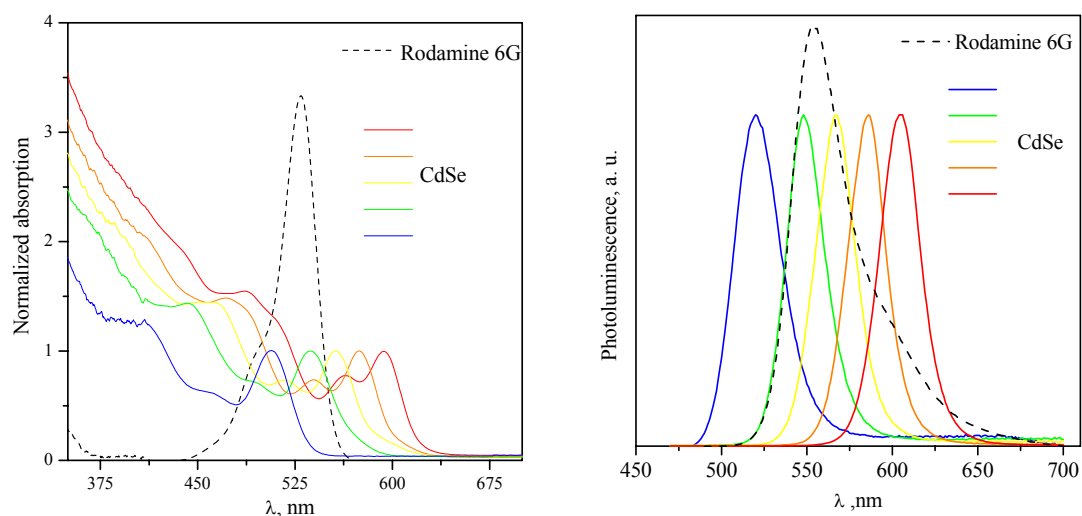


Figure 2.3.1. Comparison of the absorption and emission characteristics of CdSe nanoparticles of different size and the organic dye Rodamine 6G

Narrow emission and broad absorption spectra compared to the very broad emission peak and narrow excitation window of organic fluorophores are further advantages of nanoparticles (Figure 2.3.1). The emission colour of the nanoparticle fluorophore can be tuned by only changing the size of chemically identical species, which can be excited with the same wavelength light, since their absorption characteristics do not differ significantly in the low wavelength region. Whereas to observe multiple colours with organic dyes, chemically different species must be used and for each dye the most suitable experimental conditions (such as the excitation light wavelength) must be chosen.

These properties have induced a large interest in the use of semiconductor nanoparticles for imaging experiments. To provide for such extraordinary properties, the best synthetic method as described in the previous section is the usual choice, with the consequence that the obtained materials are neither water- nor bio-compatible. Thus, the first step in any further bioapplication of such materials is to make them water soluble. In an ever increasing number of reviews on the bioapplication of nanoparticles, special emphasis is always given to the water solubility issue.<sup>13-23</sup> Although very sophisticated methods for the phase transfer of nanoparticles have been developed, the universal answer to the aqueous solubility problem still does not exist. Generally all the developed methods to

make nanoparticles water-soluble can be divided into two basic strategies: ligand exchange reactions and encapsulation in micelle-like structures (Figure 2.3.2).

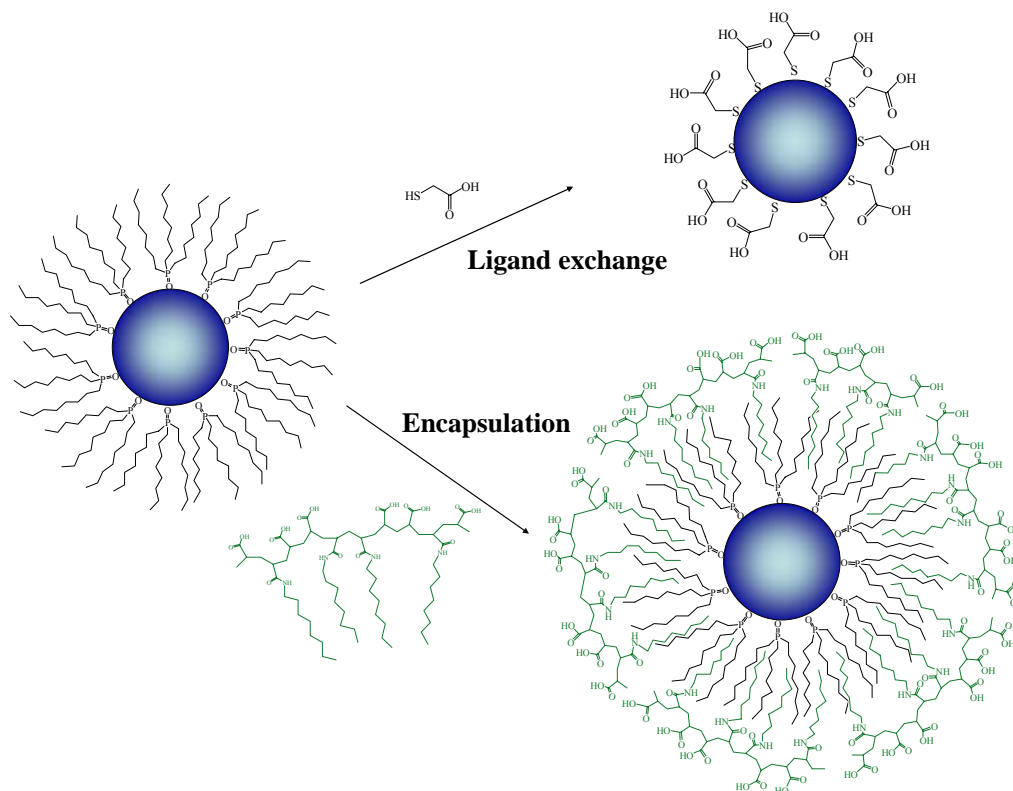


Figure 2.3.2. Schematic representation of the two strategies employed to make nanoparticles water-soluble

### 2.3.1 Solubilisation by ligand exchange

In the ligand exchange procedures, the original hydrophobic layer of organic molecules is replaced with suitable ligands which should possess a functionality reactive toward the surface atoms of the nanoparticle at one end and a water compatible functionality on the other end of molecule. In the first described ligand exchange experiment,<sup>11</sup> the ligand used was mercaptoacetic acid, which possesses an SH binding group and a carboxylic group, which provides water-solubility through the repulsive electrostatic interactions of the charged  $\text{COO}^-$  groups. The use of different mercaptohydrocarbonic acids is very broad since the phase transfer is relatively simple to perform. In addition to mercaptoacetic acid,<sup>24-27</sup> mercaptopropionic,<sup>28</sup> mercaptoundecanoic<sup>29</sup> and

mercaptobenzoic acid<sup>30</sup> have also been used. The so-obtained nanoparticles are suitable for further ligand exchange with biological molecules functionalised with groups reactive toward the nanoparticle surface, such as thiolated nucleic acids.<sup>31</sup> Although broadly used, nanoparticles stabilised with mercaptohydrocarmonic acids have many disadvantages. The bond between the SH group and the nanoparticle is dynamic so that excess ligands must be present in the solution. Crosslinking of the ligand shell around the nanoparticle has been proposed as a solution for the poor stability of the nanoparticle/ligand complex. Usually, silane molecules with an SH functionality for binding to the nanoparticle surface and a polar group for water compatibility are used.<sup>12,32,33</sup> First the ligand exchange is performed leaving methoxy groups exposed to the solvent. The silane molecules are then crosslinked by reaction of the methoxysilane groups, resulting finally in stable siloxane bonds. To improve the biocompatibility, these silanised nanoparticles can be further functionalised with poly(ethylene oxide), PEO. With this strategy, where the ligand is directly bonded to the nanoparticle, crosslinking of the carboxyl groups of the mercaptohydrocarmonic acids and further hydrophilisation with cysteine molecules have also been proposed.<sup>34</sup> Procedures involving crosslinking of the ligand molecules, although providing a much improved stability, are tentative and yields are low, which is the main reason why they are not more widely used. Another approach to increase the stability of water-soluble nanoparticles is the use of polydentate ligands, such as dihydrolipoic acid.<sup>35</sup> Multidentate ligands were also used with phosphine,<sup>36</sup> phosphine oxide,<sup>37</sup> amino<sup>38</sup> or carboxylic groups.<sup>39</sup> In many of these examples, the stabilisation in water was not provided for by the electrostatic repulsion of the charged groups. The disadvantage of nanoparticles stabilised through repulsion of the charged groups (as in the case of mercaptohydrocarmonic acids) is the poor stability in solutions of low pH and high ionic strength. To overcome this problem, ligands with non-charged groups, such as dithiothreitol, can be employed.<sup>40</sup> Moreover, the stabilisation of nanoparticles can be also achieved through steric stabilisation by the repulsion of the polymeric chains. PEO with two binding SH groups have been shown to greatly improve the properties of water-soluble nanoparticles compared to mono or bidentate mercaptohydrocarmonic acids.<sup>41</sup> One interesting example of ligands used in the ligand exchange procedure are certainly dendron molecules, where the highly branched structure

of the ligand was shown to be not only successful in providing the colloidal stability of an aqueous dispersion of nanoparticles, but also to have a positive impact on the chemical and photostability of these conjugates.<sup>42</sup>

In ligand exchange procedures, simultaneously with changes in the colloidal properties of the nanoparticles, the luminescence efficiencies can be greatly affected, since the surface states of the nanoparticles are very sensitive to any change.

### **2.3.2 Encapsulation of the nanoparticles in micelle-like structures**

The second strategy to make nanoparticles water-soluble does not involve ligand exchange and thus allows the original ligands to almost completely determine the luminescence properties. In this approach, an additional layer of organic amphiphilic molecules is added to the existing ligand layer of the original nanoparticles. The amphiphilic molecules possess a hydrophobic part which reacts with the hydrophobic molecules on the nanoparticle surface through hydrophobic interactions, while the second hydrophilic part ensures water solubility. In the first described experiment of this type of stabilisation, phospholipid molecules were used with PEO in the water-soluble part of the molecule.<sup>43</sup> The nanoparticles were trapped in ligand-formed, micelle-like structures. Other types of polymers, such as copolymers with carboxylic groups in the backbone of the molecule and hydrocarbon branches, were also used.<sup>44</sup> The side hydrocarbon branches interact with the TOPO chains and charged carboxylic groups of the polymer backbone ensure the water solubility of these structures. To obtain such polymers, poly(acrylic acid) was grafted with octyl amine through EDC-coupling (EDC = N-(3-dimethylaminopropyl)-N'-ethylcarbodiimide hydrochloride). The same reaction of the carboxylic groups with EDC has been used to stabilise these conjugates through the crosslinking of the carboxyl-group-containing shell. Also a commercially available polymer with a similar structure and with the same working principle, poly(maleic anhydride alt-1-terdecene), was used.<sup>45</sup> As in the previous case, here also some of the carboxylic groups had to be crosslinked after the encapsulation of nanoparticles, in order to ensure the stability of such structures. Encapsulation with more

complex structures, such as a triblock copolymer containing poly(butyl acrylate), poly(ethyl acrylate) and poly(methacrylic acid) segments in which the carboxylic groups were partially modified with octylamine and PEO, was also reported.<sup>46</sup> Liposome encapsulation, similar to the first described phospholipide system, resulting in directly biocompatible nanoparticles has been performed.<sup>47</sup> The extent of agglomeration occurring during encapsulation and, in the cases where it was used, during the crosslinking procedure, is questionable and usually a poorly addressed issue. It can be easily imagined that a great loss of nanoparticles occurs due to agglomeration during the preparation of such conjugates. This can, however, in part be avoided by the proper choice of concentration and reaction conditions. The encapsulation approach is, on the other hand, quite general, since it relies on the hydrophobic interaction of the organic layer of nanoparticles and is insensitive to the variation of the nanoparticle material. However, the main criticism of this type of procedure lies in the size of the final product, which increases through the formation of a multilayered structure.

### **2.3.3 Magnetic nanoparticles**

There is a growing interest in magnetic nanoparticles for use in biomedicine.<sup>48</sup> As with semiconductor nanoparticles, magnetic nanoparticles of a good crystallinity and low polydispersity are obtained with a hydrophobic ligand layer and, hence, they must be made water-compatible. Very general encapsulation procedures, either with polymeric ligands or phospholipids, were successfully applied for the water transfer of magnetic nanoparticles.<sup>45,49,50</sup> There are also reports about ligand exchange using carboxylic or phosphine groups as the binding groups for iron-oxide nanoparticles.<sup>51,52</sup> Since the ligand exchange procedure has the advantage of retaining the small size of the end product, this strategy should be more broadly used in the case of magnetic nanoparticles, where a drop in the luminescence intensity, which usually accompanies this procedure with semiconductor nanoparticles, is not an issue.

## 2.4 Properties of water-soluble nanoparticles

As may be seen from the previous section, the strategies to make nanoparticles water-soluble are versatile and there is still no approach preferred over the other. Very often the nanoparticles are made water-soluble in a way that will suite the potential application the most. There are very few reports dealing with comparisons of any important properties, such as optical properties, size and stability of the nanoparticles, after phase transfer using different procedures.<sup>53,54</sup> If the size is an issue in the designed biological experiment, then the nanoparticles should be stabilised with a thin organic layer which is, in turn, not the best choice when high stability to the influence of the environment is required. The biocompatibility of nanoparticles is important for any type of biological experiment. Regardless of the way in which the nanoparticles are brought into an aqueous environment, they are very often, either during phase transfer or after it has been performed, decorated with PEO molecules. PEO, which is known to be bio-inert and non-toxic, is already broadly used in other fields of biotechnology. The non-specific binding sometimes observed in biological experiments is usually prevented by addition the of PEO to the nanoparticle coating.<sup>55</sup>

The increased interest in biological applications has raised the question of toxicity.<sup>56-58</sup> Nanoparticles comprising of Cd or Pb can be expected to be harmful if these ions are released from the nanoparticles. The cytotoxicity correlates with the evolution of these ions into the surrounding medium. Here also, the surface coating plays the determining role in the release of these ions and, consequently, in the toxicity. It has been shown that for nanoparticles covered with a thick polymeric coating, as opposed to those coated with small molecules such as mercaptoacetic acid, the coating could prevent cytotoxicity.<sup>57</sup> A suitable coating does not only have a role as a barrier to the release of the liberated ions, but can also affect the oxidation processes leading to the formation of these ions in the first place.<sup>59</sup> Although the cytotoxicity of suitably coated nanoparticles does not appear to be problematic for *in vitro* studies,<sup>21</sup> the impact that these materials will have *in vivo* applications still needs to be determined. Again, here the coating will play a crucial role in the final properties of these materials, not only as a barrier to the influences of the

environment, but also in issues such as uptake, accumulation in tissues and release from the body. As a starting point, the use of a non-toxic, non-immunogenic coating material, such as PEO, should be considered.

Water-soluble nanoparticles designed to be used in biological applications do not only have the role of a simple imaging probes. Conjugation with biomolecules is a step further for the design of self-assembled nanostructures. Coating-directed arrangements of nanoparticles by DNA through the self-assembly processes is of current interest in the field of nanoengineering.<sup>13</sup> However, self-assembly is not limited only to biomolecules, such as DNA, it is also a usual way by which, for example, amphiphilic molecules build complex, although predictable, structures. From this aspect, engineering of the nanoparticle coating is not just a simple way to achieve the desired properties, but can be a powerful tool in controlling the structure of a nanoparticle/ligand conjugate with the desired functionality as the next step.

### 3. Results and Discussion

#### 3.1 Synthesis and characterisation of CdSe/CdS and CdSe/CdS/ZnS nanocrystals

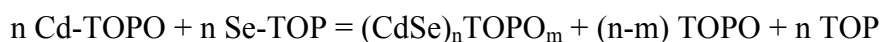
As already presented, luminescent nanocrystals have superior properties compared to organic dyes in several aspects, which recommends them for use in biolabelling experiments. Water-based synthesis would be the natural choice for such materials since the so obtained nanoparticles are hydrophilic and, therefore, more likely to be biocompatible. However, nanoparticles obtained in water-based syntheses, especially CdSe,<sup>60-62</sup> have not yet reached the level of perfection that is found in nanoparticles synthesised by the hot-injection synthesis method. Described for the first time in 1993, the hot-injection method represents a milestone in synthetic methodology in the wet-synthetic approach to obtain nanoparticles.<sup>5</sup> The method consists of the rapid injection of organometallic reagents (such as dimethyl-cadmium) into a hot coordinating solvent (trioctylphosphine oxide, TOPO, at 300 °C) to produce homogenous nucleation. The sudden temperature drop associated with the introduction of the room temperature reagents prevents further nucleation. Increasing the temperature again to higher values leads to the slow growth and annealing of the existing nuclei. Numerous adaptations of this synthetic approach have been developed leading to nanoparticles with extremely narrow size distributions and high quantum efficiencies.<sup>63</sup> Within this frame work, the hot-injection method was employed to produce high quality CdSe nanoparticles. A “greener” chemical approach was used by which the hazardous dimethyl-cadmium was replaced with cadmium-acetate, Cd(Ac)<sub>2</sub>, along with the addition of the hexadecylamine as a coordinating ligand.<sup>64</sup> Previously it was also shown that the Cd(Ac)<sub>2</sub>/pure-TOPO system is much more reproducible than the Cd(CH<sub>3</sub>)<sub>2</sub>/pure-TOPO system.<sup>65,66</sup> One more advantage of the hot-injection method compared to others is the possibility of building an inorganic passivation shell. Although organically-capped nanocrystals with

very high luminescence efficiencies can be obtained (up to 85 % for samples without any purification), they are still not robust enough for further manipulation. Their photostability is also rather poor since the organic shell is flexible and dynamic allowing the ambient chemical species to reach the surface of the nanoparticle. The robustness as well as photostability can be improved by growing a shell of a higher band gap material over the CdSe core. The lattice mismatch between CdSe and CdS is rather low (3.9 %), allowing an easy epitaxial shell growth and providing good passivation.<sup>67</sup> For increased stability, a shell of a higher band gap material is favourable, as is the case of ZnS. However, the large lattice mismatch between CdSe and ZnS (~12%) induces strain at the core-shell interface. To combine the advantages of both shell materials, nanocrystals with a double shell have been synthesized, where the middle CdS shell serves as a “wetting” layer to build the second ZnS shell.<sup>68,69</sup> These core/shell/shell nanoparticles are the most stable nanocrystals known to date.

Within the frame of this work, core/shell, CdSe/CdS, and core/shell/shell, CdSe/CdS/ZnS, nanoparticles were synthesised for use in the further ligand exchange experiments. In the following text, the synthetic route employed and the main properties of the obtained nanoparticles are presented.

### **3.1.1 Core/shell, CdSe/CdS, nanoparticles**

As already mentioned, the synthesis of CdSe/CdS nanoparticles was performed following a “greener” chemical approach in a one pot procedure.<sup>64</sup> In the first step, the CdSe core is produced in a yield low enough to allow for the unreacted Cd-precursor to be used in the further steps. As the Cd source, cadmium-acetate dissolved in trioctylphosphine was used. This solution was swiftly injected into a hot solution of Se in a coordinating mixture consisting of trioctylphosphine oxide (TOPO), trioctylphosphine (TOP), hexadecylamine (HDA) and tetradecylphosphonic acid (TDPA). During the nucleation process, the precursors combine to form small, unstable clusters, which, in the case of CdSe, can be represented in the following simplified form:



In the nucleation process, small amounts of the reactants are consumed. The further growth of the formed nuclei goes via the consumption of the reactants remaining in the solution. The reaction can be stopped at any point when the desired size of the nanoparticles is attained, while leaving excess precursors for further shell growth. Development of the size of the formed nanoparticles can be followed by spectroscopy, and the typical temporal evolution of the absorption and photoluminescence, PL, spectra is represented in Figure 3.1.1.

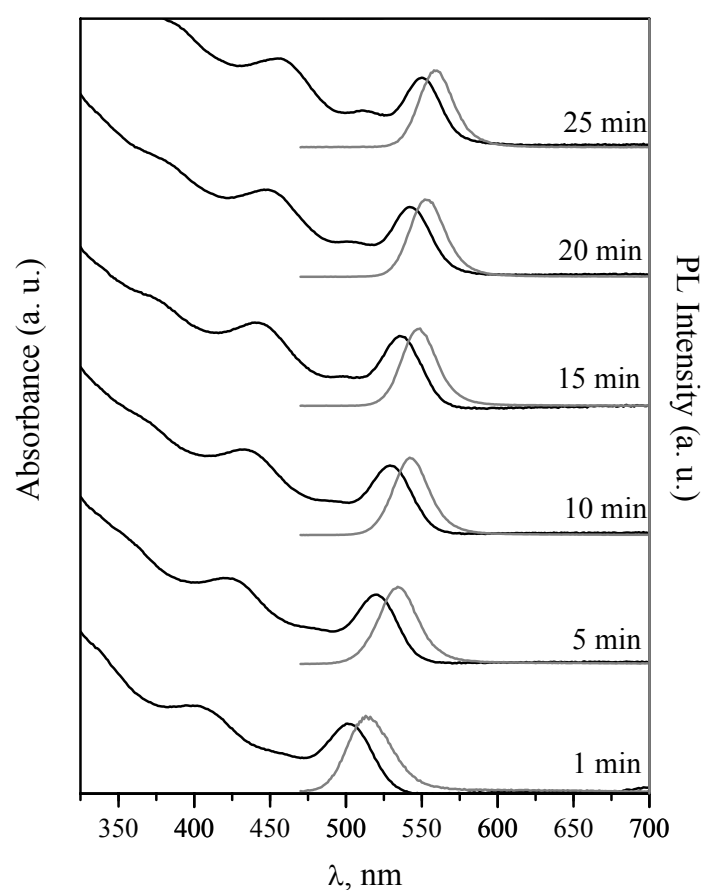


Figure 3.1.1. Temporal evolution of the absorption and PL spectra of the growing CdSe nanocrystals

The coordinating ligands provide not only the conditions for the building of the nanosized material, but also have a determining role in the quality, size distribution, kinetics, shape

even the crystal structure of the formed nanoparticles.<sup>70-76</sup> As reported before, the amine has a strong influence on the growth rate, quantum efficiency and size distribution of the product compared to the TOPO systems.<sup>71,73</sup> As can be seen in 3.1.1, the size distribution, as judged from the full width at half maximum of the PL spectra, remains narrow during the course of the reaction. This allows the calculation of the diameter of the nanocrystals from the position of the first absorption peak and, using published values of the size-dependant extinction coefficients,<sup>77</sup> the concentration of the nanoparticles.

Tetradecylphosphonic acid and hexylphosphonic acids were recognized as the main impurities in the technical TOPO which was used as the coordinating solvent in the first published hot-injection synthesis with  $\text{Cd}(\text{CH}_3)_2$  as the precursor. In the further development of this synthetic approach, usually a mixed reaction solvent consisting of high grade TOPO and phosphonic acids was used. It was found that without the addition of the strong ligand, phosphonic acid, the  $\text{Cd}(\text{CH}_3)_2$  decomposes at high temperatures and a cadmium precipitate is generated in pure TOPO.<sup>74</sup> Instead of phosphonic acids, fatty acids were also used in combination with different Cd precursors, such as CdO and the Cd salts of weak acids.<sup>65,78</sup> When fatty acids were used as ligands, the growth rates were so high that the isolation of small nanocrystals was not possible. It was also shown that CdO as a precursor functioned only in the presence of either fatty acids or phosphonic acids. However, it was demonstrated recently that CdSe nanocrystals can be obtained from CdO in TOP/TOPO mixtures without the addition of any acid.<sup>72</sup>

In order to avoid the presence of a strong coordinating ligand such as TDPA in the to-be-performed ligand exchange experiments, the influence of the amount of TDPA on the growth of the nanoparticles was investigated. The growth of the nanoparticles during the reaction was followed for different amounts of TDPA (0.4, 0.6 and 0.9 wt%, calculated on the total mass of the reaction mixture). The change in the size of the nanoparticles during the course of the synthesis is presented in Figure 3.1.2 for different amounts of TDPA.

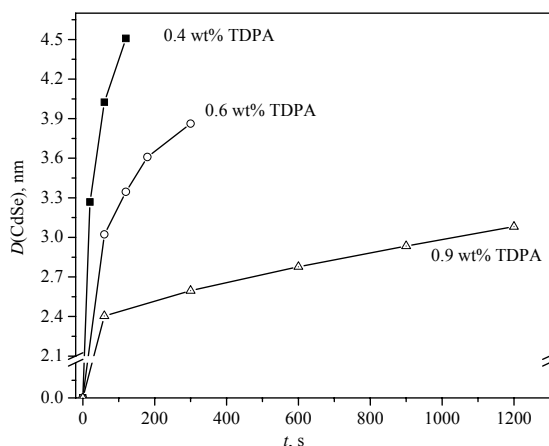


Figure 3.1.2. The change in the size of the nanoparticle during the reaction with different amounts of TDPA

Increasing the amount of TDPA strongly suppressed the growth of the nanoparticles. While the size of the nanoparticle was 3.3 nm after 20 s of reaction with 0.4 wt% of TDPA, this size was not achieved even after 20 min when the amount of TDPA was increased to 0.9 wt%. TDPA acts as a strong ligand forming a Cd-TDPA complex (precursor) and also binds to the surface of the formed nanocrystals, preventing further growth. This is in accordance with a previous kinetic study of the preparation of CdSe in the presence of oleic acid as a strong ligand.<sup>79</sup> In the case of oleic acid, it was found that it already has a strong influence in the nucleation step, determining the number and the size of the nuclei formed in the nucleation step. With increasing amount of oleic acid, the number of nuclei formed decreases almost linearly and this behaviour was explained by the strong complexation of oleic acid to Cd, which makes nucleation more difficult. To check whether TDPA has a similar influence, the overall concentration of CdSe nanoparticles after synthesis with different amounts of TDPA was calculated. Since the size distribution does not change during the course of the reaction, it can be assumed that the concentration of CdSe nanoparticles at the end of the synthesis is equal to the number of nuclei formed. The findings were contrary to the case of oleic acid, namely the amount of the TDPA had no influence on the number of formed nuclei. With increasing concentration of the strong ligand, the number of CdSe nanoparticles was constant or

slightly higher. A possible explanation of this difference may lie in the different manner of the addition of the precursors and ligands. In the oleic acid case, the Cd-stock solution already contained oleic acid before the reaction, hence complexation could have already occurred before the reaction, while in the present case, the precursor  $\text{Cd}(\text{Ac})_2$  was dissolved only in TOP and injected into the reaction mixture which contained TDPA. On injection, the competing processes, nucleation, complexation of the Cd and coordination of the formed nuclei to TDPA, occur simultaneously. This indicates that TDPA has a stronger effect in the growth phase than in the nucleation step in this case. Thus, the size of the nanoparticles can only be varied by changing the duration of the growth, and eventually, by changing the temperature of the injection.

During slow growth, the crystal structure of nanoparticles is more perfect with fewer defects. The luminescence properties are strongly affected by the perfection of the crystals. The luminescence efficiencies determined for CdSe nanoparticles obtained in the presence of different amounts of TDPA change strongly. This difference cannot be attributed only to the different size of the final nanoparticles, although there are reports that PL efficiencies are lower for larger nanoparticles than for smaller ones.<sup>65,71</sup> In all cases, a decrease of the PL efficiency with increasing size of the nanoparticles was observed during the growth. The efficiencies are lower for the nanoparticles grown with lower amounts of TDPA, i.e., with higher growth rates (Figure 3.1.3). As may be seen in Figure 3.1.3, the PL intensities of nanoparticles of similar sizes are higher when the highest amount of TDPA is used.

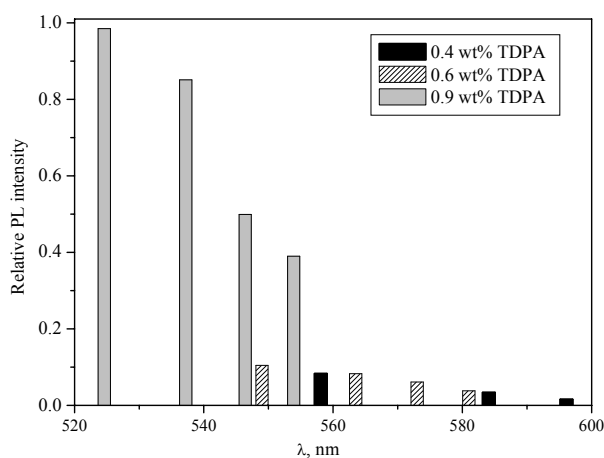


Figure 3.1.3. Changes in the PL intensities during the growth of nanoparticles with different amounts of TDPA

On the one hand, strong ligands which bind strongly to the nanoparticle surface should be avoided when the nanoparticles are intended to be used in ligand exchange experiments. On the other hand, in order to obtain highly emitting nanoparticles with good crystallinity and a small number of crystal defects, the presence of strong ligands which provide for a slow controllable growth are necessary. Thus, the CdSe nanoparticles were synthesised with the highest amount of TDPA investigated.

To improve the luminescence yield and the stability of the nanoparticles, a shell of CdS was built around the CdSe cores. This was done in a one pot synthesis via the slow injection of H<sub>2</sub>S gas and using the excess Cd precursor remaining after the synthesis of the cores. During the injection of H<sub>2</sub>S, a red shift in the absorption and PL spectra was observed, showing the growth of the nanoparticles. Simultaneously, the luminescence yield increased, as expected (Figure 3.1.4).

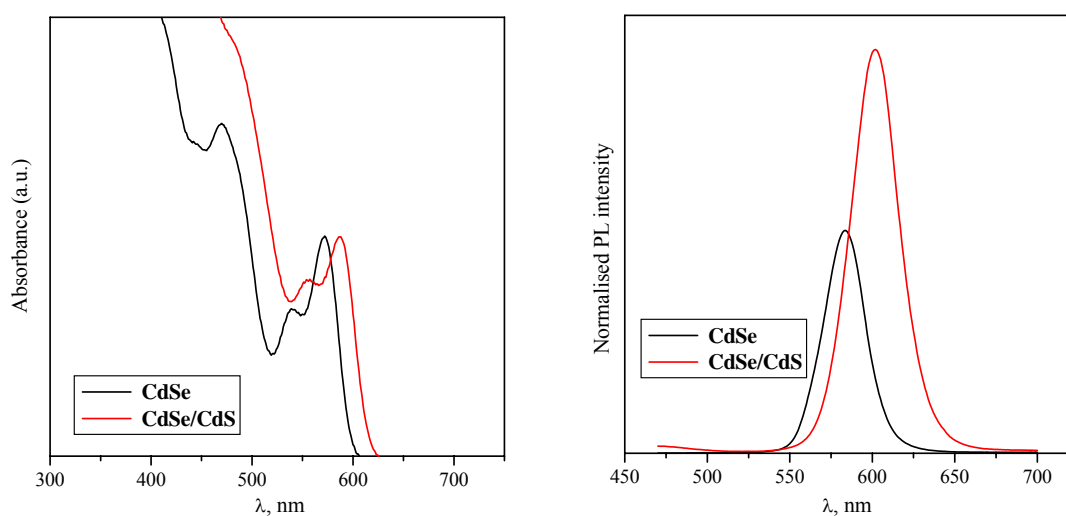


Figure 3.1.4. Changes in the absorption and PL spectra after the growth of a CdS shell on the CdSe cores

The size distribution broadens during the building of the shell, as can be seen from the full width at half maximum of the luminescence peaks. It may be seen from the transmission electron microscopy (TEM) images that the nanoparticles increased in diameter while maintaining a spherical shape on formation of the CdS shell (Figure 3.1.5).

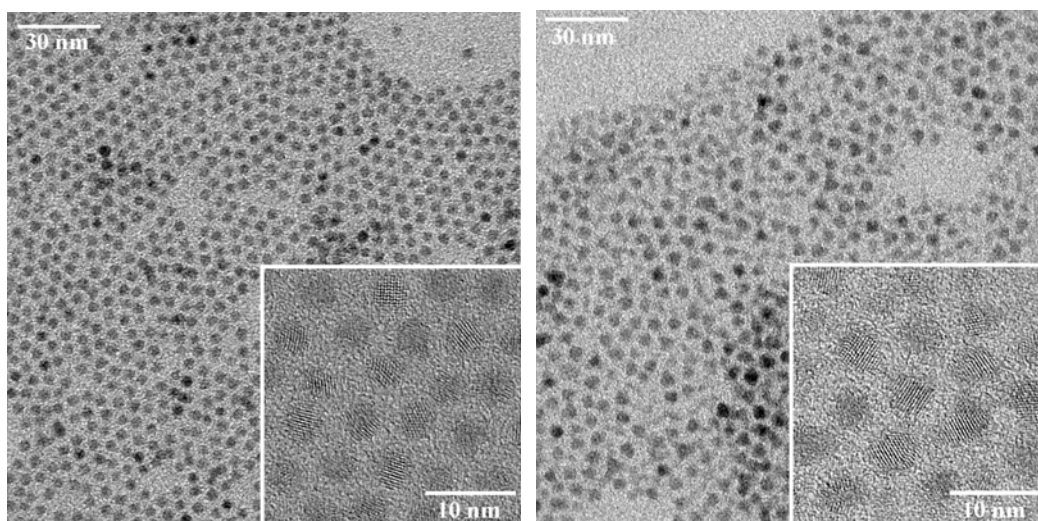


Figure 3.1.5. TEM and HRTEM images of CdSe (left) and CdSe/CdS (right) nanoparticles

The high-resolution TEM images of both the CdSe core and CdSe/CdS core/shell nanoparticles reveal a high crystallinity with continuous lattice fringes throughout the whole particle. Especially in the case of the CdSe nanoparticle, the higher hexagonal ordering is observed due to the very narrow particle size distribution and spherical shape.

### **3.1.2 Core/shell/shell, CdSe/CdS/ZnS, nanoparticles**

The same simple synthetic approach, injection of H<sub>2</sub>S gas, was used for the synthesis of CdSe/CdS/ZnS, core/shell/shell nanoparticles.<sup>62</sup> To a solution of freshly prepared CdSe/CdS nanoparticles, Zn precursor (zinc-acetate dissolved in HDA) was added which further reacted with the injected H<sub>2</sub>S to produce a ZnS shell. The growth of the second shell could also be observed by a red shift in the absorption and PL spectra during the course of the reaction (Figure 3.1.6). Together with the observed shift towards lower energies, the photoluminescence intensity further increased with the formation of a ZnS shell.

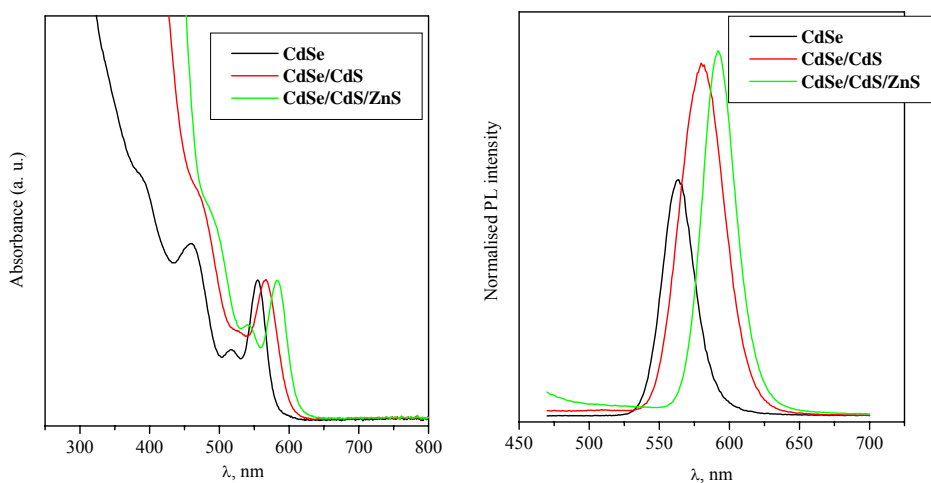


Figure 3.1.6. Absorption and PL spectra of core, core/shell and core/shell/shell nanoparticles

As observed before, the increase in PL intensity with the building of the ZnS shell is not as high as for the first CdS shell.<sup>62</sup> However, the decrease in PL in all syntheses was also not observed. It was argued before that during the growth of the ZnS shell the decrease of PL efficiency can be observed for the thicker ZnS shells. This behaviour was attributed to the possible formation of dislocations and cracks when the thicker shell was built up. The absence of a decrease in the PL efficiency can be indirect proof that the thickness of the ZnS shell is not greater than two monolayers. Calculations performed using the composition of the reaction mixture, the number of nuclei formed and the reaction yield have also shown that the thickness of the second shell should not exceed two monolayers.

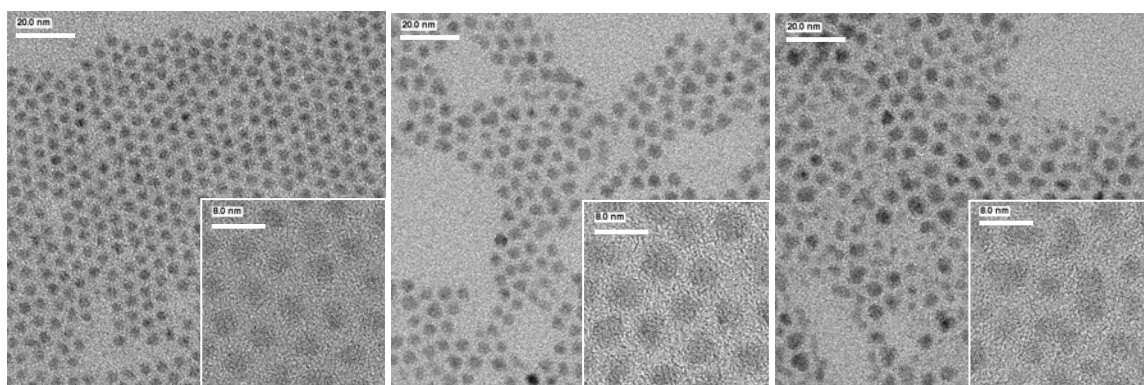


Figure 3.1.7. TEM and HRTEM images of the CdSe core (left), the corresponding CdSe/CdS core/shell (middle) and CdSe/CdS/ZnS core/shell/shell (right) nanoparticles

As for the core/shell nanoparticles, the TEM images of core/shell/shell nanoparticles indicate that the shape during the growth of the shells does not deviate very much from spherical, although, in some cases, preferential growth was observed (Figure 3.1.7). The crystal structure of all three types of nanoparticles is clearly observed in the HRTEM images.

The powder XRD patterns of the core, core/shell and core/shell/shell nanoparticles are shown in Figure 3.1.8. For all samples, peak broadening due to the small size of the nanocrystals was observed for all reflections. The CdSe core diffraction pattern exhibits peak positions corresponding to those of their bulk wurtzite crystalline structure. The XRD pattern of CdSe/CdS core/shell nanoparticles has roughly the same shape as that of the CdSe cores, but with the diffraction angles shifted to higher  $2\theta$  values.

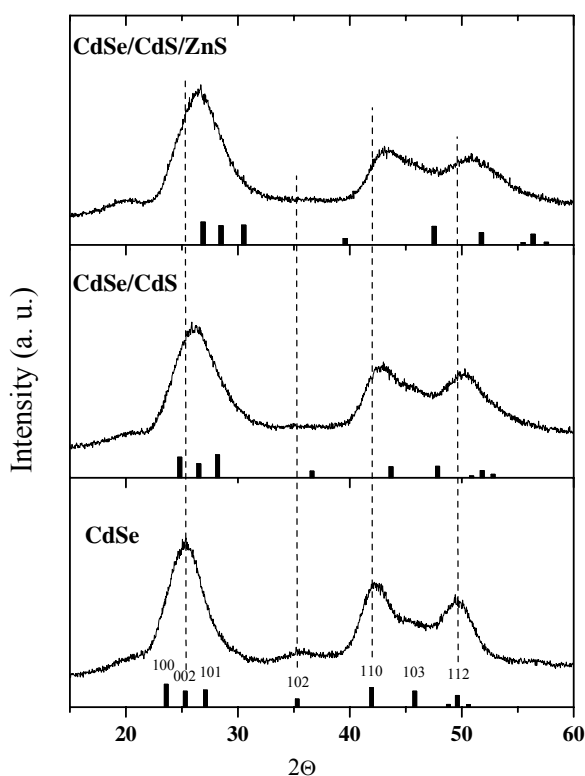


Figure 3.1.8. Powder XRD patterns of the core, core/shell and core/shell/shell nanoparticles (the bars indicate the positions of the reflections of bulk CdSe, CdS and ZnS, from bottom to top)

The shift in the peak position for the core/shell nanoparticles, together with a red shift in the absorption spectra, indicates the formation of core/shell structures rather than alloying ones.<sup>64,67</sup> A further shift towards higher  $2\theta$  positions is observed for the core/shell/shell nanoparticles. The positions of the reflections relative to pure ZnS are shifted toward smaller  $2\theta$  angles, indicating an expansion of the ZnS lattice. Simultaneously, the CdSe core reflections are further shifted towards larger  $2\theta$  angles, reflecting a compression of the CdSe lattice. This can be an indication that the internal strain in the core/shell/shell structures is not relaxed by the introduction of misfits and dislocations. The slight broadening of the peaks in the core/shell/shell pattern, although the nanoparticles increase in size, can be explained by the broad diameter distribution and irregular shapes, as observed in the TEM-images.<sup>68</sup> However, a distribution of the bond lengths resulting from the strain is another possible explanation for the peak widths becoming slightly larger.<sup>67</sup>

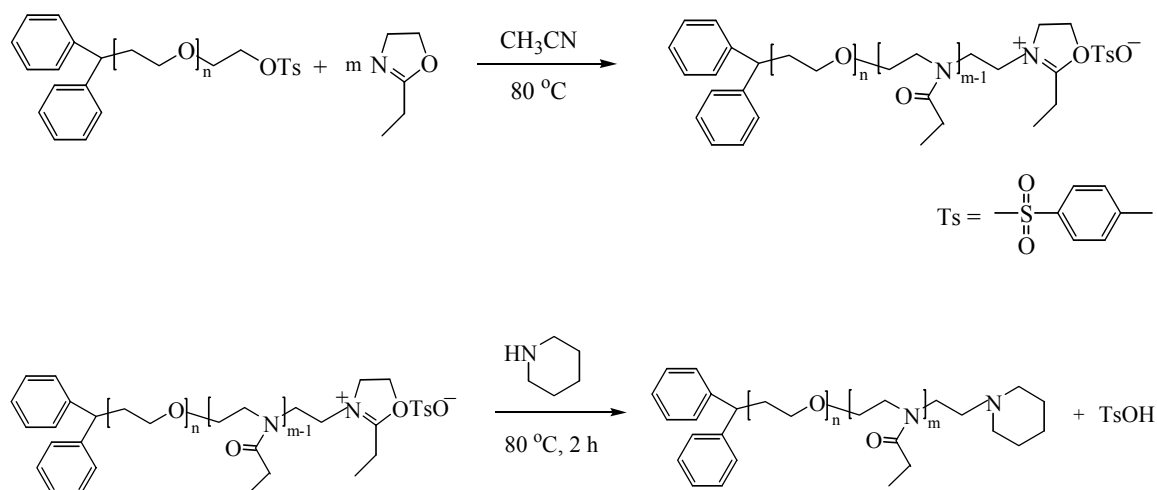
## **3.2 Synthesis and characterisation of poly(ethylene oxide)-based ligands**

In order to design ligands suitable to transfer nanoparticles into water starting from poly(ethylene oxide), it is necessary to introduce certain functional groups that can bind to the nanoparticles of interest, preferably at the end of the PEO molecule – to functionalise PEO. Amino and mercapto functionalities were chosen as binding groups and in the both cases two different approaches to functionalise PEO were employed.

### **3.2.1 Poly(ethylene oxide)-*b*-(ethylene imine) synthesised via cationic polymerization**

The first approach to introduce amino functionalities at the end of the PEO chain involved a polymerisation procedure, which would result in a binding block of highly defined structure. It is known that due to the labile hydrogen of the secondary amine groups in the product polymer, the preparation of linear poly(ethylene imine), PEI, by the ring opening cationic polymerization of ethylamine yields a highly branched structure.<sup>80</sup> Thus, the synthesis of linear poly(ethylene imine) was achieved through the hydrolysis of poly(*N*-acylalkyleneimines). The poly(*N*-acylalkyleneimines) (or poly(oxazolines) POxz) can be obtained by the isomerisation polymerisation of unsubstituted or 2-substituted-2-oxazolines. The ring opening polymerisation of 2-oxazolines can be of ionic or covalent nature, depending on the monomer and the initiator used.<sup>81</sup> With sulphonates as initiators, the polymerisation of 2-ethyl-2-oxazoline proceeds via ionic species. The cationic propagation species are stable; hence, the polymerisation has a living character and is often used for the synthesis of block copolymers. The functionalisation of PEO with such sulphonates results in a macroinitiator which can be employed in the subsequent polymerisation of 2-oxazoline. Both approaches, the functionalisation of previously synthesized OH-terminated PEO, as well as functionalisation as the end step in the synthesis of PEO were reported.<sup>82,83</sup> In this work, the polymerisation of 2-ethyl-2-oxazoline was performed using a PEO-tosyl (PEO-Ts) macroinitiator which had previously been synthesised using the second approach.<sup>84</sup> The polymerisation procedure employed here was given in the same work. The degree of functionalisation was 95 %, as

determined from the  $^1\text{H-NMR}$  spectrum. The molecular weight of the PEO-Ts macroinitiator was 6080 g/mol. After thoroughly drying the macroinitiator in two freeze-dry cycles with benzene, freshly distilled 2-ethyl-2-oxazoline was added. The reaction takes place according to the following reaction scheme:



Scheme 3.2.1. Cationic ring opening polymerisation of 2-ethyl-2-oxazoline to obtain PEO-POxz

After the complete consumption of the monomer, the oxazolinium living end groups were terminated by piperidine. The amount of monomer was varied to produce polymers with 5, 10 and 20 monomer units in the POxz block. The obtained poly(ethylene oxide)-*b*-(2-ethyl-2-oxazoline) was characterised by size exclusion chromatography (SEC) and  $^1\text{H-NMR}$  spectroscopy. The  $^1\text{H-NMR}$  spectrum of the PEO-POxz with 20 monomer units in the second block is presented in Figure 3.2.1.

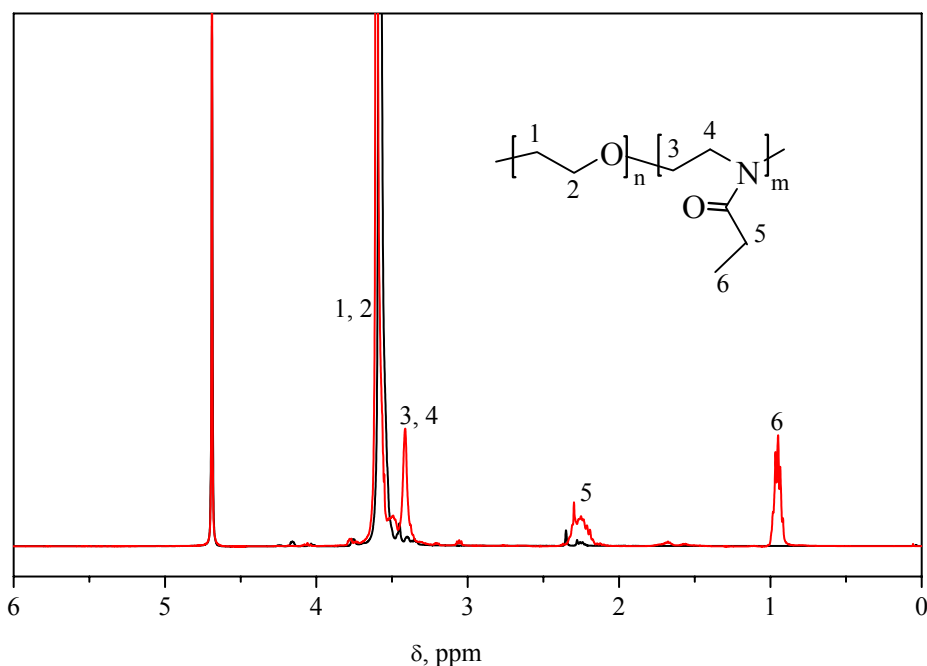
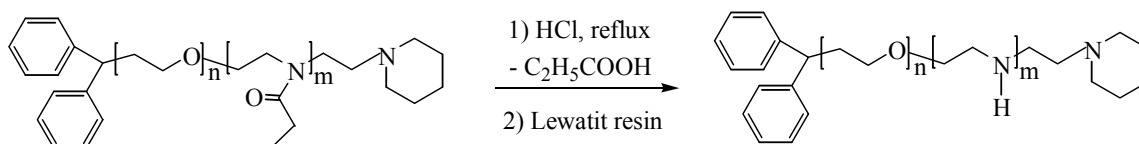


Figure 3.2.1.  $^1\text{H-NMR}$  spectra obtained in  $\text{CDCl}_3$  of the macroinitiator PEO-Ts (—) and PEO-POxz-3 (—) with 20 monomer units in the POxz block

The methylene and methyl signals of the side group of POxz are clearly visible. The ratio of the signals arising from the methylene groups of the PEO moiety at 3.65 ppm and from the methyl group in the side group of the POxz moiety at 0.95 ppm was used to calculate the corresponding block lengths. According to the calculated ratio of PEO and POxz blocks, the composition of the polymer was in good agreement with the composition of the feed (Table 3.2.1).

To finally obtain PEO-PEI, the synthesized PEO-POxz was hydrolysed with hydrochloric acid and subsequently neutralised and purified over an ion-exchange resin. The reaction procedure is presented in the following scheme:



Scheme 3.2.2. Hydrolysis of PEO-POxz to obtain PEO-PEI

As in the case of PEO-POxz, the obtained PEO-PEIs were characterised by SEC. It is known that PEI and POxz strongly bind to the column filling and in some cases, it is not possible to obtain elution curves of copolymers with long PEI or POxz blocks.<sup>84</sup> In the case of the polymers synthesised within the framework of this study, where the PEI (POxz) blocks were small compared to the PEO block, SEC was not problematic as was the case for the longer PEI blocks. However, the precise molecular weight could not be determined with certainty because some retardation of the polymer by the column filling could not be excluded. The SEC elution curves of the synthesised PEO-PEIs as well as of the intermediate PEO-POxzs are shown in Figure 3.2.2.

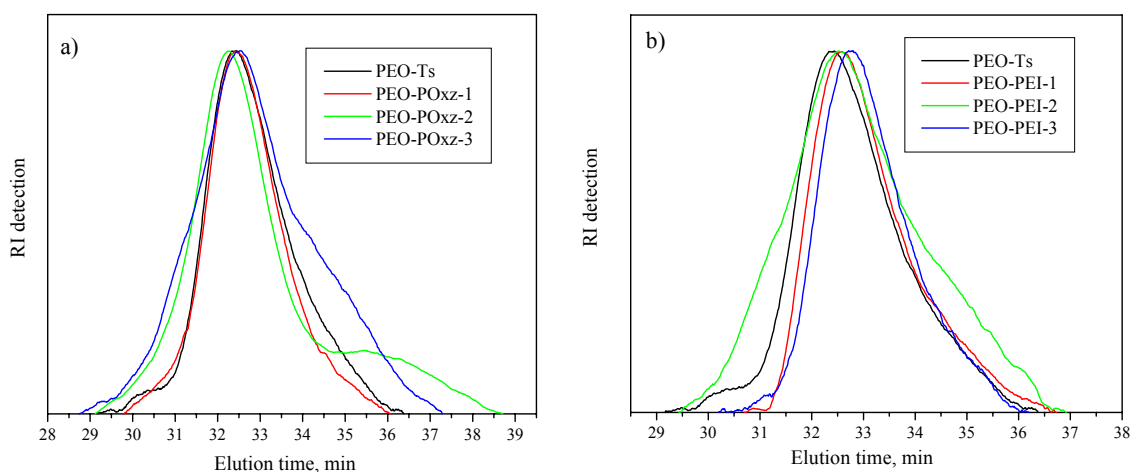


Figure 3.2.2. SEC elution curves of the macroinitiator PEO-Ts, and the synthesized a) PEO-POxzs and b) PEO-PEIs in DMF at 70 °C

As can be seen from Figure 3.2.2, the shift to lower elution times for the PEO-POxz compared to the starting PEO-Ts was very small, corresponding to a small increase in the polymer chain length relative to the first PEO block. In spite of the small POxz block length and although the SEC traces were obtained by passing the polymers over the columns at a high temperature to avoid interaction with column filling, retardation on the column could not be excluded. Among the PEO-POxz copolymers, the polymer with the highest molecular weight and the longest second block (PEO-POxz-3) has the longest elution time, which should correspond to the smallest molecular weight. This behaviour shows that the interaction with the column is more pronounced the longer the POxz

block. For the PEO-PEI copolymers, interaction with the column filling was even more pronounced. All the copolymers show longer elution times (smaller molecular weight) than the starting PEO-Ts. The molecular weight distribution remains small, as is to be expected from the nature of the cationic polymerisation synthesis. Thus, the composition dispersity is very low. To obtain more information concerning the block lengths and, consequently, the molecular weight, the  $^1\text{H-NMR}$  spectra were analysed. As an example, the overlaid  $^1\text{H-NMR}$  spectra of PEO-POxz and the corresponding PEO-PEI are shown in Figure 3.2.3.

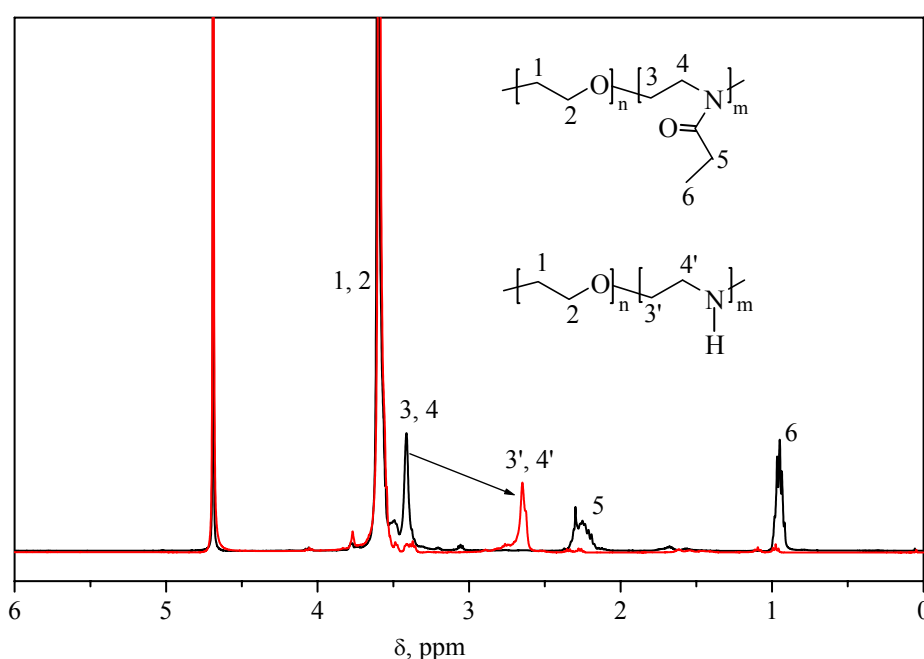


Figure 3.2.3.  $^1\text{H-NMR}$  spectra in  $\text{CDCl}_3$  of PEO-POxz-3 (—) and the corresponding PEO-PEI-3 (—) with 20 monomer units in the POxz and PEI block

The resonance signals at 0.98 ppm, ascribed to the methyl protons from the side groups in the POxz block, disappeared completely, indicating the successful hydrolysis of PEO-POxz. A shift from 3.47 to 2.78 ppm of the signal from the methylene protons adjacent to the nitrogen in POxz is observed, also proving the complete transformation of the tertiary amide groups in POxz to secondary amine groups in PEI. From the ratio of the integrals

of the signals arising from methylene protons in the two blocks, the composition of the copolymers was calculated and the results are presented in Table 3.2.1.

Table 3.2.1. The main characteristics of the PEO-*b*-PO<sub>xz</sub> and PEO-*b*-PEI polymers

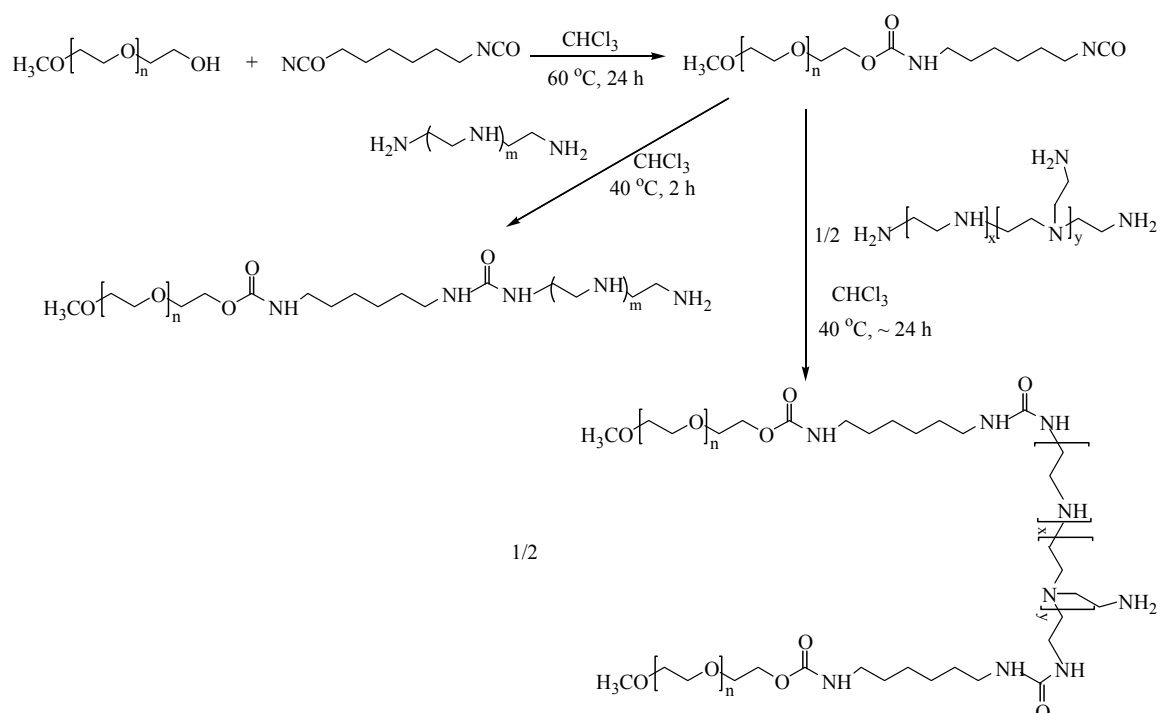
| Polymer                 | $M_{\text{NMR}}^{\text{a)}$ , g/mol | $M_{\text{p}}^{\text{b)}$ , g/mol | $PI^{\text{b)}$ | n(PEO) | n<br>PEO <sub>xz</sub> or PEI |
|-------------------------|-------------------------------------|-----------------------------------|-----------------|--------|-------------------------------|
| PEO-Ts                  | 6080 <sup>c)</sup>                  | 6689                              | 1.11            |        |                               |
| PEO-PO <sub>xz</sub> -1 | 6488                                | 6741                              | 1.08            |        | 5                             |
| PEO-PEI-1               | 6204                                | 6392                              | 1.10            |        | 4 <sup>d)</sup>               |
| PEO-PO <sub>xz</sub> -2 | 6983                                | 7101                              | 1.31            | 131    | 10                            |
| PEO-PEI-2               | 6414                                | 6516                              | 1.19            |        | 10                            |
| PEO-PO <sub>xz</sub> -3 | 7973                                | 6498                              | 1.23            |        | 20                            |
| PEO-PEI-3               | 6834                                | 6140                              | 1.08            |        | 20                            |

a) Calculated using the block lengths estimated from <sup>1</sup>H-NMR spectra; b)  $M_{\text{p}}$  and  $PI$  are the molecular weight from the peak maximum and polydispersity index from SEC measurements in DMF at 70 °C, respectively; c) obtained from MALDI-TOF measurements; d) incompletely hydrolysed sample

### 3.2.2 Functionalisation of poly(ethylene oxide) via the diisocyanate coupling reaction

The second approach to introduce amino groups into PEO-based ligands was the coupling reaction between PEO and amino group bearing molecules. This simple approach consists in the activation of PEO in the first step and coupling to the molecule of interest having a suitable functional group (an amino group in the present case). Coupling reactions of PEO to protein molecules is a well-developed area and the choice of possible reactions is versatile.<sup>85</sup> More concretely, coupling strategies to obtain PEO-PEI block copolymers for gene delivery systems or to be used as stabilisers in nanoparticle synthesis have also been developed.<sup>86-91</sup> It was decided in this work to use the isocyanate coupling reaction, which, compared to other developed activation methods, is the most elegant manner. The complete reaction from the coupling constituents is performed in only two steps, applying basically the same chemistry in both steps. Moreover, the reaction is performed without side products, making the purification procedure an easy task, and, from the chemical

nature of the isocyanate reaction, complete conversion is very easy to achieve in both reaction steps. The isocyanate coupling reaction was successfully applied to graft PEO onto high molecular weight branched PEI.<sup>87</sup> In the framework of this study, the grafting of PEO onto small molecular weight branched PEI (423 g/mol) was performed, as well as the coupling between PEO molecules and small molecular weight amines (diethylenetriamine, DETA, and hexaethylenepentamine, HEPA) (Scheme 3.2.3).



Scheme 3.2.3. Synthetic route of the synthesis of amino-functionalised PEO via the diisocyanate coupling reaction

In the first step, hydroxyl terminated PEO was reacted with a difunctional isocyanate (hexamethylenediisocyanate, HMDI) with the goal that only one of the functional groups of HMDI reacts, while the second should serve as the active centre in the second step. In order to prevent both isocyanate groups from reacting and, thus, forming a polymer of double molecular weight, a large excess of HMDI was used. The unreacted isocyanate was then removed in multiple precipitation steps, which were followed by IR spectroscopy. The IR spectra obtained after each precipitation step are presented in Figure 3.2.4. The strong absorption observed at 2269 cm<sup>-1</sup> corresponds to unreacted

isocyanate. The bands appearing at 3339 and 1716  $\text{cm}^{-1}$  correspond to N-H and C=O stretching, respectively, from the formed urethane group. At 1106  $\text{cm}^{-1}$ , the absorption from the C-O ether stretching could be observed.

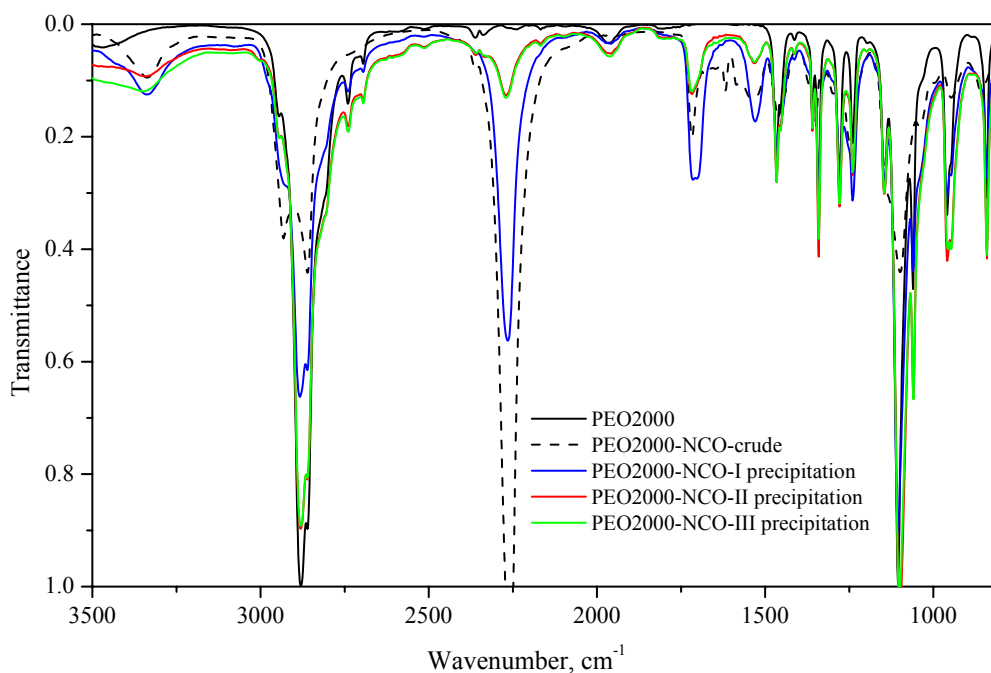


Figure 3.2.4. FT-IR spectra of the starting PEO2000 and PEO2000-NCO after successive purification steps

Under the conditions applied for the precipitation, only two cycles of precipitation were necessary to remove all the unreacted isocyanate. As can be seen in Figure 3.2.4, after two precipitations, the relative intensity of the isocyanate band compared to the C-O stretch band did not change with further precipitations. All the polymers were, consequently, purified in two precipitation steps. The purity of the synthesised PEO-NCO was also confirmed by  $^1\text{H-NMR}$  spectroscopy (Figure 3.2.5). The same intensities of the signals arising from the methylene protons adjacent to the formed urethane bond (3.15 ppm) and the protons from the methylene group next to the isocyanate group (3.30 ppm) indicate that no excess HMDI was present.

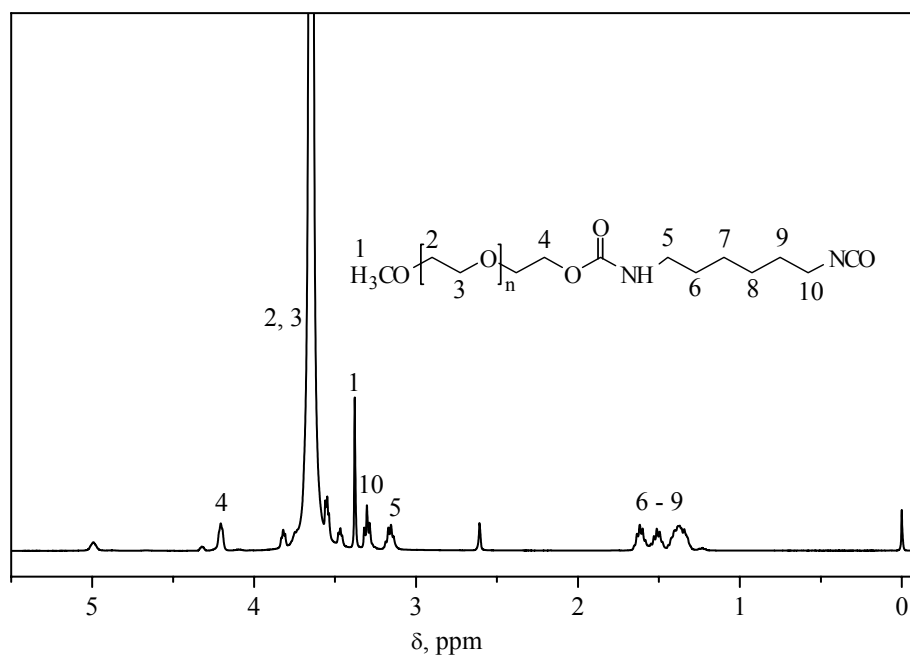


Figure 3.2.5. <sup>1</sup>H-NMR spectrum in CDCl<sub>3</sub> of PEO2000-NCO after two precipitations

The formed PEO-NCO was further used to couple either a small amine molecule or a branched poly(ethylene imine) of small molecular weight. In the case of the small amine it was also important to avoid the formation of double molecular weight product and the same strategy as in case of NCO activation was applied: a large excess of the amine was employed. The progress of the reaction was followed by IR spectroscopy to show complete conversion of the NCO groups. However, information about the final structure was obtained from <sup>1</sup>H-NMR spectroscopy. As an example, the <sup>1</sup>H-NMR spectrum of PEO2000-DETA is shown in Figure 3.2.6. From the ratio of the ethylene oxide/ethylene imine units, the successful removal (in repetitive precipitation steps) of excess DETA was also confirmed.

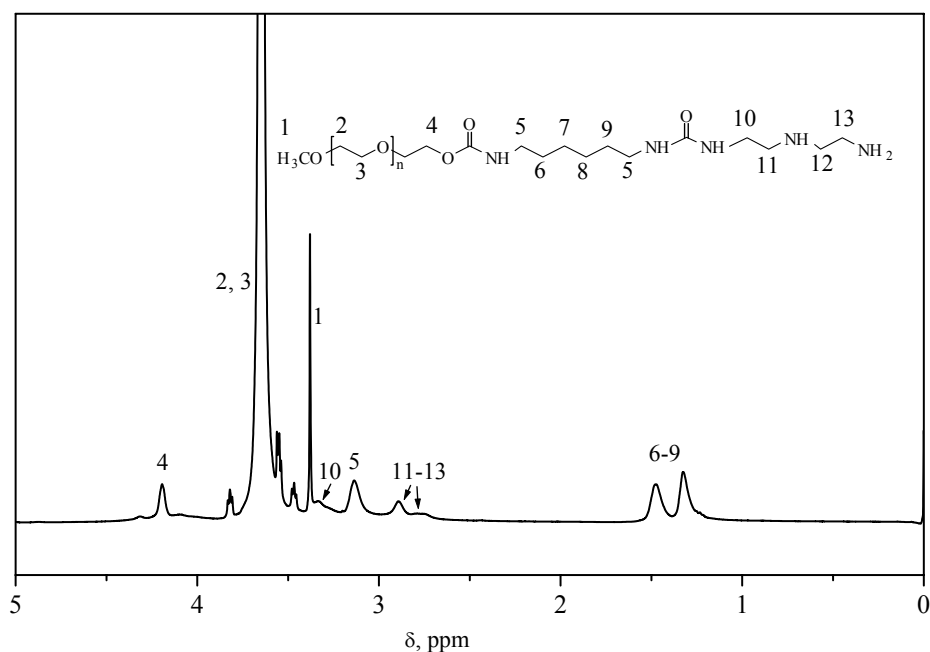


Figure 3.2.6. <sup>1</sup>H-NMR spectrum in CDCl<sub>3</sub> of PEO2000-DETA

In the case of the synthesis of PEO-PEI-branched, the final molecular structure was predetermined by the composition of the reaction mixture. The polymers were designed to have two PEO chains grafted onto each PEI molecule. The PEI-branched molecules used had a molecular weight of 423 g/mol. <sup>13</sup>C-NMR spectroscopy was used to confirm the branched structure and to estimate the average number of secondary and primary amino groups (Appendix 1). Also in this case, the disappearance in the IR spectrum of the strong band of the NCO group confirmed the successful reaction, and the ratio of distinct signals from the two different units (PEO and PEI) in the <sup>1</sup>H-NMR spectrum was used to confirm the desired structure.

The most useful characterisation to show if the reaction in which a double molecular weight product is formed had occurred is SEC. This is important in the first step of the synthesis (NCO activation of PEO) as well as in the second step in the synthesis of PEO with a small amine. As can be seen in Figure 3.2.7, the formation of the double molecular weight product was completely suppressed by the chosen ratio of HMDI to PEO for all PEO molecular weight.

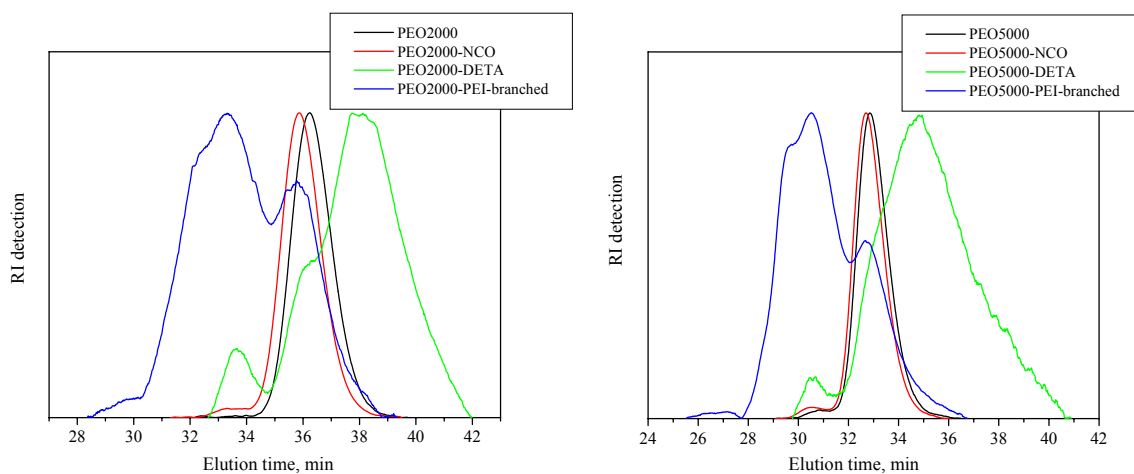


Figure 3.2.7. SEC elution curves of PEO-NCO, PEO-DETA and PEO-PEI-branched and the corresponding PEO of molecular weight of 2000 or 5000 g/mol

In the second step (coupling to the amine molecule), however, a small amount of by-product with a double molecular weight was formed in both cases, as can be seen from the appearance of a small second peak at low elution volume. However, the relative abundance of the by-product is not high. The crucial point to avoid the formation of this by-product is the ratio of the reactants. All the ratios tried smaller than the one here applied (mole excess of the amine of 100) resulted in either exclusively the double molecular weight product or this product was formed in much greater amounts than was the case with the here chosen ratio. What is also striking in the elution curves of the PEOs modified with a small amine is the strong shift towards high elution volumes, indicating a strong adsorption of the polymer on the columns. This behaviour has already been observed for PEO-*b*-PEI and the same explanation could be applied in this case, although here it is more pronounced. The polydispersity of the PEO-PEI-branched is broad and heterogeneity in the structure is very likely. The SEC elution curves of the PEO-PEI-branched samples show, in addition to the main peak corresponding to the desired product, a small peak with a position close to that of the starting polymer and a shoulder in the high molecular weight region. Structures such as PEO-PEI-branched with only one PEO branch or with more than two branches can not be excluded. However, the main product is obviously the one with two branches, as was designed in the recipe.

Under the applied reaction conditions, it was not possible to obtain PEO modified with small amine without a large presence of the by-product from PEO of a molecular weight of 1100 g/mol. Since in the case of this polymer the reaction to obtain PEO-PEI-branched was also unsuccessful, it could be concluded that the NCO activation was not performed successfully. However, SEC as well as  $^1\text{H-NMR}$  analysis of PEO1100-NCO gave the expected results and confirmed the successful NCO-functionalisation of PEO1100. The reason for this undesirable behaviour is probably due to the very low stability of PEO1100-NCO connected with the greater reactivity of the shorter polymer.

The main characterisation results of all the synthesized polymers are summarised in Table 3.2.2.

Table 3.2.2. The main characteristics of PEO-DETA, PEO-PEHA and PEO-PEI-branched polymers

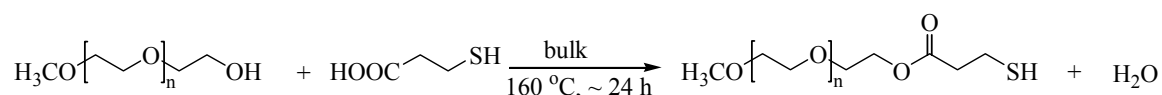
| Polymer              | $M_{\text{theor}}$ , g/mol | $M_p^{\text{a)}$ , g/mol | $PI^{\text{a)}$ | n(PEO) | $N_{\text{amino groups}}^{\text{b)}$ |
|----------------------|----------------------------|--------------------------|-----------------|--------|--------------------------------------|
| PEO5000              | 5000                       | 4923                     | 1.06            |        |                                      |
| PEO5000-NCO          | 5168                       | 5211                     | 1.08            |        |                                      |
| PEO5000-DETA         | 5751                       | 3045                     | 1.30            | 112    | 2                                    |
| PEO5000-PEHA         | 5400                       | 4886                     | 1.20            |        | 5                                    |
| PEO5000-PEI-branched | 10759                      | 12330                    | 1.38            |        | 6                                    |
| PEO2000              | 2000                       | 1992                     | 1.04            |        |                                      |
| PEO2000-NCO          | 2168                       | 2195                     | 1.06            |        |                                      |
| PEO2000-DETA         | 2271                       | 1242                     | 1.15            | 44     | 2                                    |
| PEO2000-PEHA         | 2400                       | 2112                     | 1.10            |        | 5                                    |
| PEO2000-PEI-branched | 4759                       | 4370                     | 1.34            |        | 6                                    |
| PEO1100              | 1100                       | 1151                     | 1.04            |        |                                      |
| PEO1100-NCO          | 1268                       | 1428                     | 1.06            |        |                                      |
| PEO1100-DETA         | 1371                       | 2727/1213 <sup>c)</sup>  |                 | 23     | 2                                    |
| PEO1100-PEHA         | 1500                       | 2542/1340 <sup>c)</sup>  |                 |        | 5                                    |
| PEO1100-PEI-branched | 2959                       | 2772/1242 <sup>c)</sup>  |                 |        | 6                                    |

a)  $M_p$  and  $PI$  are the molecular weight from the peak maximum and polydispersity index from SEC measurements in DMF at 70 °C, respectively; b) theoretical number of secondary and primary amino groups; c)  $M_p$  of both peaks appearing in the SEC elution curves

### 3.2.3 Poly(ethylene oxide) with SH end groups obtained via esterification with mercaptopropionic acid

Mercapto groups are widely used as anchoring/binding groups in the synthesis of nanoparticles, as well as in ligand exchange experiments. The potential of mercapto-functionalised PEO is very high as mercapto group containing molecules are not only used in the functionalisation of Cd-based nanoparticles, but also in other systems, especially gold nanoparticles.<sup>93,94</sup> In order to obtain SH functionality on the chain end of PEO, a simple approach, consisting of the esterification of the OH end group of PEOs using mercaptopropionic acid (MPA), was employed. The OH end functionality is easy to obtain at one end of the PEO chains, while the other chain end can be kept protected during anionic polymerisation. In this way, this type of functionalisation opens new routes for further functionalisation of the protected chain end of PEO. To prove the concept of SH functionalisation via esterification, in this study commercial PEOs with an OH group at one chain end were used, while the other end was a simple methylether group.

Three PEOs of different molecular weight were functionalised following the same simple reaction scheme:



Scheme 3.2.4. Synthesis of PEO-SH via esterification with mercaptopropionic acid

The SEC elution curves obtained after esterification and purification of the polymers show the expected trends (Figure 3.2.8).

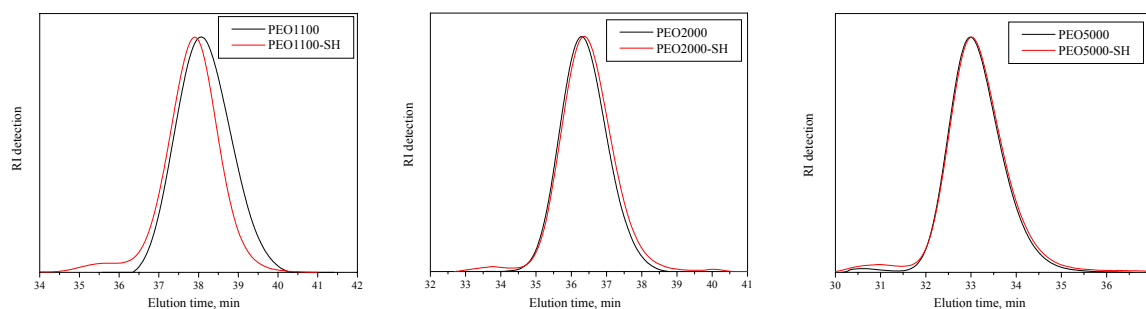
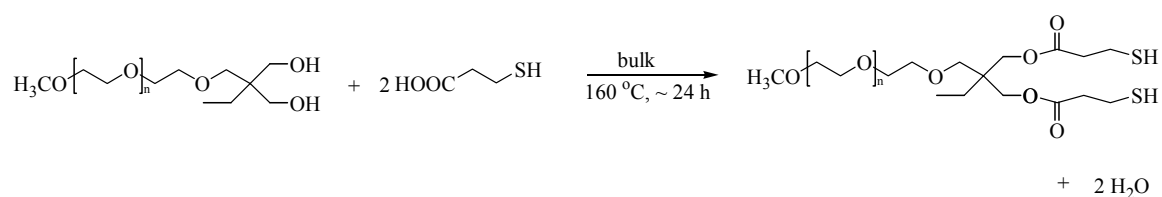


Figure 3.2.8. SEC elution curves obtained in DMF at 70 °C of the PEO-SH polymers

A small shift toward shorter elution times (higher molecular weights) was observed. This shift was smaller for higher molecular weights of the starting PEO, as expected from the relative increase of the molecular weight.

The synthesis and the application of PEO modified with two SH groups, in analogy to the frequently used bidentate dihydrolipoic acid, for the stabilisation and transfer of nanoparticles to an aqueous environment has already been reported.<sup>41</sup> In order to obtain PEO with two SH binding groups, the authors used a tentative three-step procedure. Here a simple method to obtain a polymer with two SH binding groups at the end of the chain by esterification with MPA is presented. A commercial PEO polymer from the Degussa Company with two hydroxyl groups was used and the same chemistry as in the previous case was applied. The chemical structure of the starting polymer and of the obtained PEO with two SH groups are presented in Scheme 3.2.5.



Scheme 3.2.5. Reaction scheme for the synthesis of PEO-(SH)<sub>2</sub>

As in the case of PEOs with one OH group, also here SEC showed that the molecular weight was shifted towards higher values, while the polydispersity was not affected, which was to be expected (Table 3.2.3.).

All the functionalised polymers were characterised by <sup>1</sup>H-NMR spectroscopy, whereby the ratio of the signals of the methylene groups from the PEO moiety at 3.65 ppm and the

methylene groups next to the formed ester bond at 4.27 ppm enabled the quantification of the functionalisation of the polymers. As an example, the  $^1\text{H-NMR}$  spectrum of PEO2000-SH is presented in Figure 3.2.9. Calculated from  $^1\text{H-NMR}$  spectra, the functionalisation was complete in all cases, except in the case of PEO1100 (86%).

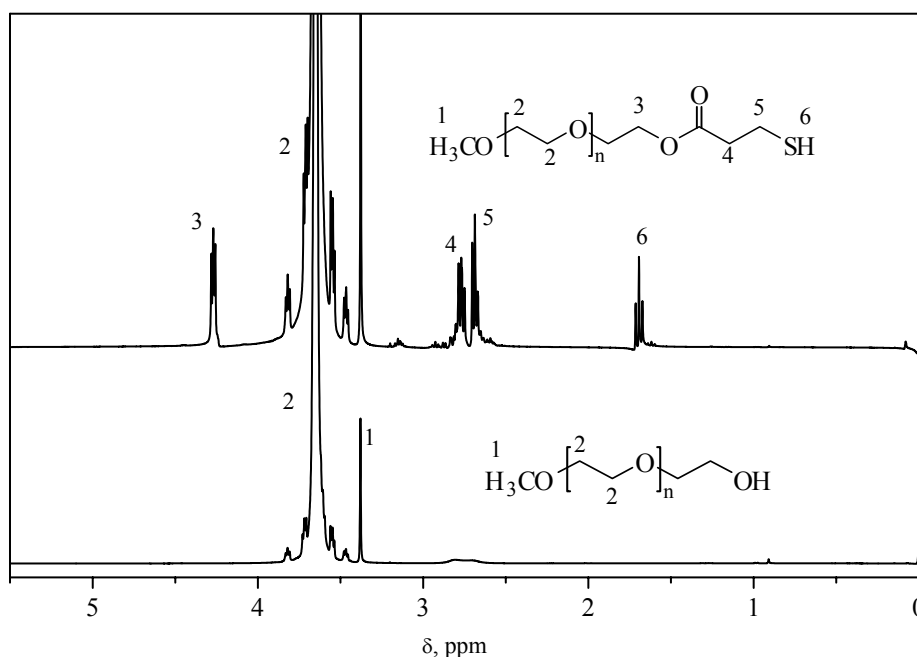


Figure 3.2.9.  $^1\text{H-NMR}$  spectra in  $\text{CDCl}_3$  of the starting PEO2000 and the obtained PEO2000-SH polymers

The main characteristics of the SH-functionalised PEOs are summarised in Table 3.2.3.

Table 3.2.3. The main characteristics of the obtained PEO-SH polymers

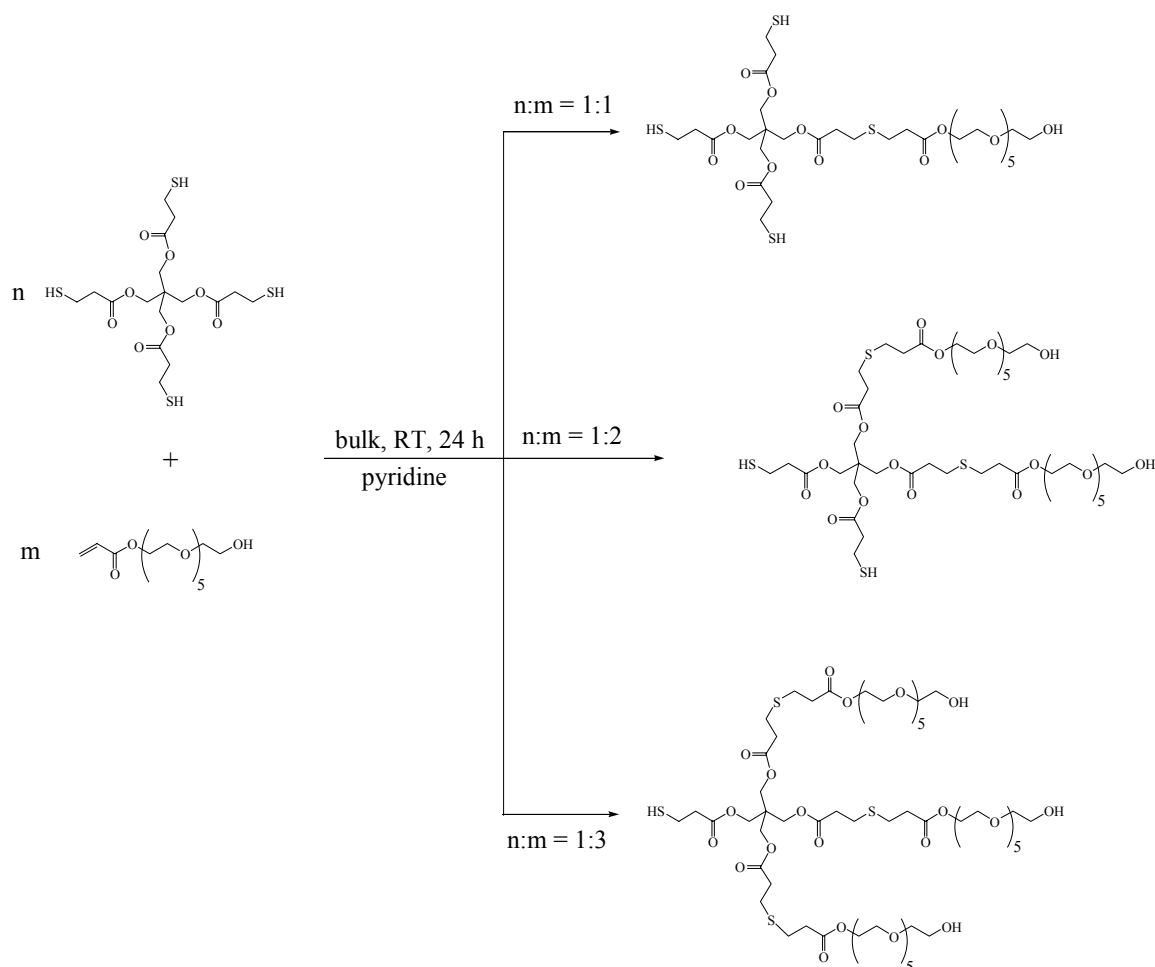
| Polymer                   | $M_{\text{theor}}$ , g/mol | $M_p$ , g/mol <sup>a)</sup> | $PI$ <sup>a)</sup> | n(PEO) | $N(\text{SH})$ <sup>b)</sup> |
|---------------------------|----------------------------|-----------------------------|--------------------|--------|------------------------------|
| PEO1100-SH                | 1228                       | 1227                        | 1.07               | 23     | 1                            |
| PEO2000-SH                | 2128                       | 1929                        | 1.04               | 44     | 1                            |
| PEO5000-SH                | 5128                       | 4812                        | 1.06               | 112    | 1                            |
| PEO1200-(SH) <sub>2</sub> | 1456                       | 1465                        | 1.08               | 23     | 2                            |

a)  $M_p$  and  $PI$  are the molecular weight from the peak maximum and polydispersity index from SEC measurements in DMF at 70 °C, respectively; b) theoretical number of mercapto groups at the end of the polymer chain

### 3.2.4 Poly(ethylene oxide) with SH end groups obtained via the Michael type addition reaction

In order to produce PEO molecules having one or more SH groups, a Michael type addition was used. This type of reaction (conjugate addition reaction between electron-poor olefins and nucleophiles, such as thiols) has already been used for the conjugation of peptides<sup>95</sup> to polymeric substrates and in the production of degradable bifunctional polymer networks for tissue engineering and control release.<sup>96,97</sup> It has also found application in the functionalisation of polymers,<sup>98</sup> as well as surface functionalisation.<sup>99</sup> There are a number of strong points which recommend the employment of this reaction: mild character and high yield; tolerance to a wide range of functional groups, avoiding protection/deprotection steps; no necessity for a metal catalyst.

In the framework of this study, the reaction between a molecule with four SH groups (pentaerythritol tetrakis(3-mercaptopropionate)) and poly(ethylene oxide) with an acrylate end group was performed. Since the employed PEO possessed an  $\omega$ -hydroxyl group which does not interfere with the actual reaction, the thus obtained ligands, in addition to a binding group, would possess a suitable functional group for further functionalisation either before or after ligand exchange. The number of PEO branches can be varied by varying the composition of the reaction mixture. The reaction pathway is shown in Scheme 3.2.6.



Scheme 3.2.6. Synthesis of (PEO)<sub>x</sub>-(SH)<sub>y</sub> molecules via a Michael type addition

This type of reaction is catalysed by electron-donor compounds and in this case pyridine was chosen as the catalyst. The amount of catalyst required for a successful functionalisation was investigated.

The reaction could be followed by IR spectroscopy by monitoring the disappearance of the absorption peaks of the carbon-carbon double bond at 1636 and 1620 cm<sup>-1</sup> and the out of plane stretch at 810 cm<sup>-1</sup>. In Figure 3.2.10, the FT-IR spectra of the starting PEO with an acrylate group and the spectra of the samples taken after 6.5 and 24 h of reaction are presented. The reaction was performed with 1 equivalent of pyridine and the ratio of the reactants was chosen to produce a molecule with two PEO branches.

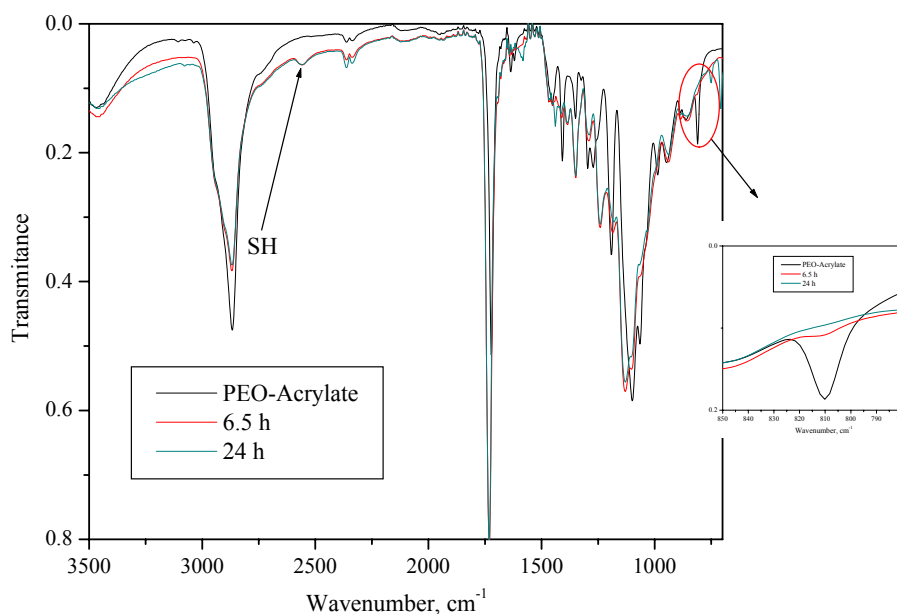


Figure 3.2.10. FT-IR spectra of the starting PEO-Acrylate and of the samples taken during the reaction with pentaerythritol tetrakis(3-mercaptopropionate)

According to the complete disappearance of the band at 810 cm<sup>-1</sup> from the FT-IR spectra, it could be concluded that the reaction was completed after 24 h. However, after inspection of the <sup>1</sup>H-NMR spectra, some residual acrylate groups could still be observed, although in the small amount of 1 %. Identical results were obtained for the synthesis of the molecule with three PEO branches (2 % of unreacted acrylate groups after 24 h of reaction). The amount of catalyst was then increased to 2 and 5 equivalents and the reaction time was set at 24 h. As confirmed from the <sup>1</sup>H-NMR spectra, the conversion of the acrylate group was complete after 24 h of reaction, with both 2 and 5 equivalents of the catalyst. As an example, the <sup>1</sup>H-NMR spectra of PEO-Acrylate and the product obtained in the reaction with 5 equivalents of pyridine are shown in Figure 3.2.11.

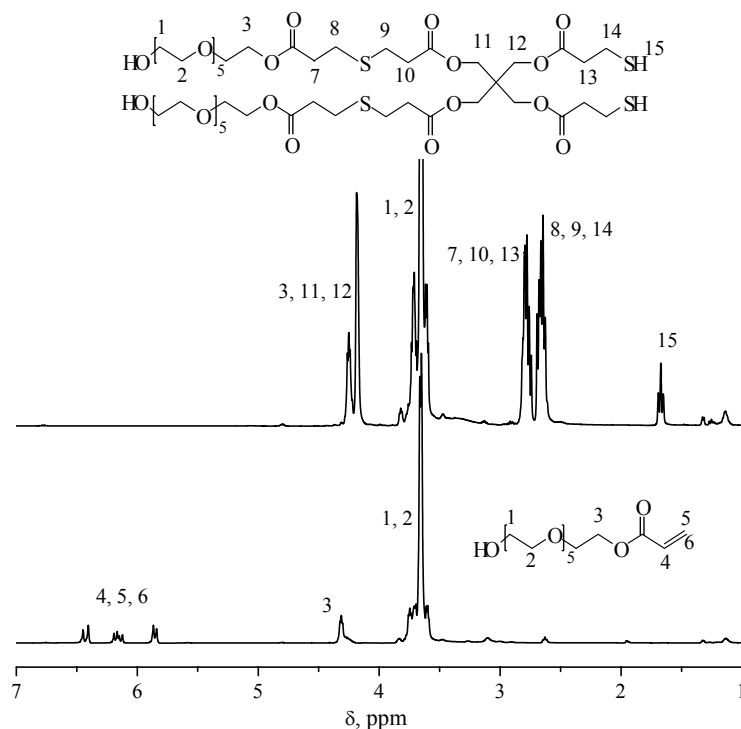


Figure 3.2.11.  $^1\text{H}$ -NMR spectra in  $\text{CDCl}_3$  of the starting PEO-Acrylate and the obtained  $(\text{PEO})_2\text{-SH}_2$

The length of the PEO, which was relatively small, allowed the direct calculation of the number of SH groups from the strong signal at 1.67 ppm arising from the proton in the mercapto group.

The final reaction conditions were set to be 24 h with 2 equivalents of the pyridine. Molecules with one, two and three PEO branches and consequently three, two and one SH groups, respectively, were synthesized. From the SEC curves presented in Figure 3.2.12, the trend of increasing molecular weight in the series with increasing number of PEO branches is clearly observed. The polydispersity of the samples increases with increasing molecular weight. This fact, as well as the asymmetry of the signals in the SEC elution curves could be the consequence of the formation of molecules having more or less PEO branches than was predetermined by the composition of the reaction mixture.

However, the increase of  $M_p$  in the series indicates that the desired product was the main product in the mixture.

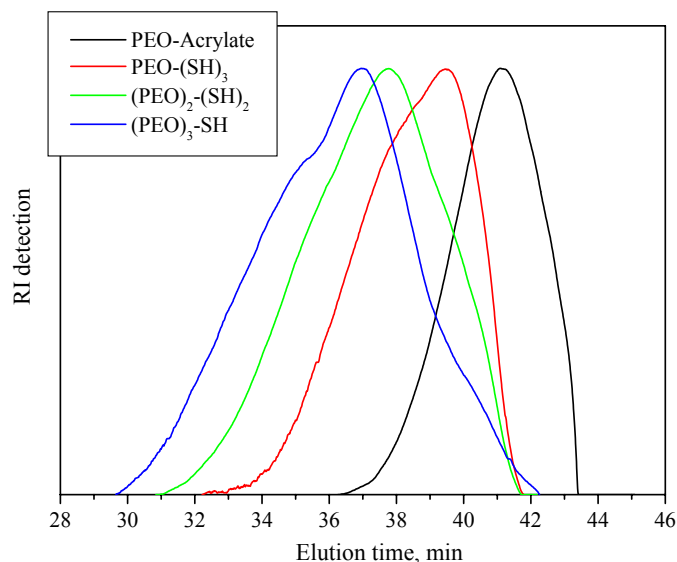


Figure 3.2.12. SEC elution curves obtained in DMF at 70 °C of PEO-Acrylate and PEO-SH polymers

The main properties determined from the SEC elution curves and the  $^1\text{H-NMR}$  spectra of the synthesised ligands are summarised in Table 3.2.4.

Table 3.2.4. The main characteristics of PEO-SH polymers synthesised via Michael type addition reaction

| Polymer                               | $M_{\text{theor}}$ , g/mol | $M_p^{\text{a)}$ , g/mol | $PI^{\text{a)}$ | $N(\text{SH})^{\text{b)}$ |
|---------------------------------------|----------------------------|--------------------------|-----------------|---------------------------|
| PEO-Acrylate                          | 336                        | 492                      | 1.12            |                           |
| PEO-(SH) <sub>3</sub>                 | 785                        | 727                      | 1.19            | 3                         |
| (PEO) <sub>2</sub> -(SH) <sub>2</sub> | 1161                       | 1151                     | 1.37            | 2                         |
| (PEO) <sub>3</sub> -SH                | 1497                       | 1448                     | 1.51            | 1                         |

a)  $M_p$  and  $PI$  are the molecular weight from the peak maximum and polydispersity index from SEC measurements in DMF at 70 °C, respectively; b) determined from  $^1\text{H-NMR}$  spectra

### **3.3 Ligand exchange with amino-functionalised poly(ethylene oxide)s**

#### **3.3.1 Ligand exchange with mono-amino poly(ethylene oxide), PEO-NH<sub>2</sub>**

In the hitherto developed ligand exchange reactions for the phase transfer of nanoparticles, usually small molecules were used with a suitable functionality for binding to the nanoparticle surface on the one end of the molecule and a functionality for providing water solubility on the other end. In the present approach, instead of a single functional group (such as  $-\text{OH}$  or  $-\text{COO}^-$ ), the poly(ethylene oxide), PEO, chain attached to the nanoparticle surface should serve to render the nanoparticles water-soluble. Water is a very good solvent for PEO due to hydrogen bonding between the water molecules and the oxygen atoms in the polymer backbone. In a broader context, PEO is not a strongly interacting polymer. Its inertness accounts for its wide use for surface treatment to provide biocompatibility since surfaces covered with PEO have proven to be non-immunogenic, non-antigenic and protein resistant. In order to be used for changing the solubility of nanoparticles it must be properly functionalised. One of the hitherto employed functional groups which are known to interact with the surface of nanoparticles, i.e.,  $-\text{NH}_2$ ,  $-\text{SH}$ ,  $-\text{COOH}$ , should be a part of the PEO molecule. Amino groups are known to interact strongly with Cd sites<sup>110</sup> on the nanoparticle surface, and it was shown that amines used in the post-synthetic treatment of nanoparticles can improve, in some cases, the luminescent properties.<sup>101</sup> Poly(ethylene oxide) bearing one amino group at the end of the polymer chain, PEO-NH<sub>2</sub>, with the structure shown in Figure 3.3.1, was used as a ligand model to prove the feasibility of the idea.

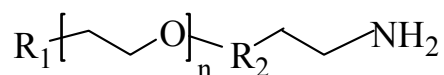


Figure 3.3.1. Structural formula of the mono-amino PEOs (PEO500-NH<sub>2</sub>: R<sub>1</sub> ≡ CH<sub>3</sub>, R<sub>2</sub> ≡ CH<sub>2</sub>CH<sub>2</sub>O; PEO2400-NH<sub>2</sub> and PEO3200-NH<sub>2</sub>: R<sub>1</sub> ≡ CH<sub>2</sub>CH<sub>2</sub>OSi(CH<sub>3</sub>)<sub>3</sub>, R<sub>2</sub> ≡ C<sub>6</sub>H<sub>4</sub>; the numbers in the abbreviations represent the molecular weight of the PEO

A simple experiment was performed by mixing chloroform solutions of nanoparticles and mono-amino PEO, in which the nanoparticles were exposed to the new potential ligands, while the old one were still present in the solution. After evaporation of the solvent from the chloroform solution containing nanoparticles and PEO-NH<sub>2</sub>, the obtained solid was soluble in methanol, which is a non-solvent for nanoparticles covered with the TOP/TOPO ligands used as stabilizing agents in their synthesis. In a control experiment where only poly(ethylene oxide) dimethyl ether was used, the addition of methanol caused the agglomeration of the nanoparticles. This showed that the amino groups attached themselves to the nanoparticles to an extent high enough to maintain colloidal stability in a solvent for the new capping ligands. The absorption and luminescence spectra of the nanoparticles in chloroform and in methanol are shown in the Figure 3.3.2.

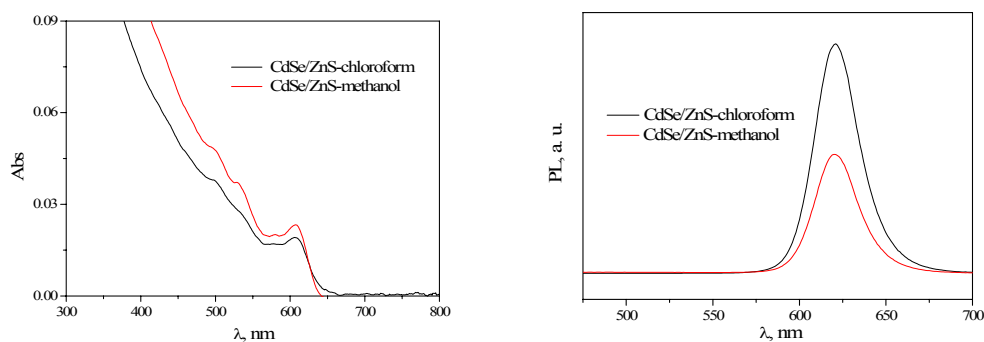


Figure 3.3.2. Absorption and luminescence spectra of CdSe/ZnS nanoparticles dispersed in chloroform (capped with TOP/TOPO) and methanol (capped with PEO2400-NH<sub>2</sub>)

The nanoparticles retain all their characteristic features in the absorption as well as in the emission spectra, although the luminescence efficiency in methanol was decreased.

Using the simple method described above, it was not possible to dissolve the nanoparticles in water. The possible reason could be an insufficient stabilization of the nanoparticles by a ligand having only one anchor group, which can alone form bonds with both the nanoparticles and the solvent. Increasing the number of binding groups should in this case improve the stability. The second reason can be the destabilising effect of the old ligands (TOP/TOPO), which are soluble in methanol but not in water, observed previously with some other systems dealing with ligand exchange.<sup>53</sup>

### 3.3.2 Ligand exchange with poly(ethylene oxide)-*b*-(ethylene imine), PEO-*b*-PEI

In order to obtain stable nanoparticle-polymer conjugates, polymers with multiple anchoring amino groups would be necessary. Polymers containing several secondary amino groups, poly(ethylene oxide)-*b*-(ethylene imine), were synthesised. The structural formula, with the characteristic block lengths of the polymers, is presented in Figure 3.3.3.

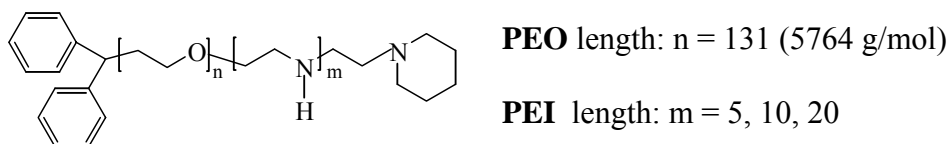


Figure 3.3.3. Structural formula of poly(ethylene oxide)-*b*-(ethylene imine), PEO-*b*-PEI

Since the very frequently employed method of direct phase transfer was not successful, a simple method using block copolymers, to transfer the nanoparticles into water was developed. The method consists of precipitation of the nanoparticles after the ligand exchange using a non-solvent for the new capping groups. When the nanoparticles are exposed to a large excess of the new ligands, ligand exchange occurs. As a method of separation from the old ligands and a proof of ligand exchange, a non-solvent for the new ligands should cause precipitation. As a non-solvent, hexane or cyclohexane (note that the nanoparticles covered with TOP/TOPO are soluble in hexane) could be used. After centrifuging, the obtained pellet was readily soluble in all solvents for the new capping

groups, including water. A control experiment was performed in which non-functionalised poly(ethylene oxide) was used. The addition of hexane to a chloroform solution containing nanoparticles and polymer resulted in precipitation of the polymer only, while the nanoparticles remained well dispersed in the chloroform/hexane mixture. This control test showed that ligand exchange had occurred when the block copolymer was used, excluding any possible agglomeration of the nanoparticles by the polymer itself.

This method was also efficient for the phase transfer of nanoparticles using the mono-amino PEOs, except the one with the lowest molecular weight (500 g/mol), probably because of the incomplete precipitation of the low molecular weight PEO. However, the aqueous solutions of nanoparticles with mono-amino PEOs were not colloidally stable for longer times; the nanoparticles precipitated in a few hours up to one day in the dark.

While the absorption properties of the nanoparticles were not altered by the ligand exchange and phase transfer, the luminescence was strongly affected. The luminescence intensities were measured to be less than 3 % for the nanoparticles in water, compared to Rodamine 6G in ethanol. In Figure 3.3.4, the luminescence intensities of water-soluble nanoparticles covered with PEO-*b*-PEIs, which were obtained with different polymer/nanoparticle ratios during the ligand exchange, are compared.

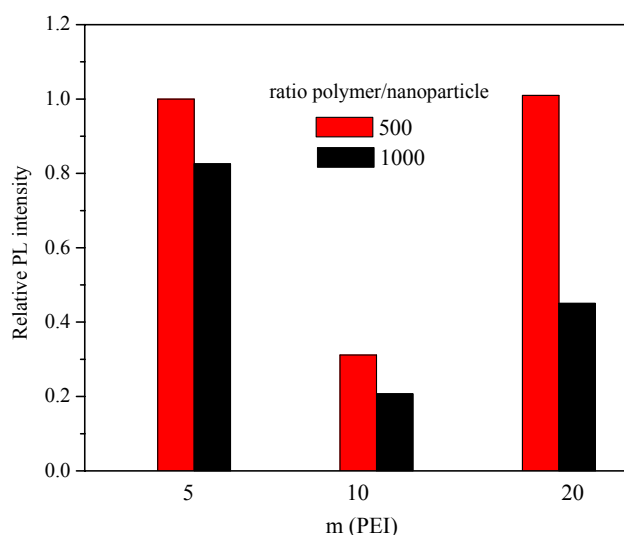


Figure 3.3.4. Relative PL intensities of CdSe/CdS nanoparticles in water stabilised with PEO-*b*-PEI polymers with different PEI lengths: 5, 10 and 20

It is noticeable that the PL intensities are higher when the polymer to nanoparticle ratio was smaller for all the three polymers used. The possible reason can be the agglomeration caused when the higher polymer/nanoparticle ratio was used. This assumption is strongly supported by the observation that agglomeration was observed even in chloroform with high amounts of the copolymer with 20 ethylene imine units. It was observed previously that the luminescence of nanoparticles decreased when large amounts of a diamine (ethylenediamine) were added to the solution, which was attributed to agglomeration caused by the bifunctional ligand.<sup>102</sup> Also, complete agglomeration was observed in attempts to perform ligand exchange with dendritic poly(amidoamine) molecules which contained 16 primary amino groups.<sup>103</sup> In order to avoid agglomeration, the number of amino binding groups had to be decreased by epoxidation. After transfer to water with the ratios presented in Figure 3.3.4, some precipitation also occurred, so that the nanoparticle solution had to be separated by centrifuging. The second observation is that there is no proportionality in the change of the luminescence with increasing number of ethylene imine groups. The PL first decreased when the number of binding groups was increased from 5 to 10, which can be due to the presence of some agglomerates in the solution. With further increase in the number of binding groups, the PL increases, although agglomeration should be more pronounced. However, since the amount of agglomeration is not known, it is difficult to draw any conclusion as to the real reason for such behaviour of the PL.

The luminescence intensities of nanoparticles of two different sizes in chloroform and in water are compared in Figure 3.3.5.

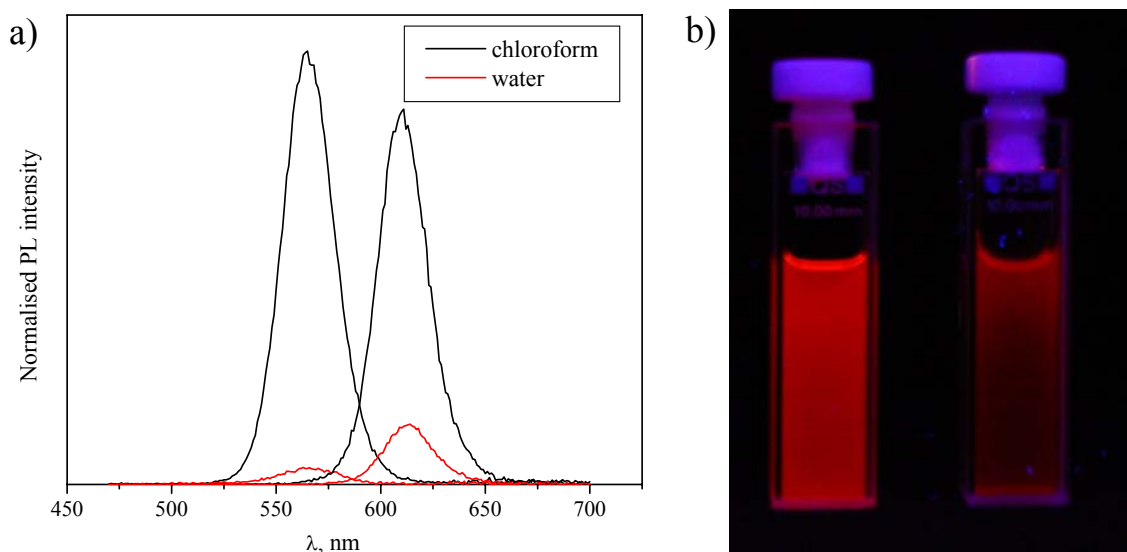


Figure 3.3.5. a) Change in the PL intensity of CdSe/CdS nanoparticles after transfer into water using a PEO-*b*-PEI with 5 PEI units; b) photograph of nanoparticles under illumination with a hand lamp in chloroform (left) stabilized with TOP/TOPO and in water (right) stabilized with PEO-*b*-PEI with 5 PEI units

The PL intensity of the smaller nanoparticles is much more reduced than that of the larger nanoparticles. Although a higher sensitivity of the smaller nanoparticles could be expected, because of their larger surface to volume ratio, agglomeration of the smaller nanoparticles caused by the polymer could also play a role. The second reason for the low PL efficiencies in both cases could be the high molecular weight of the polymers, which prevented higher grafting densities of the ligands and, consequently, good passivation of the nanoparticles could not be achieved.

The type of ligands, extent of surface coverage, as well as the solvent all have a profound effect on the luminescence properties of nanoparticles. In the following text an attempt to clarify the most important reasons for such low PL efficiencies is presented.

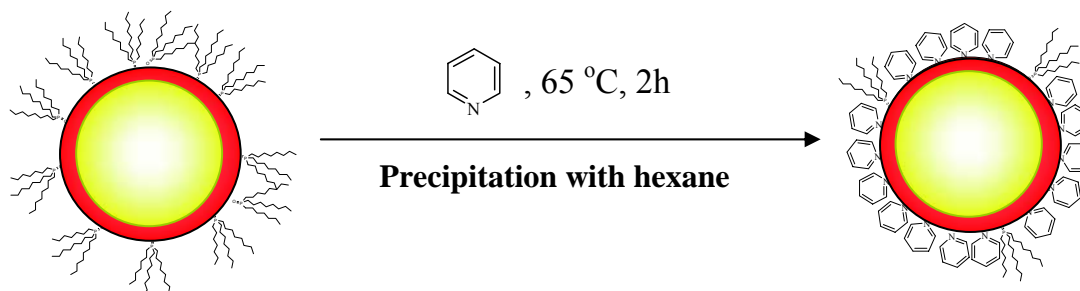
### **3.3.3 Changes in the luminescence efficiency due to ligand exchange and change of the medium**

The synthetic approaches employed nowadays for the synthesis of CdSe nanoparticles result in nanoparticles with high quantum yields due to their close to perfect structure with very few crystal defects, which could provide a pathway for the non-radiative recombination of the charge carriers. However, the processing of colloidal nanocrystals usually involves the manipulation of the monolayer of organic ligands at the surface and the surface environment of the nanoparticles. It was recognized that a change in the surface has little effect on the energetics of the radiative recombination, and that the main effect of such alterations is a change in the efficiency of luminescence.<sup>104</sup> This fact must be encountered, especially when ligand exchange and phase transfer processes are in question.

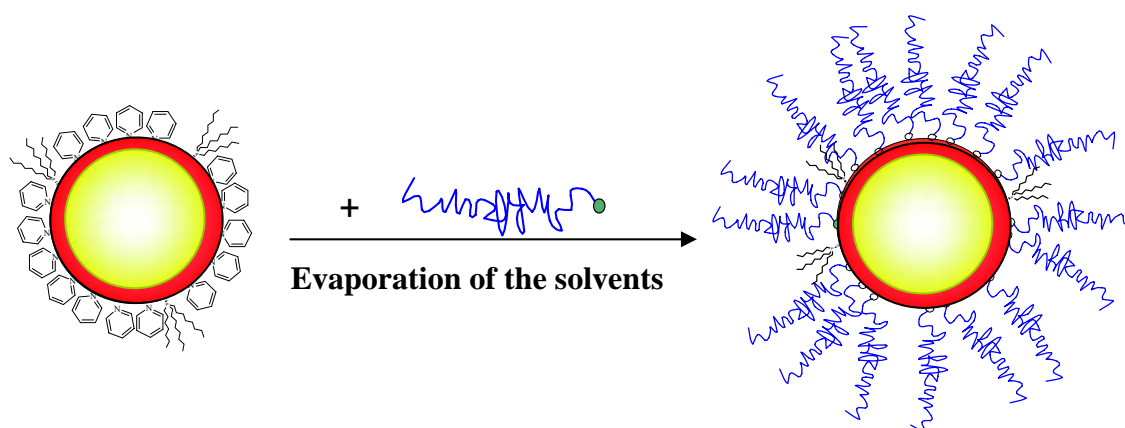
The influence of amino functionalities has been observed and investigated in a number of studies. The positive effect on the PL intensities of surface exchange with different amines has been reported for CdSe, as well as for some other semiconductor nanocrystals.<sup>101,105-107</sup> It was shown that the increase of the luminescence follows the trend: primary >> secondary > tertiary amines.<sup>105</sup> However, there are reports showing that the addition of *n*-butylamine to a nanoparticle solution quenches the luminescence.<sup>108,109</sup> Some authors experienced quite different behaviour from that previously reported for nanoparticles in the presence of *n*-butylamine and attributed the differences to the concentrations of the amine.<sup>110</sup> It was also found that the behaviour of nanoparticles in the presence of *n*-butylamine is strongly related to their size in certain nanoparticle size regimes.<sup>111-113</sup> It was also shown that, under certain conditions, controlled etching of CdSe nanocrystals is amine-assisted.<sup>114</sup> It is thus hard to predict the behaviour of a chosen system, especially when more complex systems, such as core/shell nanoparticles and long chain ligands, are involved. To investigate the influence of amino functionalities attached to a long polymer chain on the luminescence of nanocrystals involved in this study, ligand exchange experiments with polymeric ligands were performed and the changes in the luminescence intensities were followed. In order to avoid the influence of the ligands remaining from the synthesis (TOP/TOPO), first a ligand exchange with pyridine

molecules was performed. The weak bond which pyridine forms and the subsequent easy evaporation of the pyridine enable the nanoparticles to be exposed only to the ligand of interest with low as possible residue of the original ligands. The ligand exchange steps are schematically presented in Scheme 3.3.1.

a)



b)



Scheme 3.3.1. Schematic representation of the ligand exchange with a) pyridine and b) polymeric ligands

After the exchange with pyridine, a decrease in luminescence was observed, as reported previously for CdSe nanoparticles.<sup>5</sup> Evaporation of the pyridine in a nitrogen flow without the addition of the new ligands resulted in nanocrystals insoluble in chloroform. The loss of solubility indicates that the pyridine ligands can be easily removed from the nanoparticle surface, resulting in bare nanocrystals. A chloroform solution of different polymers in varying amounts was added to the nanoparticle solution in pyridine, and the

solvents were removed in a gas flow. The final result after four cycles of addition and evaporation of the chloroform was that the nanoparticles were stabilised almost exclusively with the ligand of choice. To check the influence of the primary amino group, hexadecylamine, HDA, was also used as a ligand. The luminescence efficiency changes of nanoparticles covered with different polymers, as well as HDA are presented in Figure 3.3.6.

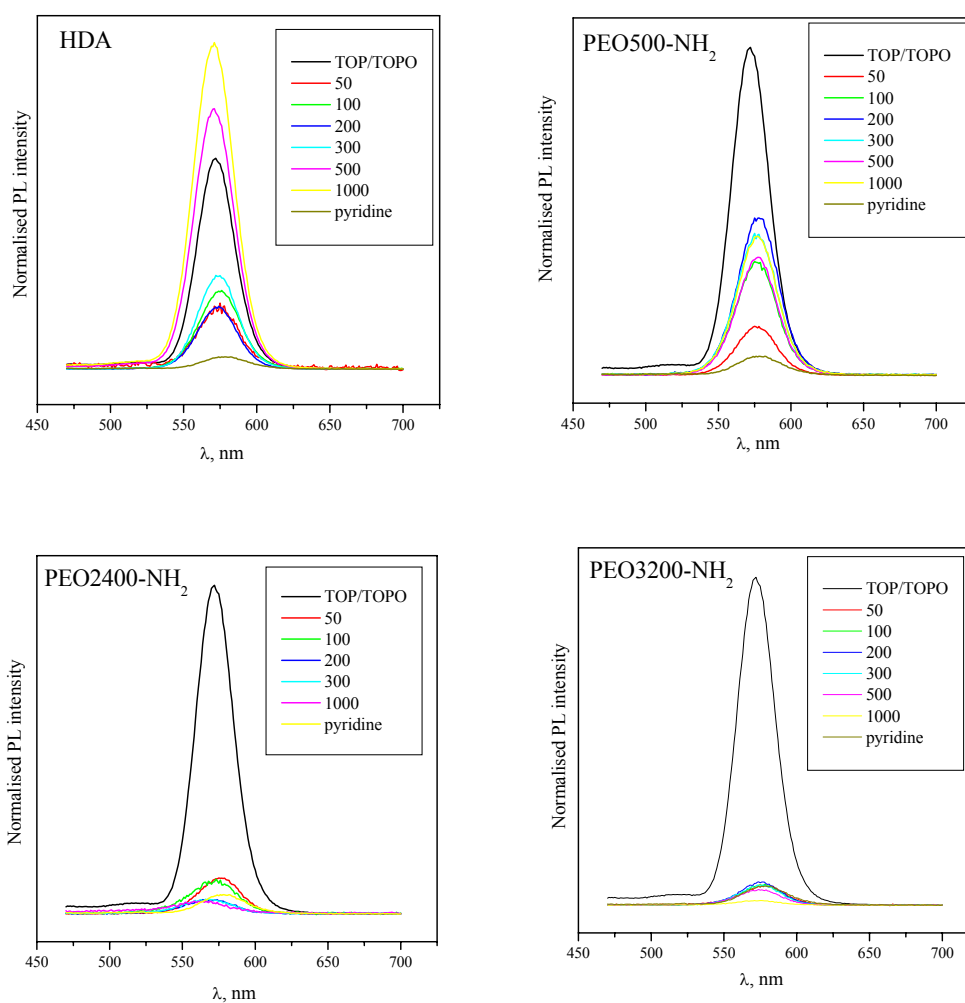


Figure 3.3.6. Changes in the luminescence intensities of CdSe/CdS nanoparticles dispersed in chloroform stabilised with TOP/TOPO, pyridine, HDA or polymeric ligands (the numbers indicate the ratio of HDA (or polymers) to nanoparticles)

The exchange of the pyridine with the HDA increases the luminescence almost proportionally to the amount of added ligand. For the higher ratios of HDA to nanoparticles (500 and 1000), this increase was so pronounced that the thus obtained nanoparticles had a higher PL intensity compared to the TOP/TOPO capped ones in chloroform. Increased luminescence compared to pyridine capped nanoparticles was also observed when PEO500-NH<sub>2</sub> was used as the ligand. The increase in luminescence was proportional to the amount of added polymer, or HDA for smaller ratios of polymer to nanoparticles and then it levelled off with further increase in the amount of ligand used in the case of PEO500-NH<sub>2</sub>, while it continued to increase in the case of HDA (Figure 3.3.7.).

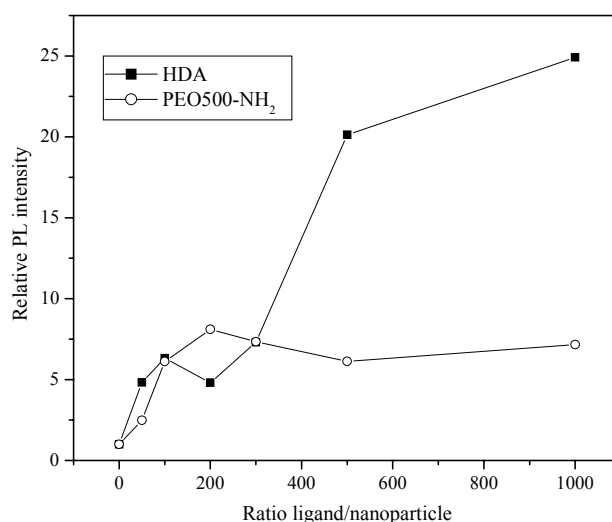


Figure 3.3.7. Relative increase in the PL intensity of CdSe/CdS nanoparticles after pyridine ligand exchange with HDA and PEO500-NH<sub>2</sub>

It could be argued at this point that the higher molecular weight ligands, due to the more difficult packing, cannot passivate the nanoparticles so efficiently as small molecules. The results presented previously concerning the insensitivity of the luminescence intensities on the molecular weight of the poly(*N,N*-dimethylaminoethyl methacrylate), PDMA, are not in accordance with the ones presented here.<sup>115</sup> However, since the binding groups in the case of PDMA are the side groups distributed along the polymer chain and

previous studies on polymers with binding side groups have shown that such polymers spread over the surface of the nanoparticles in order to maximise the number of contacts per polymer chain<sup>116</sup>, this difference can be attributed to the molecular structure with respect to the position of the binding groups. The trend of lower PL efficiency with increasing molecular weight was also observed when going from PEO500-NH<sub>2</sub> to PEO2400-NH<sub>2</sub> and PEO3200-NH<sub>2</sub>. There was not a large difference in the luminescence intensities between nanoparticles stabilized with PEO2400-NH<sub>2</sub> and PEO3200-NH<sub>2</sub>, probably due to the small relative increase in the molecular weight which cannot affect the difference in the conformation of the polymer chain significantly.

Taking into account this argumentation, it is to be expected that in the case of block copolymers, the luminescence intensities remain low due to the high molecular weight of these ligands (Figure 3.3.8.).

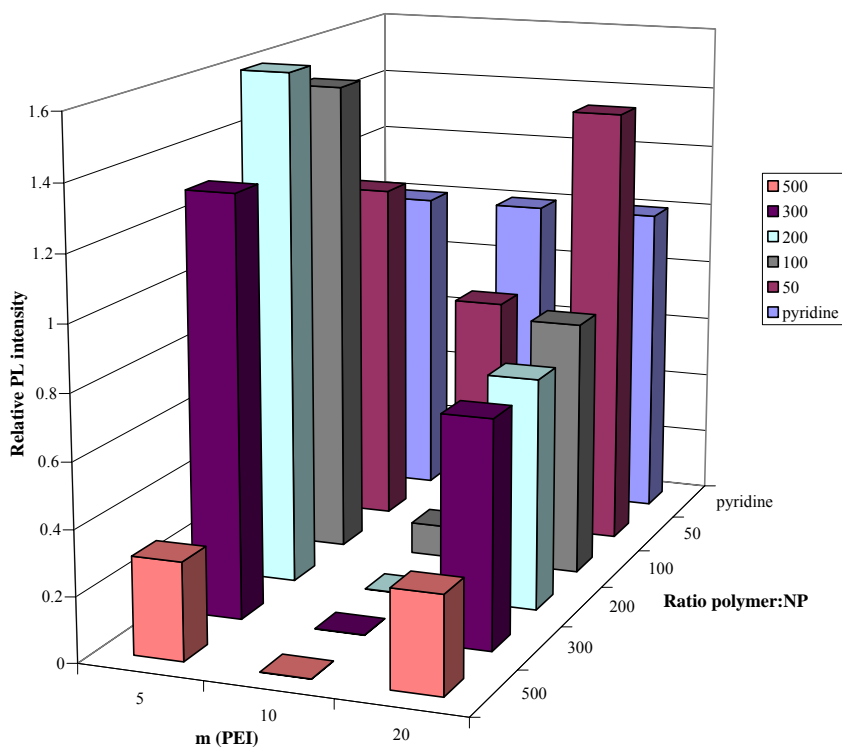


Figure 3.3.8. Comparison of the PL intensities of CdSe/CdS nanoparticles dispersed in pyridine and in chloroform stabilised with different block copolymers PEO-*b*-PEI after the pyridine/ligand exchange (the numbers indicate the ratio of copolymers to nanoparticles)

Only in the case of very low polymer/nanoparticle ratio are the luminescence intensities slightly higher compared to the pyridine covered nanoparticles, and that only for the copolymers with 5 and 20 EI moieties. This proves the potential of secondary amino groups compared to pyridine to increase the luminescence even at so low a content. However, the PL intensities are lower compared to nanoparticles stabilised with any of the mono-amino PEOs. It is not clear at this point whether this is an influence of the different type of binding groups or of the higher molecular weight of the copolymers compared to the mono-amino PEOs. With increasing polymer content, the luminescence decreased and was even quenched for very high amounts of polymer. Although no observable agglomeration was detected, it can not be excluded, which would be the explanation for the decrease of the PL intensities with higher contents of the polymer. No trend was observed in relation to the number of PEI units in the polymer chain. It remains unclear why the PL intensities are the lowest for almost all polymer/nanoparticle ratios for the copolymer with PEI block having 10 EI moieties.

To check the influence of the solvent on the luminescence efficiencies of the nanoparticles, a simple experiment was performed in which methanol was added successively to dilute the chloroform solution of nanoparticles and the changes in the luminescence were followed. The absorption and luminescence spectra were recorded after each addition of methanol. Two different nanoparticles were used: CdSe/CdS and CdSe/CdS/ZnS. In aging experiments performed on dilute solutions of nanoparticles, the observed decrease of the luminescence intensity with time was attributed to the desorption of ligands.<sup>105,107</sup> In some cases the addition of ligands resulted in a recovery and sometimes even improvement of the luminescence, which supports the hypothesis that ligand loss was the reason for the observed deterioration of the luminescence.<sup>107</sup> In order to check whether the applied extent of dilution could cause a loss of ligands, due to the increased solubility, and consequently a decrease in luminescence, in parallel with the dilution with methanol, the solution of nanoparticles was diluted to the same extent with chloroform. The luminescence spectra obtained after successive dilution with chloroform and methanol are presented in the Figure 3.3.9 and Figure 3.3.10, respectively, for CdSe/CdS and CdSe/CdS/ZnS nanoparticles.

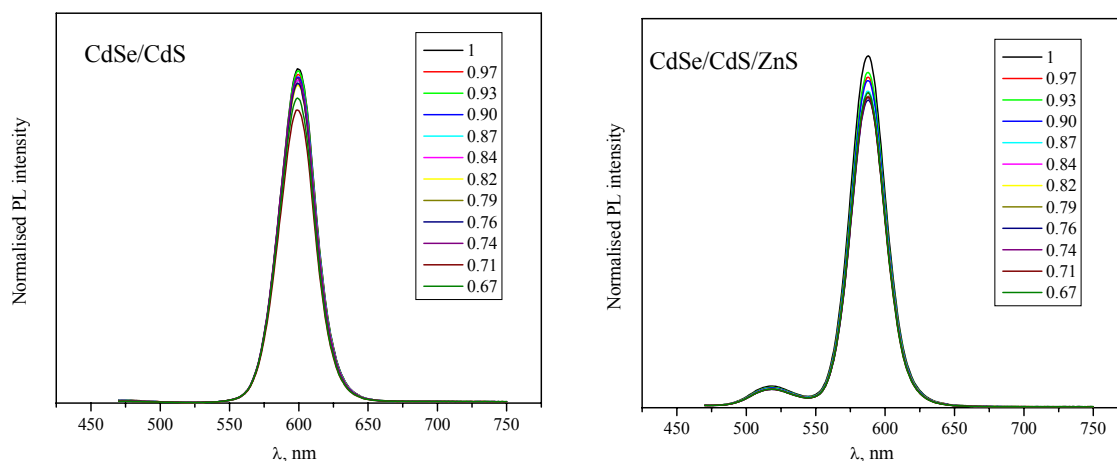


Figure 3.3.9. Changes in the PL intensity with dilution with chloroform; the numbers in the legend indicate the dilution factor ( $c/c_0$  with  $c$  the actual and  $c_0$  the initial concentration)

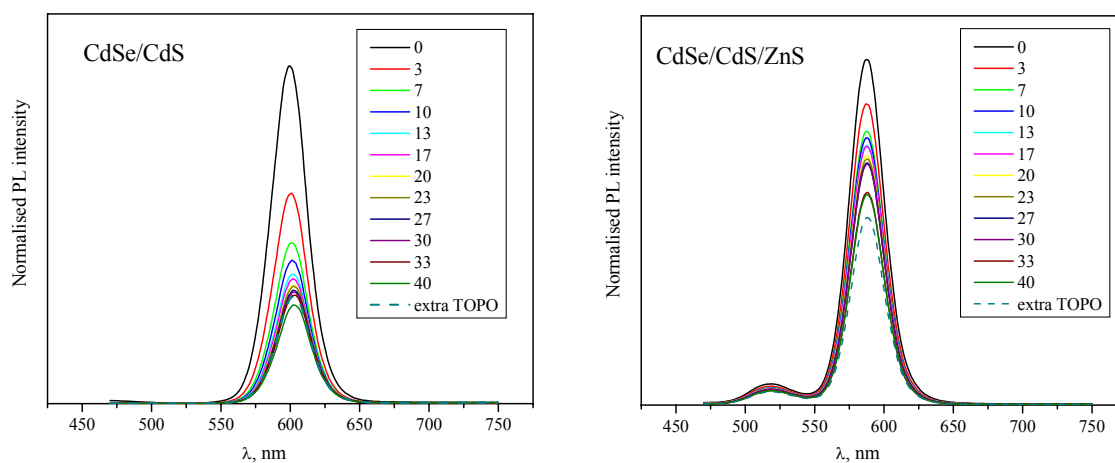


Figure 3.3.10. Changes in the PL intensity with dilution with methanol; the numbers in the legend indicate the vol. % of methanol in the chloroform/methanol mixture

The extent of the applied dilution with chloroform did not have a strong effect on the luminescence intensity of both types of nanoparticles. Some changes were observed, which however, can be attributed to experimental error. Thus, if any desorption of ligands did occur it was to an extent which did not have a significant effect on the PL efficiencies.

Dilution with methanol, however, had a more pronounced effect with both types of nanoparticles. Although methanol is a non-solvent for the nanoparticles, no precipitation was observed. As expected, the more robust CdSe/CdS/ZnS nanoparticles showed less sensitivity to the environmental changes. As previously suggested, an increased polarity of the solution and, consequently, the increased solubility of TOPO can cause desorption of the ligands, which results in a poorer passivation and lower PL efficiency.<sup>105</sup> However, the most pronounced drop in the luminescence was observed for a very low content of methanol (3 vol. %) and the further decrease in the luminescence was not so pronounced, even for very high contents of methanol. An attempt to recover the luminescence by the addition of TOPO molecules was not successful (dotted line in Figure 3.3.10). This leads to the conclusion that, in addition to changing the absorption of the ligands, solvents alone have an influence on the luminescence, by either binding to the free sites on the nanoparticle surface or changing the local dielectric constant of the surrounding medium. Murray et al. also attributed the inability to restore initial luminescence by the addition of HDA to nanoparticles purified in multiple washing steps with methanol, although some improvement was achieved, to the binding of methanol to the vacancies on the CdSe surface.<sup>107</sup>

When the experience gained in the above experiments is applied to a polymer-nanoparticle system, it is reasonable to expect that there would be a decrease in the luminescence in these systems, compared with the luminescence of fully passivated nanoparticles in apolar solvents, which is the usual luminescence value reported in the literature. The surface coverage when large and bulky molecule are used instead of small ones, and the change in the medium which promotes the solubility of the ligand and can have an effect on the luminescence alone, are both reasons to expect a decrease in luminescence of the nanoparticles after ligand exchange and phase transfer.

### 3.3.4 Ligand exchange with amino-functionalised PEOs with different architectures of the binding blocks

In order to obtain amino-functionalised PEOs with the possibility of easily changing the type of the binding group, a new synthetic strategy was developed. Using the isocyanate coupling reaction, PEOs with binding blocks of different architectures containing primary as well as secondary amino groups were synthesised. Binding blocks containing the amino functionalities: diethylenetriamine (DETA), pentaethylenhexamine (PEHA) and branched polyethyleneimine (PEI-branched) of low molecular weight (423 g/mol), were connected to PEOs of different molecular weights (2000 or 5000 g/mol). The structural formulas of the polymers are presented in Figure 3.3.11. In the case of the polymer with PEI as the binding block, the molecule was designed to have two PEO branches connected to the binding core (PEI).

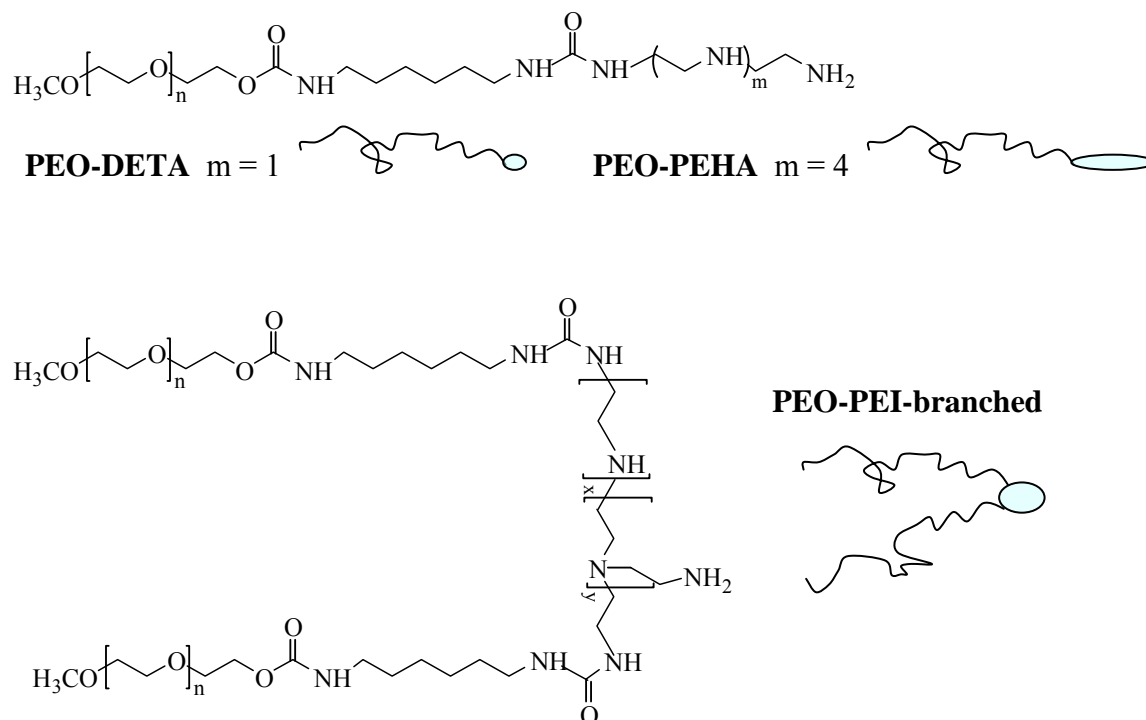


Figure 3.3.11. Structural formulas of the amino-functionalised PEOs synthesised using the diisocyanate coupling reaction

Transfer into water was achieved using the same procedure developed for the block copolymers: precipitation using a non-solvent for the PEOs. The nanoparticles could be

transferred into methanol as well as into water and the obtained concentrated solutions were stable for months when kept in the dark at room temperature. The luminescence efficiencies in methanol were generally higher than in water. This indicates that due to the formation of strong hydrogen bonds some loss of the ligand occurred in water. Compared to the PEO-*b*-PEI stabilized nanoparticles, the luminescence efficiencies in water were higher with all these PEO ligands. Although a thorough study was not performed and the molecular weights are not comparable, it can be indirectly concluded that the primary groups are a better choice than the secondary ones for the passivation of the nanoparticles. In Figure 3.3.12, the PL intensities of nanoparticles dispersed in water with different PEO ligands are compared with the PL intensity of the TOP/TOPO capped ones in chloroform.

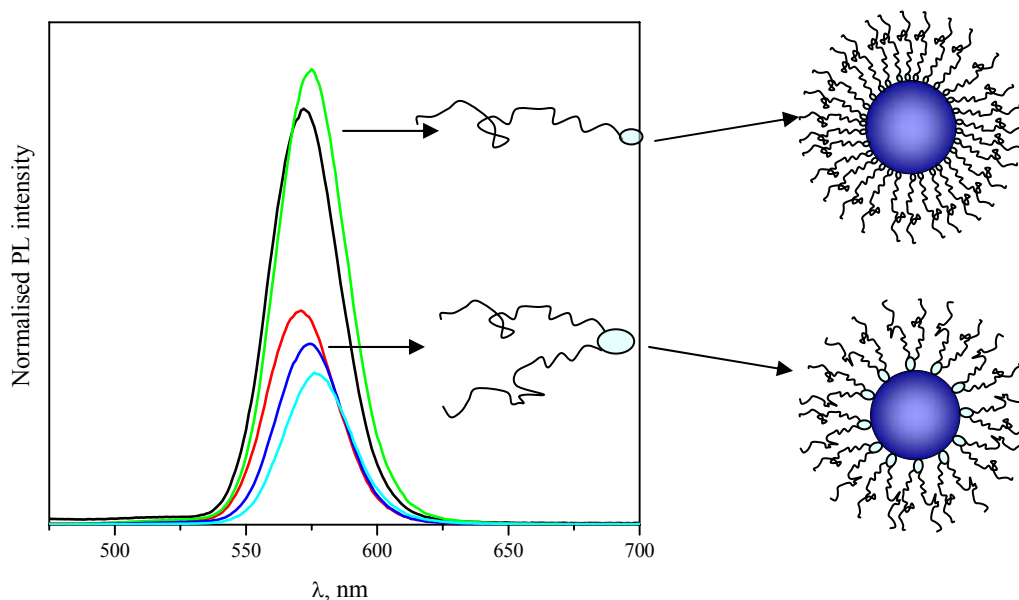


Figure 3.3.12. PL spectra of CdSe/CdS nanoparticles: — in chloroform and in water with, — PEO2000-PEI-branched, — PEO2000-DETA, — PEO5000-PEI-branched, and — PEO5000-DETA

Interestingly, luminescence efficiencies (up to 20 % reproducible for different batches of nanoparticles) as high as those for the TOP/TOPO capped nanoparticles in chloroform were observed for the nanoparticles in water covered with PEO of 2000 g/mol modified with diethylenetriamine. On the basis of the results of the ligand exchange experiments

performed with polymeric ligands and the influence of the solvent on the PL described in the previous section, it is surprising that luminescence efficiencies as high as those for nanoparticles covered with small molecules in chloroform were obtained. The slight PL intensity increase after ligand exchange with polymeric ligand is probably due to the poor surface passivation of the starting nanoparticle sample.<sup>117</sup> In order to promote mass driven ligand exchange, low as possible content of the original ligands is desired and, hence, all the samples were thoroughly washed before the ligand exchange procedure. At the same time, an almost linear dependence of the PL intensity on the polymer to nanoparticles ratio used in the ligand exchange procedure, was observed only in the case of the polymer with which the highest PL intensities in water were achieved. The influence of the polymer/nanoparticle ratio employed during ligand exchange on the PL for different polymeric ligands is presented in Figure 3.3.13.

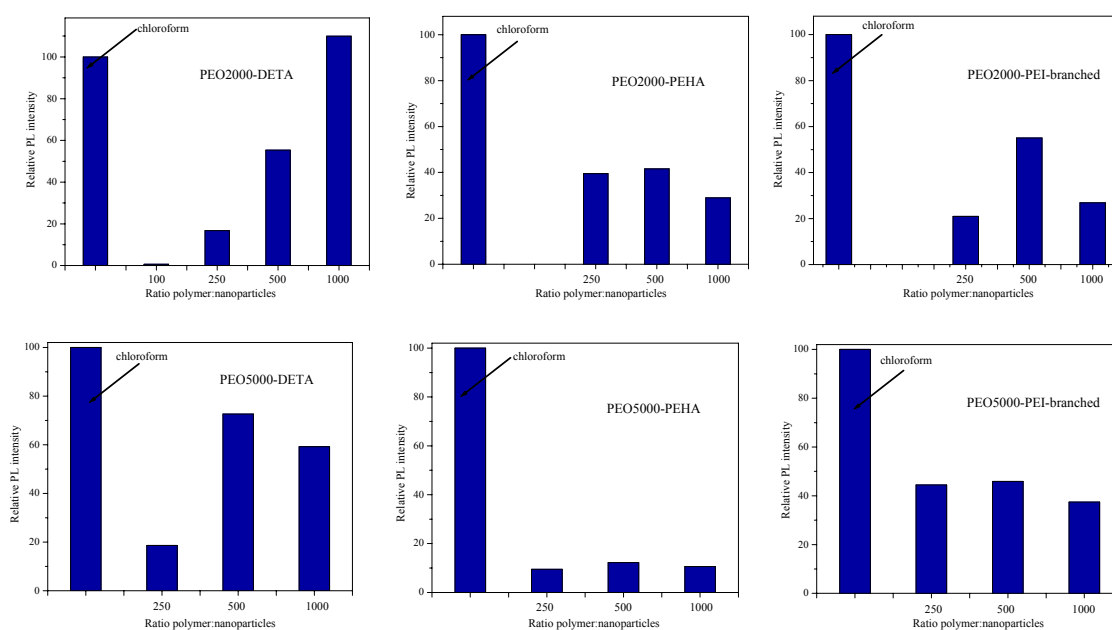


Figure 3.3.13. Relative PL intensities of CdSe/CdS nanoparticles dispersed in water as a function of the polymer/nanoparticle ratio employed during the ligand exchange

Except in the case of PEO2000-DETA, no dependence of the PL intensity on the polymer/nanoparticles ratio was observed. The dependence observed for the PEO2000-DETA ligand suggests that the PL intensity is directly related to the surface

coverage of the nanoparticles and that it is very high when high PL intensities are observed. In other cases, steric hindrance (bulky binding groups and high molecular weights) prevents high grafting densities to be achieved. This leaves the surface states unpassivated which allows the small molecules of polar solvents to approach the surface of the nanoparticles, thus also affecting the luminescence.

#### ***Influence of pH and increased ionic strength***

The most frequently used water soluble system obtained by the ligand exchange procedure is that in which the nanoparticles are stabilised with mercaptoacetic acid. However, these nanoparticles, which are electrostatically stabilised (by the repulsion of the charged  $\text{COO}^-$  groups), are very sensitive to changes in the pH of the medium and changes in the ionic strength. In this case, it is even impossible to obtain stable water solutions in the pH region below 7. The stability and luminescence efficiencies in solutions of different pH and ionic strength were investigated for nanoparticles stabilised with amino-functionalised PEOs.

In these cases, it was possible to obtain stable nanoparticle dispersions in solutions with pH as low as 4. In the course of a few weeks, however, the nanoparticles precipitated out of the solutions with low pH values (4-7), while maintaining their luminescence in the precipitate. The luminescence intensities of freshly prepared solutions of nanocrystals stabilised with amino-functionalised PEOs in buffer solutions of different pH values are compared in Figure 3.3.14.

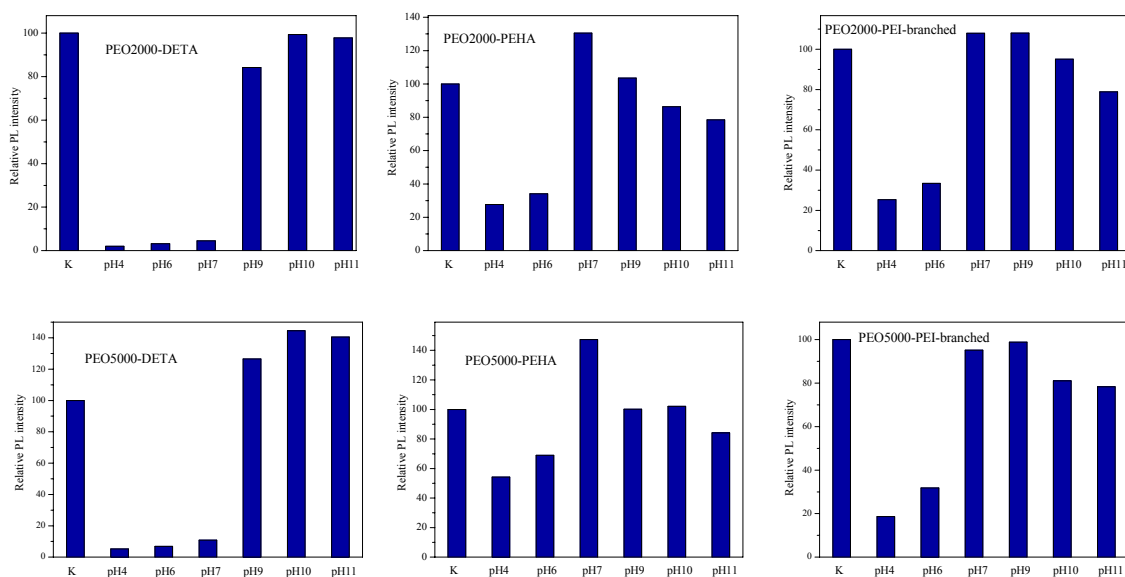


Figure 3.3.14. Relative PL intensities of nanoparticles dispersed in buffer solutions of a different pH

In the region of low pH values, the luminescence intensities were lower compared to the control sample in de-ionised water (K in the Figure 3.3.14). In the region of low pH values, ionisation of the amino group occurred and there were fewer amino groups with a free electron pair remaining for coordination to the Cd sites. The more amino groups are present in the binding unit (PEO-PEHA and PEO-PEI-branched), the less is the luminescence affected with increasing proton concentration. All the samples which showed a strong decrease in the luminescence intensity compared to the control sample precipitated after three weeks, while the samples in solutions of high pH values were stable for months. This experiment showed that amino-stabilised nanoparticles, although having a limited stability in low pH media, could be efficiently used as fluorescence probes in short-term experiments. For experiments where the pH value of the medium is low, the natural choice would be nanoparticles stabilised with ligands containing a binding group with a higher number of amino groups.

In addition to pH stability, the behaviour of nanoparticles capped with amino-functionalised PEOs in aqueous solutions of various ionic strengths was

investigated. Resistance to agglomeration in solutions of high ionic strength is important for the possible application of these nanoparticles in intracellular studies, where the ionic concentration is known to be high. Since PEO covered nanoparticles are not electrostatically stabilised colloids, increasing the ionic strength of the solution should not affect the colloidal stability. The colloidal stability, as well as the photoluminescence properties, were investigated by dispersing PEO stabilised nanoparticles in solutions of increasing concentration of NaCl, from 0.1 to 1 mol dm<sup>-3</sup>. Over this concentration range of NaCl, no agglomeration of the nanoparticles was observed and all the samples were stable for months. The changes in the luminescence properties with increasing ionic strength are presented in Figure 3.3.15.

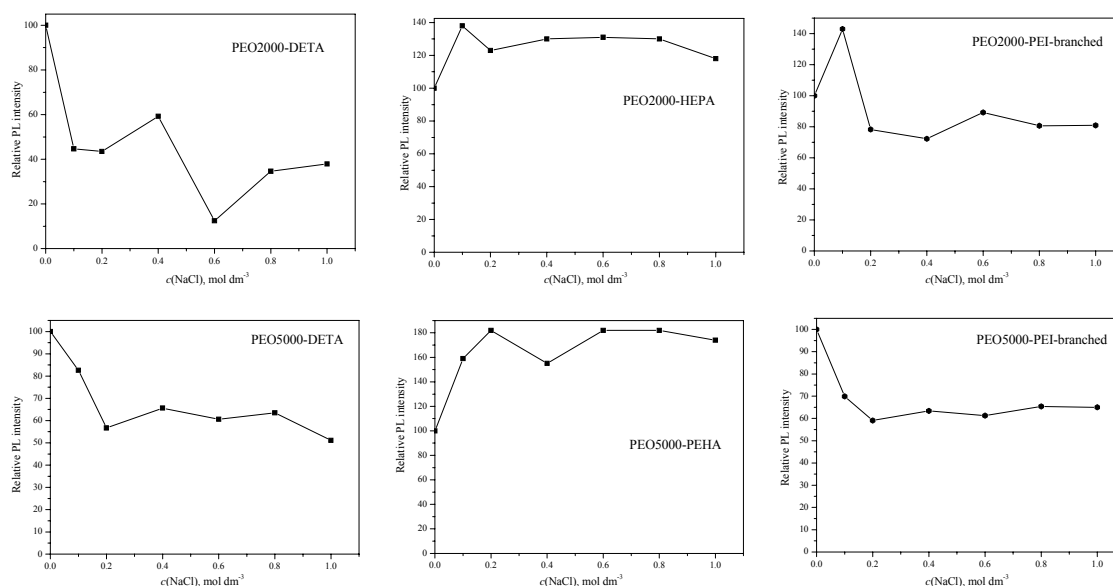


Figure 3.3.15. Relative PL intensities of CdSe/CdS nanoparticles dispersed in solutions of different monovalent salt concentrations

A decreasing tendency of the luminescence was observed in all cases, except when the polymer with five amino groups in the linear binding part was used as the stabilising ligand. It was shown that the chain conformation of PEO is not affected by ionic strength due to the absence of any interactions between the salt and PEO in pure water.<sup>117,118</sup> Thus, a change in the grafting density as a consequence of a change in the conformation of the

polymer is not to be expected. The reason for the decrease in the luminescence should be searched for in the direct effects that charged species have either on the binding group of the polymer or on the surface states of the nanoparticles. The presence of impurities of unknown origin is a probable reason for the different behaviour of PEO-PEHA capped nanoparticles. This ligand was synthesised using PEHA of technical grade and the low luminescence intensities of aqueous nanoparticles covered with this ligand are likely to be the result of the interaction of the impurities present with the nanoparticles. The increase in the luminescence upon the addition of salt indicates that the negative effect that these impurities have on the nanoparticles is somewhat screened. However, since the exact nature of the impurities is not known, speculation about the type of interactions which exist in the solutions with and without salt and possible further suppression of the negative effects which these impurities have on the PL of water soluble nanoparticles is difficult.

#### *Application of amino-functionalised PEOs for other types of nanoparticles*

The use of the developed amino-functionalised ligands and the method for ligand exchange is not only limited to CdSe nanoparticles. Independent of the nature of the ligands covering the surface of the nanoparticles after the synthesis, these amino-PEOs could also be employed to obtain aqueous solutions of magnetic nanoparticles (such as  $\text{Fe}_3\text{O}_4$  and  $\text{CoPt}_3$ ). Photographs of aqueous solutions of different nanoparticles are presented in Figure 3.3.16.

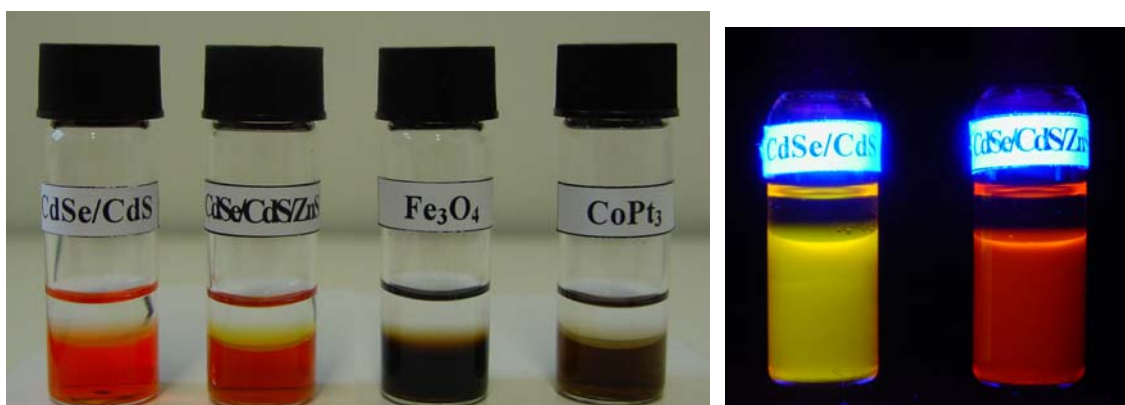


Figure 3.3.16. Different nanoparticles dispersed in the aqueous phase below a hexane phase

It was noticed that ligand exchange was promoted when the use of acid in the synthesis was avoided. For magnetic nanoparticles synthesised in the presence of acid, it was necessary to perform a thorough washing in multiple precipitation steps, up to the point of precipitation before the ligand exchange. For  $\text{Fe}_3\text{O}_4$  nanoparticles which were synthesised using only HDA as the coordinating ligand, the pre-treatment before the ligand exchange was the same as for the CdSe/CdS nanoparticles. Either the binding of the carboxylic group is so strong that ligand exchange for amino-functionalised molecules is not feasible, or a possible protonation of the amino groups prevents their binding to the metal sites. TEM images of  $\text{Fe}_3\text{O}_4$  nanoparticles before ligand exchange and after transfer into water are presented in Figure 3.3.17. After transfer into water, no agglomeration was detected.

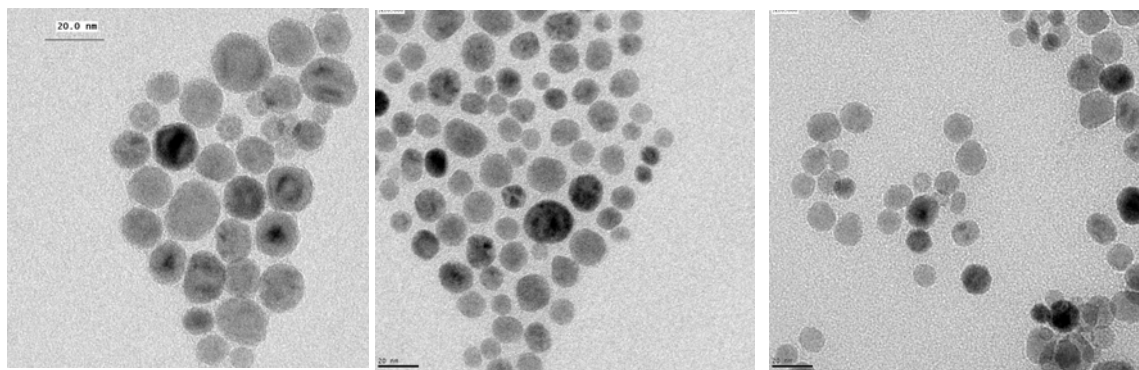


Figure 3.3.17. TEM images of  $\text{Fe}_3\text{O}_4$  nanoparticles dispersed in toluene (left) and in water with PEO2000-DETA (middle) and PEO2000-PEI-branched (right)

Nanoparticles capped with PEO ligands are soluble not only in water, but in any solvent for PEO, including chloroform. After ligand exchange with two types of PEO-PEI-branched, differing in the molecular weight of the PEO,  $\text{CoPt}_3$  nanoparticles were dissolved in chloroform and analysed by TEM. TEM images of  $\text{CoPt}_3$  nanoparticles with different ligand shells are presented in Figure 3.3.18.

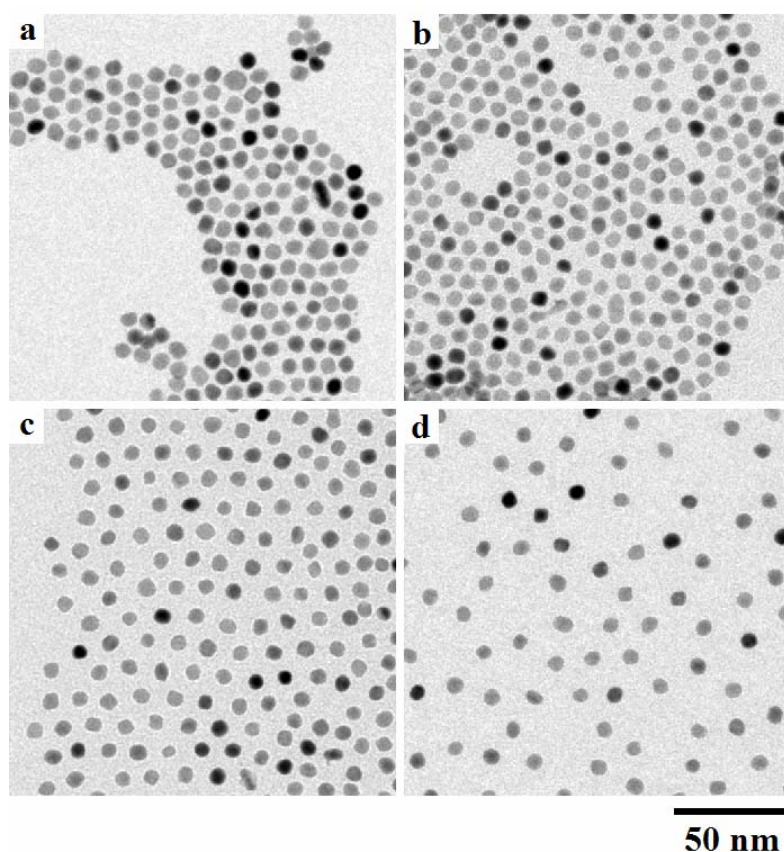


Figure 3.3.18. TEM images of  $\text{CoPt}_3$  nanoparticles with a) a ligand shell from the synthesis, b) after mixing with unmodified PEO5000 and after ligand exchange with c) PEO2000-PEI-branched, and d) PEO5000-PEI-branched

As can be seen from the TEM images, the distance between the nanoparticles changes with changing size of the stabilising ligand. In order to avoid the influence of different concentrations on the coverage of the TEM grid, the same amounts of nanoparticles were used in all the ligand exchanges, as well as the control experiments, and the nanoparticles were dissolved in the same amount of solvent. The concentration of nanoparticles was the same in all samples since no loss of nanoparticles occurred during the ligand exchange. Thus, the difference in the distance between the nanoparticles can not be ascribed to the difference in the concentration of the samples. The distance between the nanoparticles covered with polymer is larger compared to the distances when small molecules are the stabilising ligands (Figure 3.3.18 a, c and d). The longer the polymer chain, the bigger is the distance between the nanoparticles. Also, a control experiment with unmodified PEO

of 5000 g/mol molecular weight was conducted. The distances between the nanoparticles in the presence of unmodified PEO were not altered compared to the distances observed in the sample with small molecules. This shows that the arrangement of the nanoparticles is not affected by the presence of the polymer and that the different distances observed in the samples after ligand exchange are the consequence of the different size of organic shell as an integral part of the nanoparticle-polymer conjugate.

### *Size of nanoparticle-PEO conjugates and self-organisation*

The size of the nanoparticles to be used in labelling experiments is of critical importance for certain types of biological applications. The size of the nanoparticle-polymer conjugate will, in the end, determine the specific use.<sup>53</sup> Dynamic light experiments were performed in order to investigate the changes in the size of the hydrodynamic radii of nanoparticles capped with different polymeric ligands as a function of the size of the PEO part of the molecule (Figure 3.3.19).

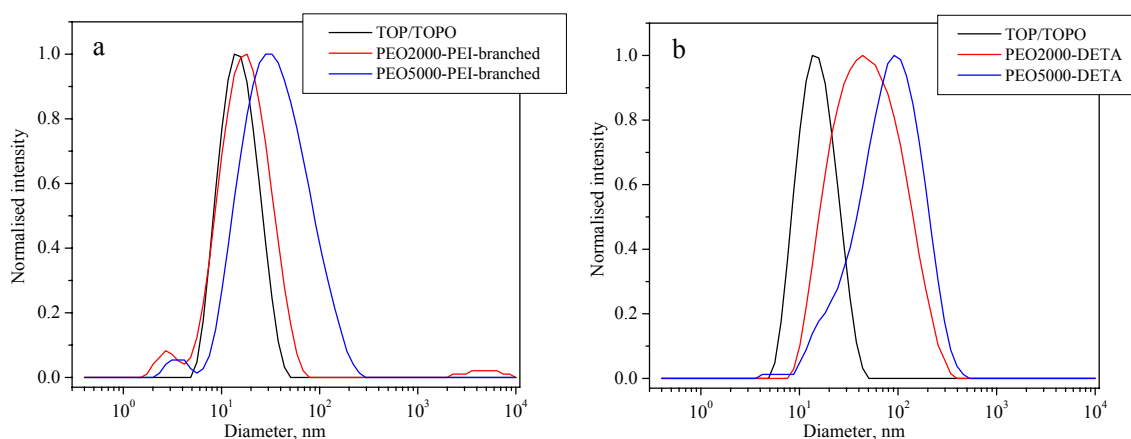


Figure 3.3.19. Size distribution of CdSe/CdS nanoparticles before (in chloroform-TOP/TOPO) and after ligand exchange (in water) with a) PEO-PEI-branched and b) PEO-DETA ligands

The values of the obtained hydrodynamic radii are higher than the simple sum of the radius of a particle and the length of a fully stretched polymer chain and cannot be taken as absolute values. Even for the nanoparticles covered with TOP/TOPO ligands, the value of 10 nm for the diameter is too high considering that the diameter of the nanoparticle core determined from spectroscopy measurements is 3.3 nm. However, from this

measurement, two conclusions can be reached: first, for both series, with increasing polymer chain length, a trend of increasing hydrodynamic radius was observed, and second, the formation of larger agglomerates can be excluded. Unexpectedly, the values of the hydrodynamic radii in the PEO-DETA series were considerably larger compared to the corresponding values in the PEO-PEI-branched series. It is to be expected that, for example, nanoparticles covered with PEO2000-DETA and PEO200-PEI-branched would show similar values of the hydrodynamic radii; however, the values were 22 and 9 nm, respectively, which are too diverse to be attributed to a different packing of the PEO ligands on the nanoparticle surfaces. Samples of nanoparticles covered with different polymeric ligand were subjected to TEM analysis in order to reveal the reasons for the difference in the hydrodynamic radii observed in the DLS measurements. The TEM images are presented in Figure 3.3.20.

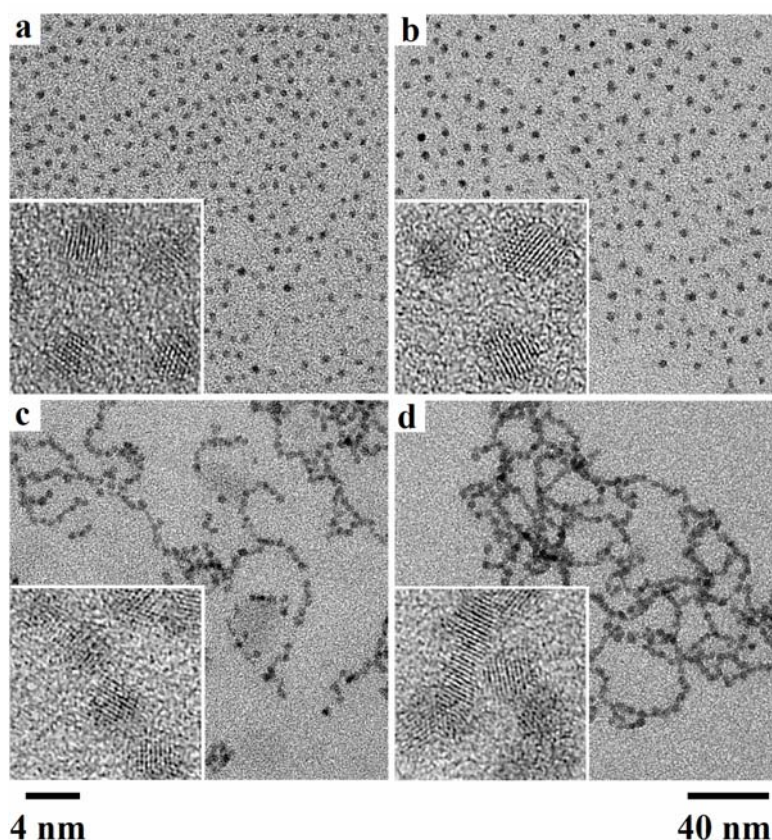


Figure 3.3.20. TEM images of water-soluble CdSe/CdS nanoparticles modified with a) PEO2000-PEI-branched, b) PEO5000-PEI-branched, c) PEO2000-DETA and d) PEO5000-DETA

In the PEO-PEI-branched series (Figure 3.3.20 a and b), single well-separated nanoparticles were observed. Even though the samples were prepared by evaporation of water from the TEM copper grid, which is associated with difficulties in obtaining a good distribution of nanoparticles over the grid, it can be seen that the distances between the nanoparticles change with the changing length of the PEO. In the PEO-DETA series, no single particles were observed, only wormlike agglomerates. Inspection of a frozen solution of the samples with cryo-TEM (Figure 3.3.21) showed that in the present case, the observed wormlike micelles already existed in the solution and hence, that the changes in the concentration during the evaporation of the solvent from the

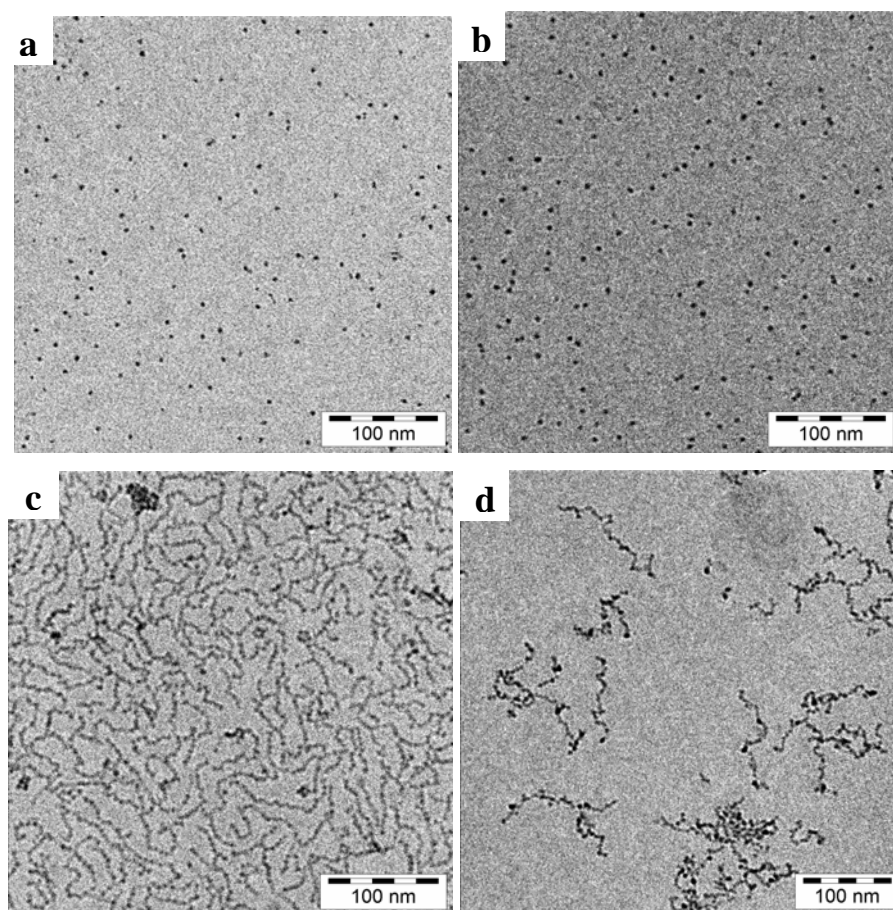


Figure 3.3.21. Cryo-TEM images of water soluble CdSe/CdS nanoparticles modified with a) PEO2000-PEI-branched, b) PEO5000-PEI-branched, c) PEO2000-DETA and d) PEO5000-DETA

TEM grid were not responsible for the formation of micelle aggregates. The larger values of the hydrodynamic radii observed in the DLS measurements for the PEO-DETA series are probably the consequence of the formation of wormlike micelles in the aqueous solution of nanoparticles covered with these polymers.

Cylindrical micelle structures of copolymers loaded with nanoparticles have hitherto been observed for several combinations of nanoparticle-[block copolymers].<sup>119-121</sup> However, all of these systems were prepared from polymers that alone can make different architectures depending on the hydrophobicity/hydrophilicity ratio of the constituent units. In a control experiment, it was confirmed by cryo-TEM that amino-functionalised polymers have no tendency of organising themselves in water in the absence of nanoparticles, as expected from their chemical composition. The structures observed here are unique self-organising systems obtained only through interaction between the nanoparticles and the polymeric ligands.

The first observation in the formation of a nanoparticle-polymer conjugate is that a change in the morphology is induced by the change in the architecture of the polymeric ligand. The effect of the geometry of an amphiphile on the aggregation behaviour has already been observed for the poly(styrene)-poly(propylene imine), PS-dendr-PPI, dendrimer molecules.<sup>122</sup> It was shown that in aqueous phases, PS-dendr-(NH<sub>2</sub>)<sub>32</sub> forms spherical micelles, PS-dendr-(NH<sub>2</sub>)<sub>16</sub> forms micellar rods and PS-dendr-(NH<sub>2</sub>)<sub>8</sub> forms vesicular structures (Figure 3.3.22)

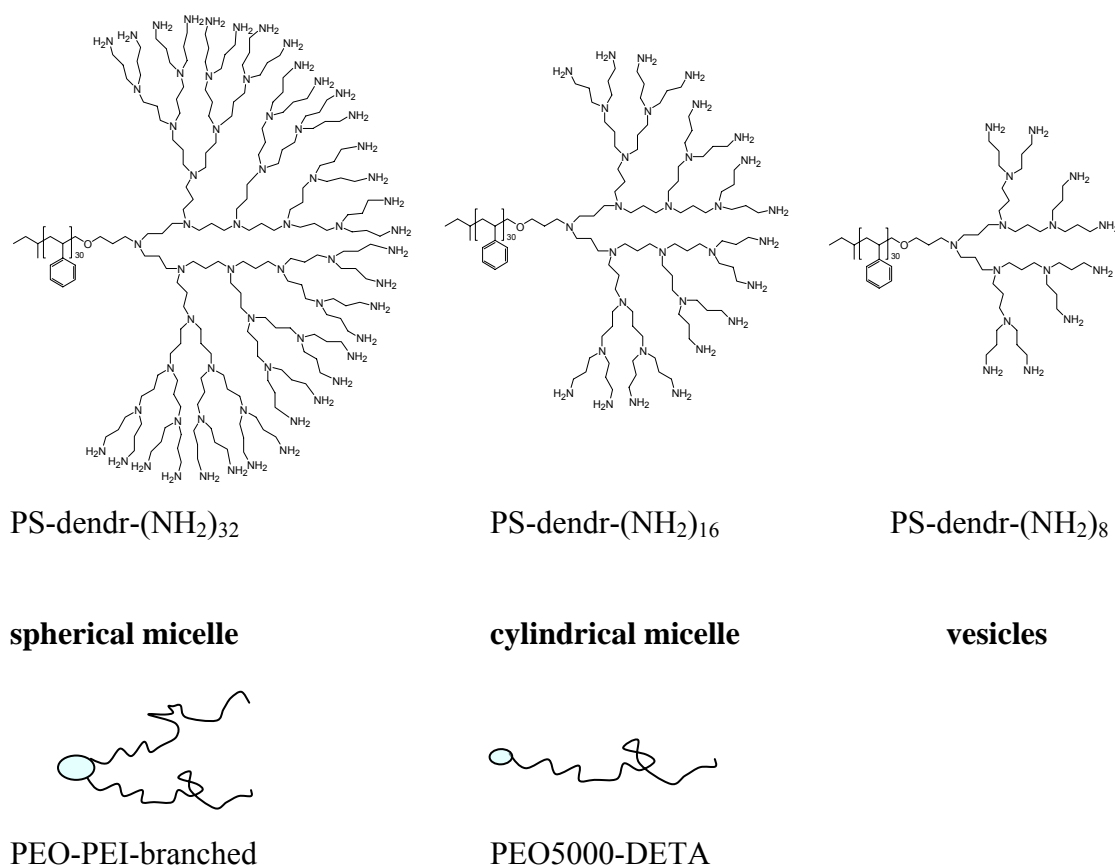


Figure 3.3.22. Comparison of dendritic polymers which self-organise into different morphologies depending on the molecular structure and the polymeric ligands

The argumentation of the effect of geometry of an amphiphile on the type of morphology observed in the case of PS-dendr-PPI was supported by the Israelachvili theory of the influence of tenside geometry on the self-assembly structure in solution.<sup>123,124</sup> The striking similarity of the architecture of the PS-dendr-PPI molecules and the PEO ligands studied here, with the same effect on the morphology found in solution indicates the similarity of the nature of the self-organisation of tenside molecules, block copolymers and nanoparticle-polymer conjugates.

Further investigation of the conditions for the formation of different morphologies in an aqueous dispersion of nanoparticles revealed that cylindrical micelles were formed only for certain polymer/nanoparticle ratios applied during the ligand exchange (Figure 3.3.23.)

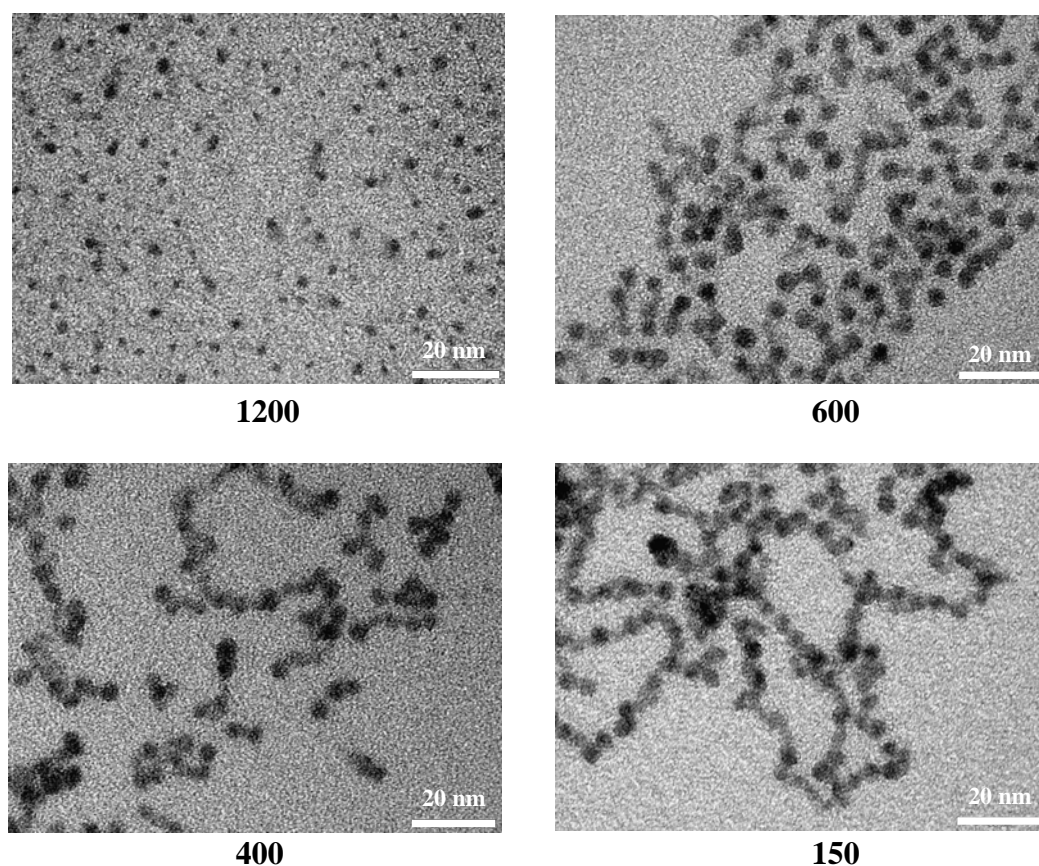


Figure 3.3.23. TEM images of water soluble CdSe/CdS nanoparticles (with a diameter of 3.9 nm) obtained with different PEO2000-DETA/nanoparticle ratios (the numbers below each image indicate the applied ratio) during the ligand exchange

For very high polymer/nanoparticle ratios, single particles were observed. By decreasing the polymer/nanoparticle ratio, starting from the ratio of 600, the gradual formation of cylindrical micelles can be followed. However, changing the polymer/nanoparticle ratio within the limit applied in the case of PEO2000-DETA induced no change in the morphology in the case of nanoparticle/PEO2000-PEI-branched conjugates (Figure 3.3.24).

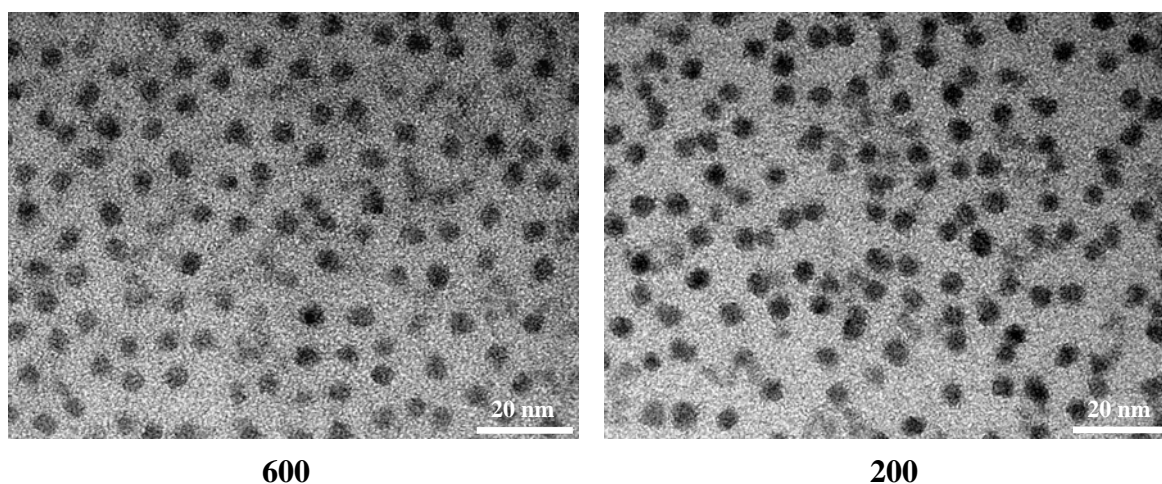


Figure 3.3.24. TEM images of water-soluble CdSe/CdS nanoparticles (with a diameter of 3.9 nm) obtained with different PEO2000-PEI-branched/nanoparticle ratios (the numbers below each image indicate the applied ratio) during the ligand exchange

The polymer/nanoparticle ratio at which the formation of cylindrical micelles is to be expected is influenced by several factors, such as the pre-treatment of the nanoparticles and the size of the nanoparticles. When smaller nanoparticles are employed, in order to induce the formation of cylindrical micelles, the polymer/nanoparticle ratio had to be lower than the one applied for the larger nanoparticles in order to obtain organised structures (Figures 3.3.23. and 3.3.25). When, in the case of smaller nanoparticles, the ratio was 300 (Figure 3.3.25), a few isolated self-organised structures are visible in the TEM image, although the majority of the nanoparticles were individually encapsulated. All other higher ratios gave simple spherical nanoparticle-polymer micelles containing a single encapsulated nanoparticle. On decreasing the ratio to 150, on the other hand, the vast majority of the nanoparticles were contained in self-assembled structures, with only a very few individual nanoparticles.

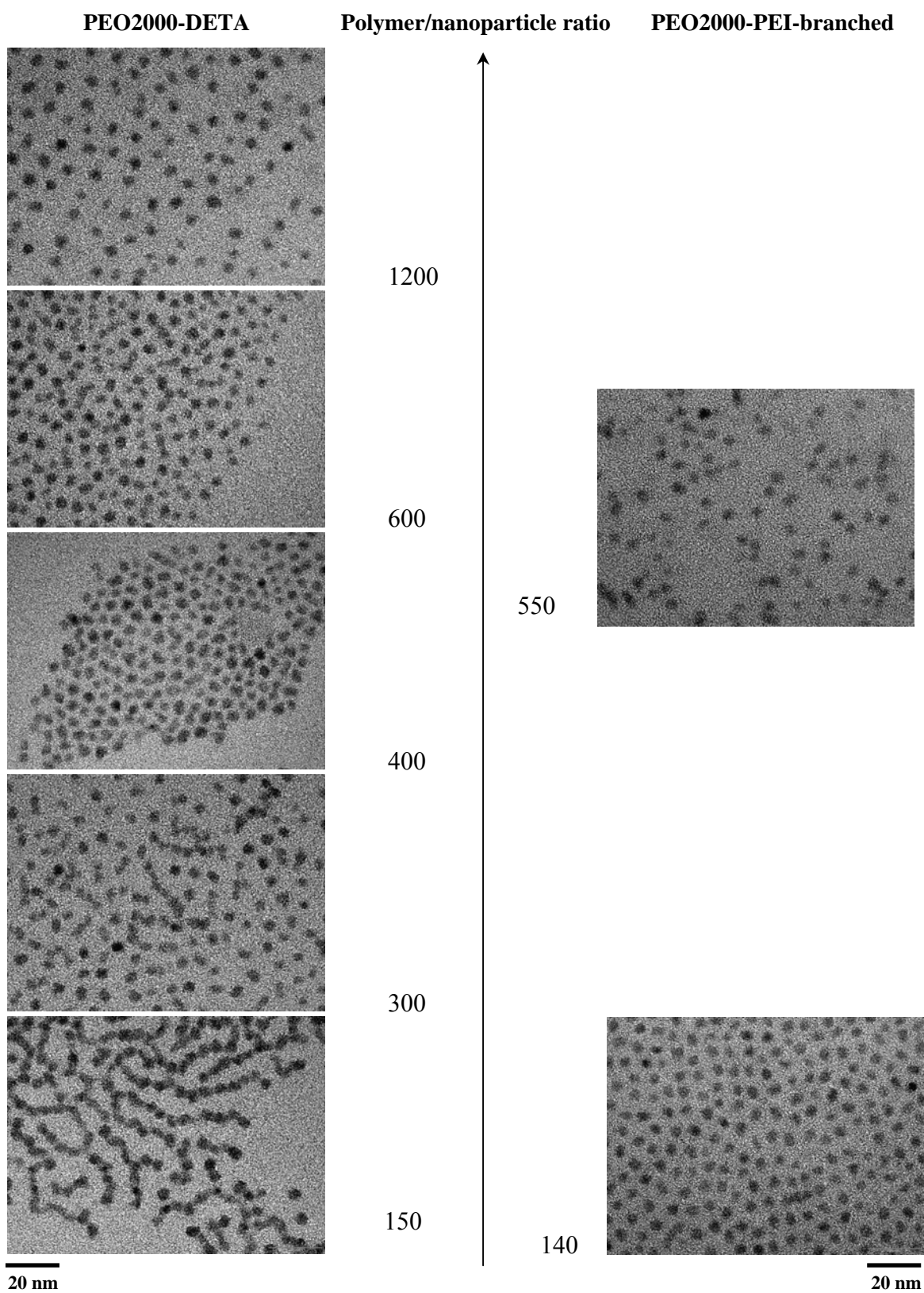


Figure 3.3.25. TEM images of water-soluble CdSe/CdS nanoparticles (with a diameter of 3.4 nm) obtained with different polymer/nanoparticle ratios during the ligand exchange

As expected, with the PEO-PEI-branched ligand and smaller nanoparticles, it was also not possible to obtain structures other than single nanoparticle-polymer conjugates even with the lowest employed polymer/nanoparticle ratio (Figure 3.3.25.).

Further investigation of the dependence of the morphology changes on the type of ligand was performed by changing the length of the binding part of the ligand with the same architecture of the ligand and the same PEO length (PEO2000-PEHA versus PEO2000-DETA). For the same polymer/nanoparticle ratio, while nanoparticles covered with PEO2000-DETA (short binding block) were organising into cylindrical aggregates, nanoparticles covered with PEO2000-PEHA (long binding block) were still well separated, similar to the case when PEO2000-PEI-branched was used (Figure 3.3.26.).

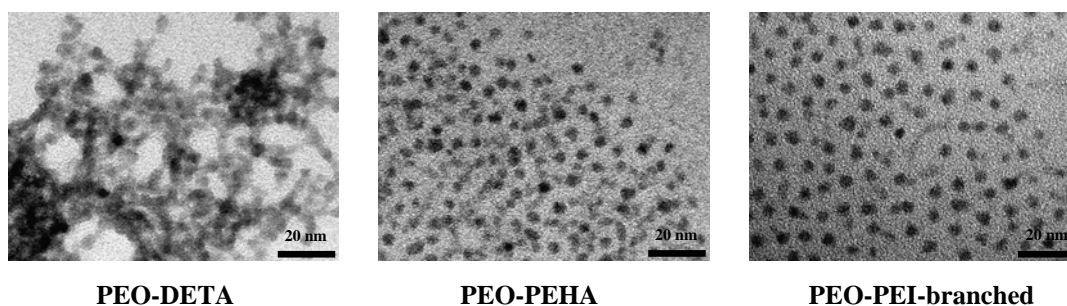


Figure 3.3.26. TEM images of water-soluble CdSe/CdS nanoparticles obtained with polymers having the same PEO length (PEO2000) but with different binding parts (the polymer/nanoparticle ratio was the same (150) during the ligand exchange)

The type of self-assembly observed for nanoparticle-polymer conjugates resembles those typical for tenside molecules and already observed for highly asymmetric, amphiphilic block copolymers.<sup>125,126</sup> Manipulation of the relative block lengths in the structure of the block copolymer can lead to the formation of a variety of morphologies in a solution. One way to describe and predict the preferred shape of the assembly of a block copolymer in solution is influenced by the theory of the organisation of small surfactant molecules, which is described by the value of a dimensionless packing parameter,  $P$ :<sup>123</sup>

$$P = \frac{v}{a_0 l} \quad \left\{ \begin{array}{ll} < 1/3 & \text{spherical micelle} \\ < 1/2 & \text{cylindrical micelle} \\ 1/2 - 1 & \text{vesicle} \end{array} \right.$$

where, for a small surfactant molecule,  $v$  is the volume fraction of the hydrophobic core per surfactant molecule,  $l$  is the critical length of the hydrophobic part of the surfactant and  $a_0$  is the optimal interfacial area per surfactant molecule. The packing parameter theory takes into account the geometrical constraints for a given molecule which would lead to the preferred formation of only one morphology. Thus, for a certain molecule with a given  $v$  and  $l$ , and optimal  $a_0$ , which depends only on the type of the polar surfactant group, a spherical or cylindrical micelle, or a vesicle will be formed.

Interestingly, all the observed changes of the morphology of the nanoparticle-polymer conjugates in the described experiments can be qualitatively described by the packing parameter formalism. If the packing parameter formalism is to be applied in a nanoparticle-polymer system, then  $l$  is the radius of the nanoparticle  $R$ ,  $v$  is the partial volume of the nanoparticle per polymer ligand and can be expressed as  $v = V/N$ , where  $N$  is the number of polymeric ligands per nanoparticle and  $V$  the nanoparticle volume (Figure 3.3.27).

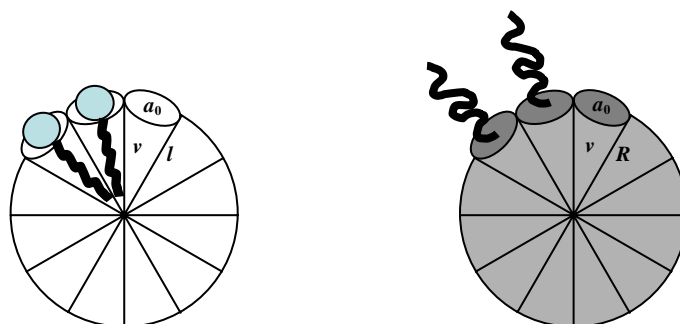


Figure 3.3.27. Schematic representation of a surfactant micelle and a spherical nanoparticle-polymer conjugate

The packing parameter would then be:

$$P = \frac{V}{Na_0R} = \frac{4\pi R^2}{3Na_0}$$

As observed, the transition from spherical to cylindrical morphology is dependant on the polymer/nanoparticle ratio used during the ligand exchange. It can be easily assumed that

a proportionality exists between the polymer/nanoparticle ratio employed during the ligand exchange and the total number of polymeric ligands attached to a nanoparticle ( $N$ ) after the ligand exchange. This is further supported by the observed change in the distance between the nanoparticles (in the case where a good coverage of the TEM grid is achieved) with changing nanoparticle/polymer ratio. As the polymer/nanoparticle ratio decreases, the distance between the nanoparticles also decreases (Figure 3.3.25). When this distance is thought of as being proportional to the amount of the polymer molecules attached to the nanoparticle, this means that with decreasing polymer/nanoparticle ratio in the ligand exchange experiments, the number of attached polymers also decreased. If the number of ligands per nanoparticle decreases, then the packing parameter increases, eventually reaching the critical condition for the formation of a cylindrical micelle.

On decreasing the size of the nanoparticle ( $R$ ) for the same type of polymeric ligand (constant  $a_0$ ), the number of attached polymeric ligands necessary to reach the critical condition for cylindrical micelle formation should be lower. This can explain why cylindrical micelles are observed at a lower polymer/nanoparticle ratio for smaller nanoparticles.

Using a ligand with a longer or bulkier binding block, the optimal interfacial area  $a_0$  increases, meaning that a cylindrical micelles can be formed with a lower number of polymeric ligands per nanoparticle for the ligand with a longer or bulkier binding part. For the same polymer/nanoparticle ratio, cylindrical micelles were observed with PEO2000-DETA, while in the case of ligands with more binding amino groups PEO2000-PEI-branched and PEO2000-PEHA, single encapsulated nanoparticles were the only morphologies observed.

According to the packing parameter model, when the critical condition for the formation of a cylindrical micelle is close to  $1/2$ , small vesicles are formed, which coexist with the long cylindrical micelles. Only in case of PEO2000-DETA, structures resembling vesicles were observed in the cryo-TEM images (Figure 3.3.28).

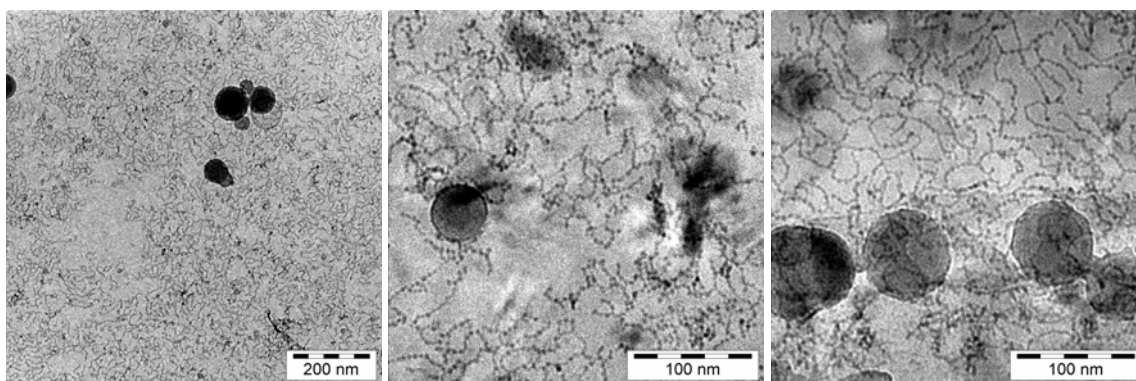


Figure 3.3.28. Cryo-TEM images of CdSe/CdS nanoparticles with PEO2000-DETA polymeric ligand aggregates

Structures resembling vesicles were observed only with PEO2000-DETA and only cylindrical micelles were present for the nanoparticles covered with PEO5000-DETA. Under all restrictions concerning the observed vesicle-like structures, their absence with PEO5000-DETA leads to the expected conclusion that the self-organisation is also determined by the lengths of the PEO blocks.

It is natural to assume that the optimal interfacial area is determined by the type of the ligand with respect to its binding group and the size of the ligand. The optimal interfacial area is determined by the forces of interfacial tension between the hydrophobic surface and water, and the repulsive forces between the polymeric chains. In a study of the micellisation of block copolymers,<sup>127</sup> a dimensionless packing parameter was introduced, with formalistic analogy to the packing parameter for surfactant molecules:

$$\Delta = \frac{v_0^{2/3}}{b^2} = \frac{v}{a_0 l} = P$$

where  $b$  is the average distance between the polymeric chains in the micelle corona and  $v_0$  is the monomer volume of the core-forming, hydrophobic part of the block copolymer molecule. In the analogy developed,  $b^2 = a_0$ ,  $v = N_A v_0$  and  $l = N_A v_0^{1/3}$  (where  $N_A$  is the degree of polymerization of the core building part of the molecule). This analogy allows a direct correlation between the optimal surface area and the length of the hydrophilic corona-forming part of the block copolymer to be derived. For a block copolymer,  $b$  is a

function of the size of the hydrophilic part expressed through the degree of polymerization ( $N_B$ ) of this block and is given by the expression:

$$b = b_0 N_B^\varepsilon$$

Using the values of  $b_0$  and  $\varepsilon$  given for alkylpoly(ethyleneglycol)s,<sup>127</sup> the value of  $b$  for PEO2000 was calculated to be 0.917 nm, and of  $b^2 = a_0$  to be 0.841 nm<sup>2</sup>. The good distribution of the nanoparticles on the TEM grid allowed the calculation (Appendix 2) of the surface area per polymeric ligand for the nanoparticle-conjugates obtained for different polymer/nanoparticle ratios. The obtained values are plotted in Figure 3.3.29. and compared with  $b^2 = a_0$  calculated using literature data.

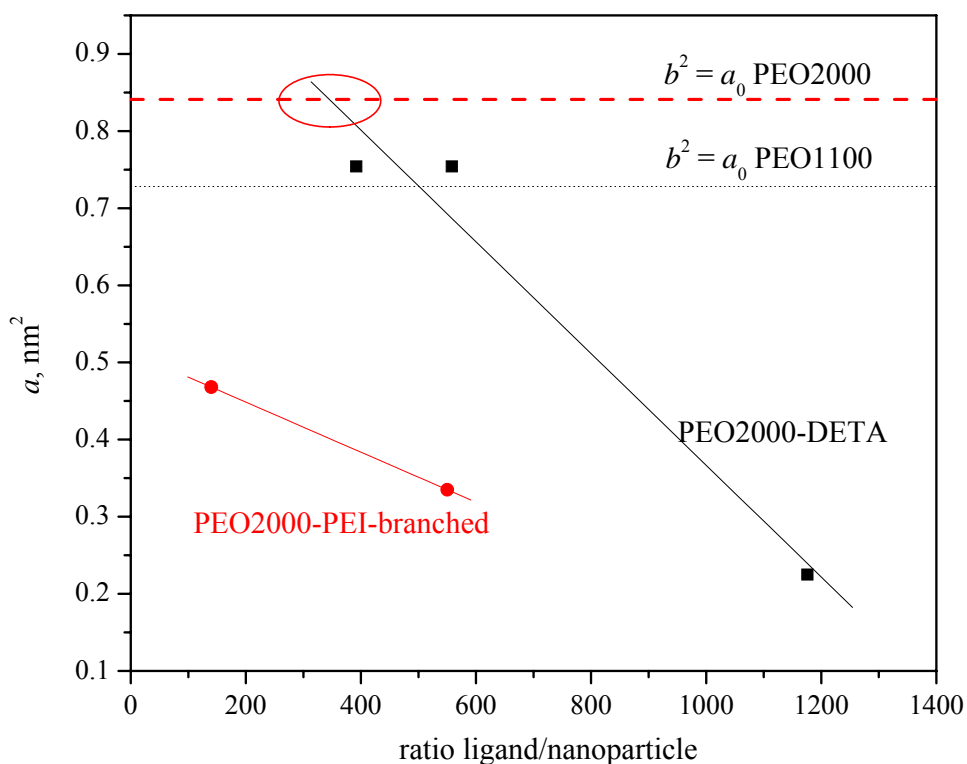


Figure 3.3.29. The dependence of the surface area per ligand molecule on the polymer/nanoparticle ratio applied in the ligand exchange

At a PEO2000-DETA/nanoparticle ratio of about 300, cylindrical micelles began to form (see Figure 3.3.25), as would be expected from the crossover section of the fitted data and the calculated  $b^2$  value (Figure 3.3.29). At a lower ratio of 150, the only structures observed were cylindrical micelles, indicating that the surface area of the nanoparticle per polymer should be well above the critical  $a_0$ , if the structure were to stay spherical. The argumentation of geometrical constraints employed in the development of the packing parameter model for small surfactant molecules can also be applied to describe the formation of cylindrical micelles in nanoparticle-polymer conjugates. It can be thought of as when the critical value of  $b^2 = a_0$  is reached, the interfacial tension between the bare nanoparticle surface and water is so high that the attractive forces between the nanoparticles drive the morphological changes and by mutual coalescence reduce the surface area occupied by the ligand molecule. For the given system, in order to drive the morphological changes further, the polymer/nanoparticle ratio should be very low, bringing into question efficiency of the ligand exchange.

For the PEO2000-PEI-branched-nanoparticle conjugate, it is to be expected that the value of the optimal  $a_0$  is higher since the binding group is the bulky PEI and the ligand has a branched structure. Additionally, the values of surface area of nanoparticle per polymer molecule for this ligand are surprisingly low (Figure 3.3.29), which leads to the conclusion that this system is far removed from spontaneous morphological changes.

The argumentation used so far leads to the logical conclusion that the morphological changes going from spherical to cylindrical to vesicular structures for a given nanoparticle and type of ligand would be easier to induce when a polymeric ligand of lower molecular weight would be used. As shown in Figure 3.3.29, the critical value of  $b^2 = a_0$  is at a lower value for PEO1100, which was also used to synthesise amino-functionalised ligands. Attempts to obtain vesicles with ligand PEO1100-DETA failed.

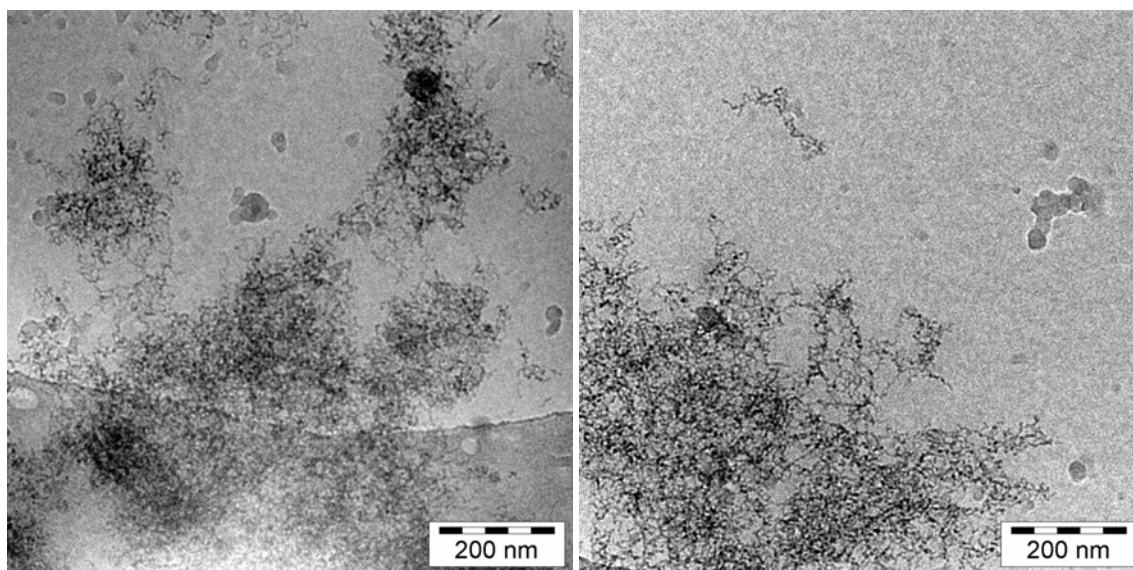


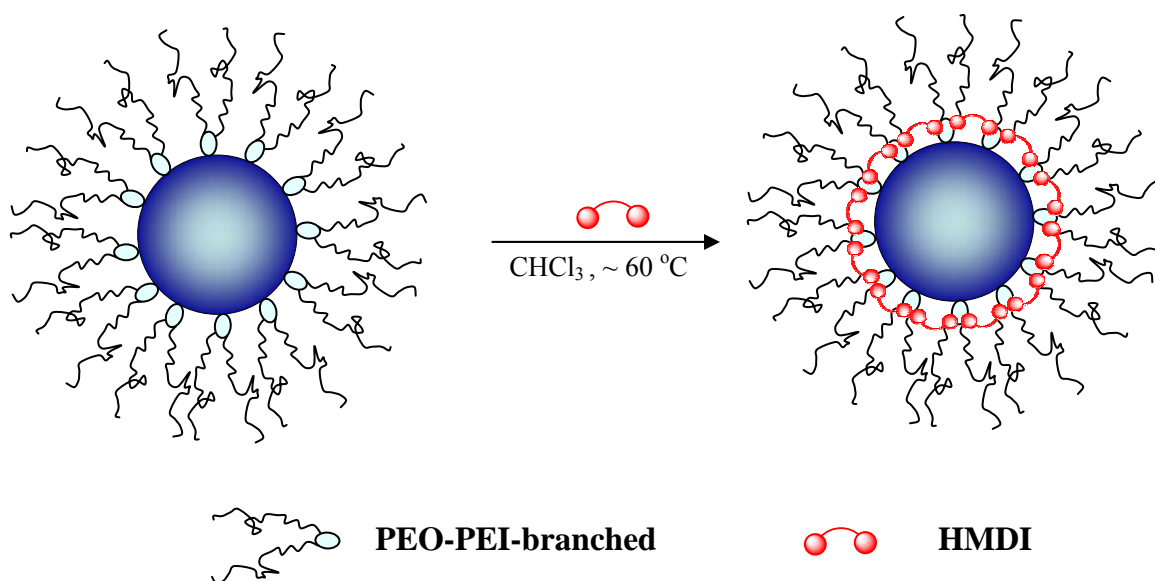
Figure 3.3.30. Cryo-TEM images of CdSe/CdS nanoparticles covered with PEO1100-DETA obtained with a polymer/nanoparticle ratio of 150 during the ligand exchange

As can be seen in Figure 3.3.30, cylindrical micelles were the only structures observed. The solution of nanoparticles was instable and precipitated readily. The reason can be the poor quality of the synthesised ligand (see 3.2.2), containing a large amount of double molecular weight by-product. However, the possibility that vesicle formation (which means a further increase of the surface area per total volume of the formed structure) is not sustainable because of the very large difference in the density of the core and that of the corona forming material, can not be excluded.

#### ***Crosslinking of the organic stabilising shell***

The main reason for the poor stability of nanoparticles, as well as for the problems encountered during bioactivation of biocompatible nanoparticles is the dissociation of the organic ligands from the inorganic core. In addition to the frequent use of multidendate ligands, a strategy employed to overcome this problem is the crosslinking of the organic shell around the nanoparticle, which would prevent the detachment of the ligands. There are two reasons which recommend PEO-PEI-branched ligands for further stabilisation of nanoparticle/ligand complexes through the crosslinking strategy. The first is the sufficient

number of amino groups of the binding PEI-branched part, which could be involved in the crosslinking reaction next to the surface of the nanoparticle. The second is that the overall branched structure of the ligand should allow the molecule used for the crosslinking to approach the inner binding part of the molecule (Scheme 3.3.3). In this study an attempt was made to crosslink the PEO-PEI-branched polymeric shell using hexamethylenediisocyanate, HMDI, as the crosslinking reagent, as it readily reacts with the amino groups under mild conditions to form urea bonds.



Scheme 3.3.3. Crosslinking of the PEO-PEI-branched ligands around the nanoparticles using hexamethylenediisocyanate

The ligand exchange was performed with the ratio polymer/nanoparticles as low as 250 in order to avoid the presence of free ligands in the solution. After the addition of the crosslinker molecule to the nanoparticles in chloroform solution, the reaction of the isocyanate with the amino group can be easily followed by IR spectroscopy through the disappearance of the band at  $2269\text{ cm}^{-1}$ , characteristic of the isocyanate group. In order to investigate the optimal amount of the crosslinker, two different ratios of hexamethylenediisocyanate/PEO2000-PEI-branched were used: 0.5/1, which is the lower limit for the successful crosslinking and 2/1, which should lead to a higher crosslinking density, however with a higher probability of interparticle crosslinking. After the

completion of the reaction, as proved by IR spectroscopy, the nanoparticles remained well dispersed in the solution and could withstand the subsequent purification steps and phase transfer, indicating that interparticle crosslinking had not occurred to a significant extent. The absorption spectroscopic characteristics of the nanoparticles remained unaltered after the crosslinking reaction. The PL intensities of the nanoparticle after transfer to water were comparable with those of the nanoparticle covered with unreacted PEO2000-PEI-branched (Figure 3.3.31).

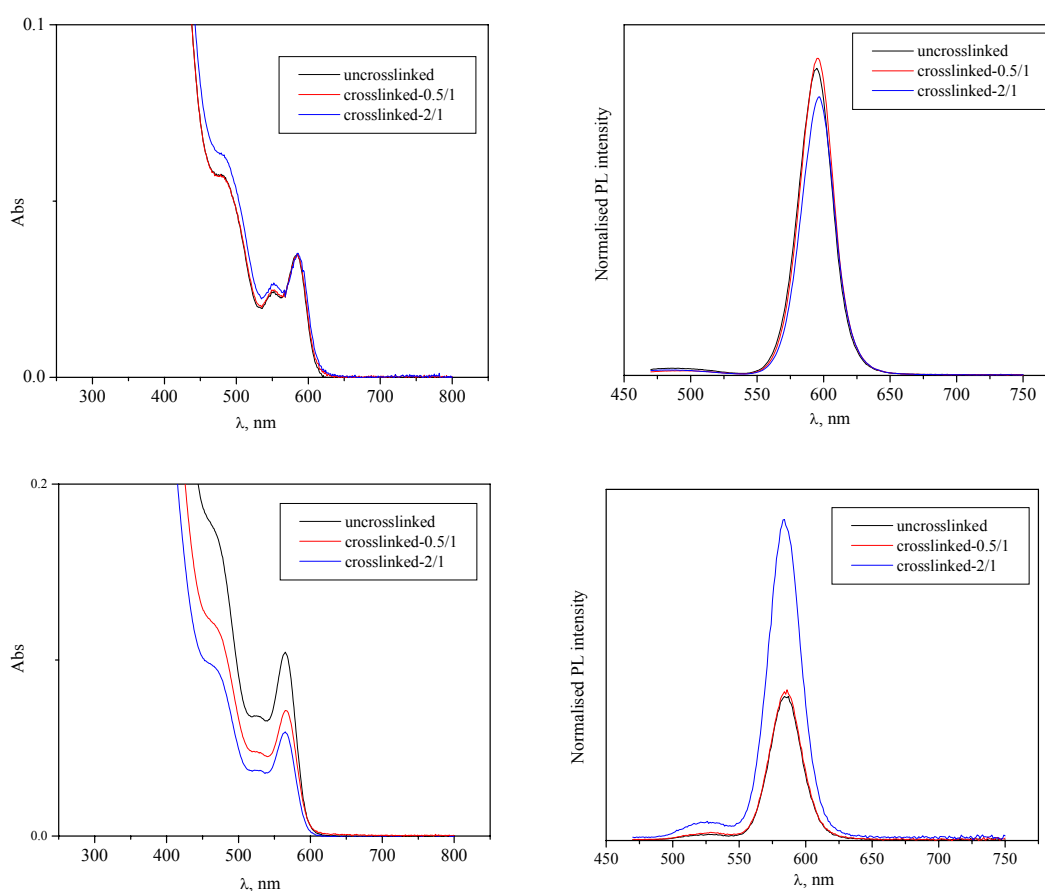


Figure 3.3.31. Absorption and luminescence spectra of water-soluble CdSe/CdS nanoparticles of two different diameters (3.9 nm upper row and 3.4 nm lower row) before (uncrosslinked) and after the crosslinking reaction with two different ratios of HMDI/PEO2000-PEI-branched

Based on the presented experimental evidence, it can be stated that hexamethylenediisocyanate can be successfully applied for the reaction of the

PEO-PEI-branched ligands after performance of the ligand exchange reaction. However, it is not certain if the reaction occurred on the ligand layer around the nanoparticles or whether free ligands were involved in the reaction. Reaction of free ligands with hexamethylenediisocyanate would lead to the formation of an insoluble high molecular weight product, the presence of which was not detected, showing that this reaction was not the main event occurring during the crosslinking. However, the participation free ligands in the reaction, even to a small extent, would decrease the probability of the crosslinking of the ligand shell around the nanoparticles, leading to the insufficient stabilisation. In studies of the crosslinking of organic dendron molecules around nanoparticles, it was shown that the nanoparticles with a crosslinked shell exhibit improved chemical stability against the action of a strong acid and a strong oxidant compared to those with an uncrosslinked shell.<sup>128,129</sup> The main reason for such an improvement of chemical resistance is the hindered diffusion of etchant molecules through the crosslinked undynamic organic shell. In order to reveal the nature of the organic shell of nanoparticles in this work, etching experiments with hydrochloric acid were performed before and after crosslinking. Two different nanoparticle sizes were used. The change in the optical density at the first absorption maximum with exposure time was used as a measure of the deterioration of the nanoparticles due to the action of hydrochloric acid (Figure 3.3.32).

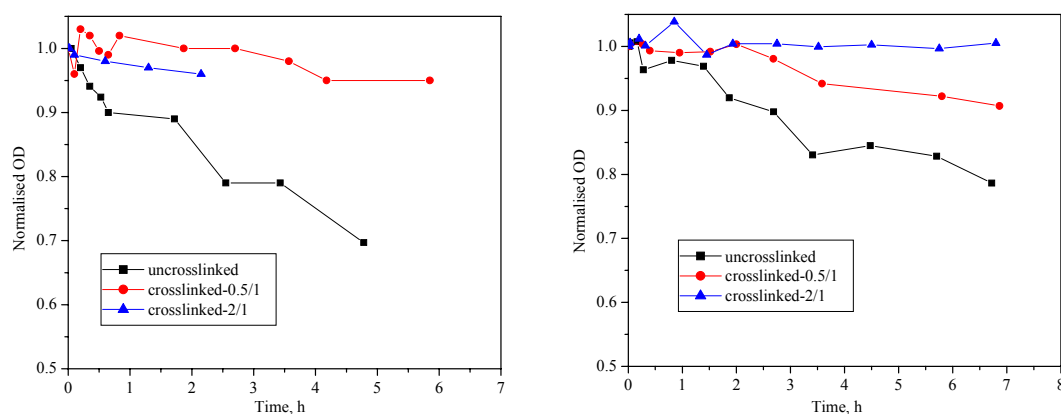


Figure 3.3.32. Optical density change during the reaction of CdSe/CdS nanoparticles of two different diameters (3.9 nm left and 3.4 nm right ) with HCl before (uncrosslinked) and after the crosslinking reaction using two different ratios of HMDI/PEO2000-PEI-branched

As can be seen from Figure 3.3.32, the nanoparticles after performance of the crosslinking reaction were more stable against the action of hydrochloric acid in both cases. However, a clear trend of increased stability with increasing amount of crosslinking agent was not observed. This fact, as well as the low reproducibility of the results lead to the conclusion that the increased stability of the nanoparticles can be a consequence not of the slower diffusion of the etchant through the crosslinked organic shell, but of the consumption of the acid in the hydrolysis reactions of the ligands (in the reaction with hydrolysable urea and urethane) themselves. Thus, the etching reaction was performed with a strong oxidant, in which case reaction with the organic shell can be completely excluded. The results of the temporal change of the optical density during the oxidation of the nanocrystals with  $H_2O_2$  are presented in Figure 3.3.33.

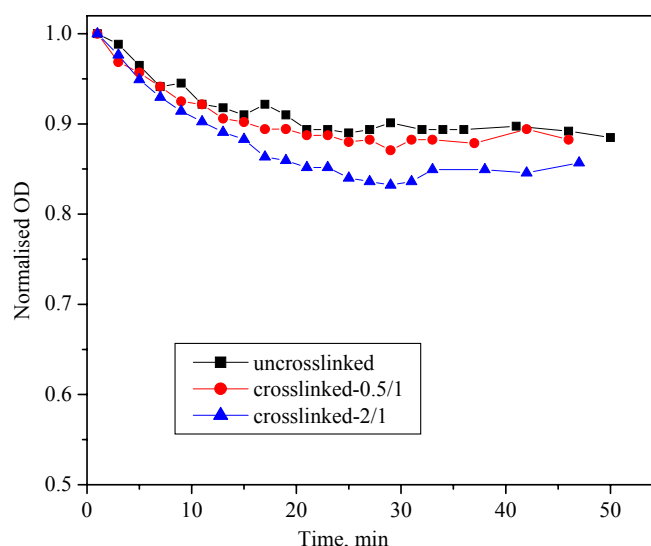


Figure 3.3.33. Temporal change of OD of CdSe/CdS nanoparticles (3.4 nm) during the reaction with  $H_2O_2$  before (uncrosslinked) and after the crosslinking reaction with two different ratios of HMDI/PEO2000-PEI-branched

As opposed to that observed for the reaction with hydrochloric acid, the oxidation of the nanocrystals by  $H_2O_2$  proceeded at almost the same rate regardless of the treatment applied to the polymeric shell. At this point, it can be speculated that either the polymeric shell was not crosslinked and thus not making a sufficient barrier to the oxidant

molecules, or that the shell is crosslinked but that the crosslinking in this case is not an efficient barrier to the diffusion of  $\text{H}_2\text{O}_2$ . Although the differences were rather small, it can be observed that the untreated nanoparticles and the nanoparticles treated with the lowest amount of HMDI showed the highest resistance to the action of  $\text{H}_2\text{O}_2$ . Such a trend can be explained if detachment of the PEO2000-PEO-branched during the crosslinking reaction is assumed. However, in that case, higher amounts of insoluble products would be formed during the crosslinking with the higher amount of HMDI, which was not observed. It seems that the first argumentation of insufficient crosslinking or insufficient hindrance of the diffusion of  $\text{H}_2\text{O}_2$  is more likely.

In the present case the chemical stability experiments might not be the most suitable way to prove the crosslinking of organic shell (which is crosslinked just next to the inorganic core), as it is in a case where the outer part of organic shell was crosslinked.<sup>128,129</sup>

To determine whether with crosslinking the stability of the nanoparticle-polymer conjugate is improved with respect to the dissociation of the polymeric ligands from the nanoparticle surface, long-term experiments in which the luminescence efficiency, which should be affected by ligand dissociation, was followed with time for the crosslinked and uncrosslinked samples (Figure 3.3.34).

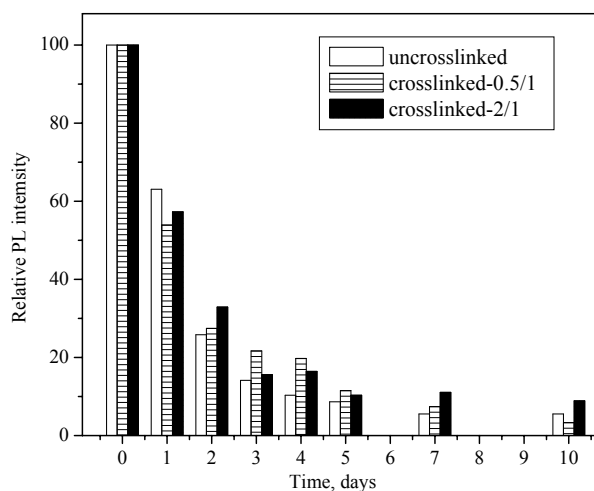


Figure 3.3.34. Temporal change in the luminescence intensity of the nanoparticles stabilized with PEO2000-PEI-branched (uncrosslinked) and after the reaction of the polymeric shell with HMDI (crosslinked) with two different ratios of HMDI/PEO2000-PEI-branched

The decrease in the PL intensity over ten days, caused by the dissociation of the ligands from the nanoparticle surface, was the same for all the investigated samples, i.e. the sample with an untreated shell and two samples in which the PEO2000-PEI-branched shell had been treated with two different amounts of the crosslinking agent. The results obtained also indicate, as assumed from the previous oxidation experiment, that the crosslinking of the PEO2000-PEI shell did not occur to an extent high enough to prevent the ligands from leaving the surface of the nanoparticle. The possible reason can be an inefficient diffusion of the crosslinking agent, HMDI, through the thick PEO shell, which is thus hindered to reach and react with inner PEI binding part. Thus, shorter PEO could be a better choice for the design of the PEO-PEI ligands suitable for further crosslinking. A further reason could be small PEI binding part of the ligand. By using a branched PEI of higher molecular weight, the number of active amino groups available for the crosslinking reaction would be increased. Simultaneously, the larger binding part of such a molecule, from the packing argumentation, would provide for a less dense organic layer, facilitating also in this way the diffusion of the crosslinking agent. Optimisation is also possible in the choice of the crosslinking agent, which could be smaller than the one employed here.

### 3.4 Ligand exchange with mercapto-functionalised poly(ethylene oxide)s

#### 3.4.1 Ligand exchange with linear mercapto-functionalised poly(ethylene oxide)

As previously stressed, the most frequently employed method to transfer nanoparticles from apolar, non-protic solvents to water is to perform ligand exchange with a small bifunctional molecule possessing a suitable water-compatible functionality. The mercapto (or thiol) group is the functional group most frequently used to bind to nanoparticles. In the previous subchapter, it was shown that PEO can serve to render nanoparticles water soluble while having a suitable functionality to bind to the Cd sites. To broaden the approach, mercapto groups were also used as anchoring groups attached to the end of PEO chains. PEOs with the structural formulas given in Figure 3.4.1, having one or two thiol groups at the end of the chain, were synthesised by an esterification reaction using mercaptopropionic acid.

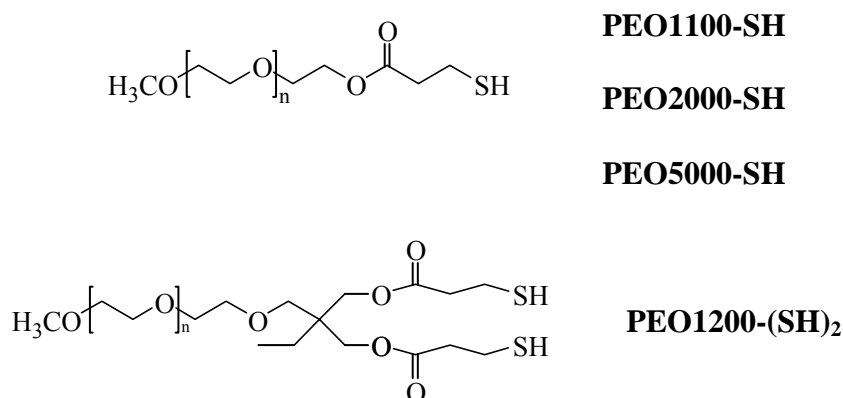


Figure 3.4.1. Structural formulas of PEOs with a thiol end group; the numbers in the abbreviations represent the molecular weight of the PEO

PEO molecules with SH functionality also have great potential for the stabilisation of a variety of types of nanoparticles, since molecules containing thiol groups can be used for

the stabilisation of Au, CdTe and Fe<sub>3</sub>O<sub>4</sub>.<sup>130-134</sup> Contrary to the effect of thiols on the luminescence of CdTe, a number of studies of CdSe nanoparticles indicated that ligand exchange with thiol-containing molecules usually leads to a reduced luminescence intensity compared to the starting nanoparticles. This remarkable difference between thiol-capped CdTe and CdSe nanoparticles was explained by the difference in the position of the top of the valence band with respect to the redox energy level of the thiol molecule, which is positioned above the top of the valence band of CdSe, promoting hole trapping in this case.<sup>135</sup> However, it was recently reported that the blinking of polymer encapsulated CdSe/ZnS was almost completely suppressed by the addition of a small amount of ( $\beta$ -mercaptoethanol).<sup>136</sup> This issue was further investigated by Jeong et al. who found that the effect of thiols on the luminescence of nanoparticles can be favourable or detrimental depending on different conditions.<sup>137</sup> Thiulates rather than thiols are responsible for the quenching of luminescence, which can be regulated by the pH conditions. These findings promise that further investigation and a better understanding of the role of thiol surface ligands could lead to the production of stable, luminescent, non-blinking nanoparticles under properly chosen conditions.

It is known that the mercapto group binds strongly to Cd and that this should be stronger than the binding of the amino group. The use of molecules containing thiol rather than amino groups for attachment to the nanoparticle surface should provide less vulnerable, long-term stable nanoparticle-polymer conjugates.

Using mercapto-functionalised PEOs by the method developed for amino-functionalised PEOs, the nanoparticles could be transferred into water. The spectral characteristics of PEO-SH capped nanoparticles in water were not altered, although the luminescence intensities were lower.

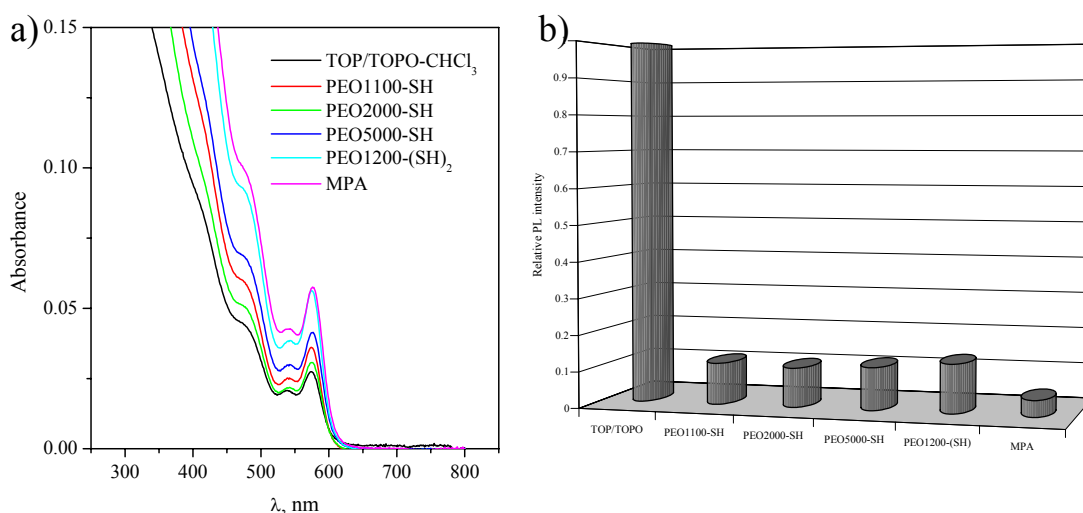


Figure 3.4.2. Absorption spectra (a) and comparison of the PL intensities (b) of the CdSe/CdS nanoparticles in chloroform and in water with different ligands

The absorption spectra of the nanoparticles in chloroform and of nanoparticles in water stabilised with different PEO-SHs together with a comparison of the relative luminescence intensities are presented in Figure 3.4.2. For comparison, the ligand exchange was also performed with mercaptopropionic acid (MPA), a very frequently used ligand to achieve the phase transfer of nanoparticles. As expected, the luminescence intensities of all the nanoparticles in water are lower compared to the starting TOP/TOPO stabilised nanoparticles in chloroform. The MPA-covered nanoparticles, however, exhibit the lowest PL intensity. Since MPA nanoparticles are electrostatically stabilised by the repulsion of the charged  $\text{COO}^-$  groups, it was suggested that this local electrostatic/polar environment affects electron-hole recombination<sup>138,139</sup>. This behaviour was further supported by the observed increase in the luminescence once the surface charges had been neutralised by self-assembly with negatively charged molecules. It can also be explained by the presence of thiolates rather than thiol groups,<sup>137</sup> since MPA-covered nanoparticles are stable only in solutions of high pH, where the carboxylic groups are ionised. Stabilisation of nanoparticles with PEO-SH does not require a specific pH of the solution because the nanoparticles are sterically stabilised by the repulsion of the polymeric chains, which probably leads to the improved luminescence.

Of the PEO-SH stabilised nanoparticles, the highest luminescence intensities were repeatedly observed for the ligand with two SH binding groups. Multidentate ligands provide for a more stable bond, which in turn results in better protection of the nanoparticles from the negative effect that the solvent alone (water) can have on the luminescence efficiency.

The water-soluble nanoparticles were subjected to TEM investigations (Figure 3.4.3).

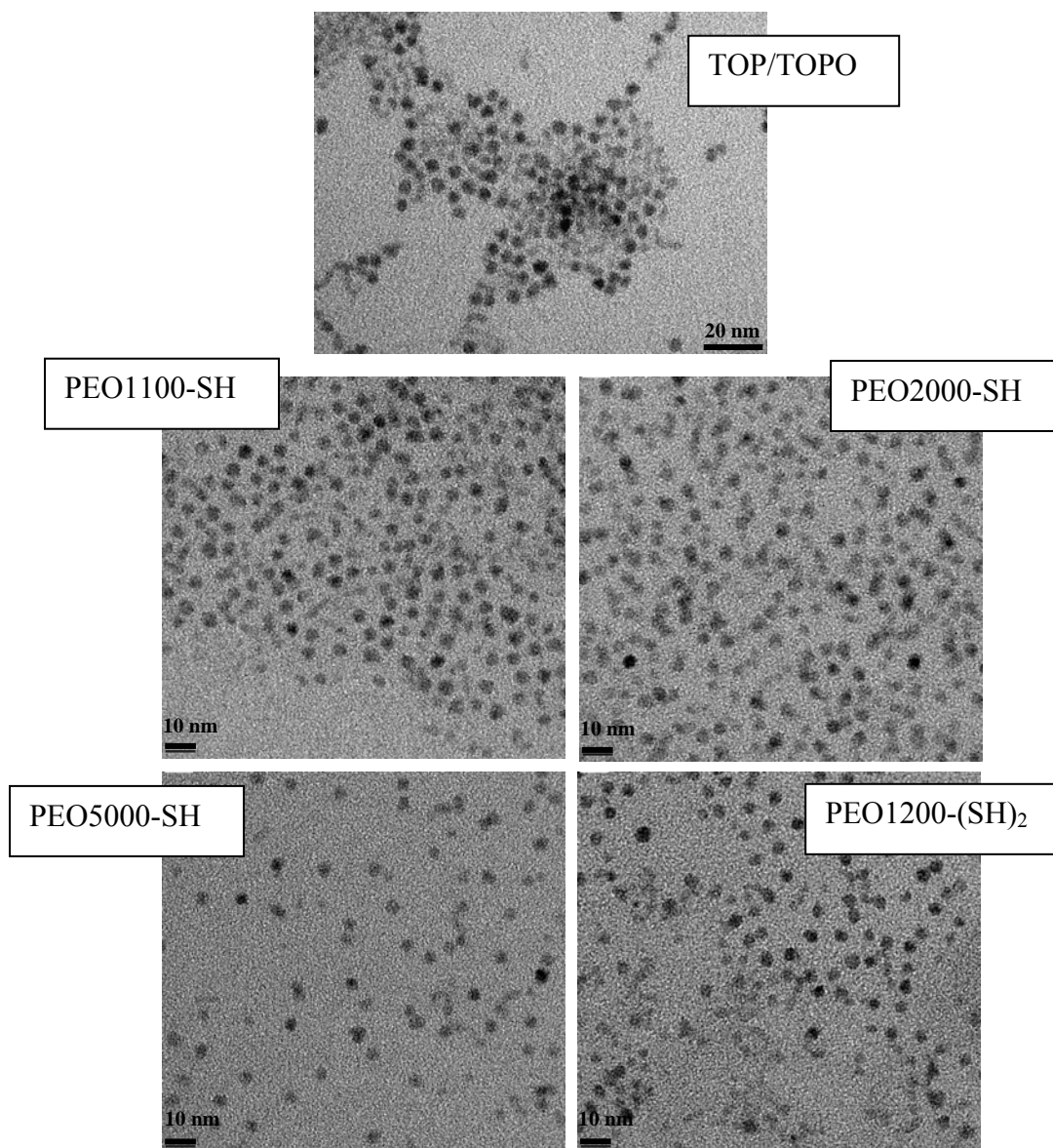


Figure 3.4.3. TEM images of the CdSe/CdS nanoparticles in chloroform (with TOP/TOPO ligands) and in water after ligand exchange with different SH-containing polymers

As can be seen from Figure 3.4.3 and as expected from the peak position in the absorption spectra, the size of the nanoparticles is not altered by the ligand exchange and phase transfer. Although the distance between the nanoparticles with a polymeric shell is larger compared to the distances observed for nanoparticles covered with TOP/TOPO, no tendency was observed with increasing polymer chain length, since the distribution of the nanoparticles on the TEM grid was very irregular.

In order to see how the different polymer coatings influence the size of the nanoparticle-polymer conjugates, DLS measurements were performed in chloroform and in water after ligand exchange (Figure 3.4.4.).

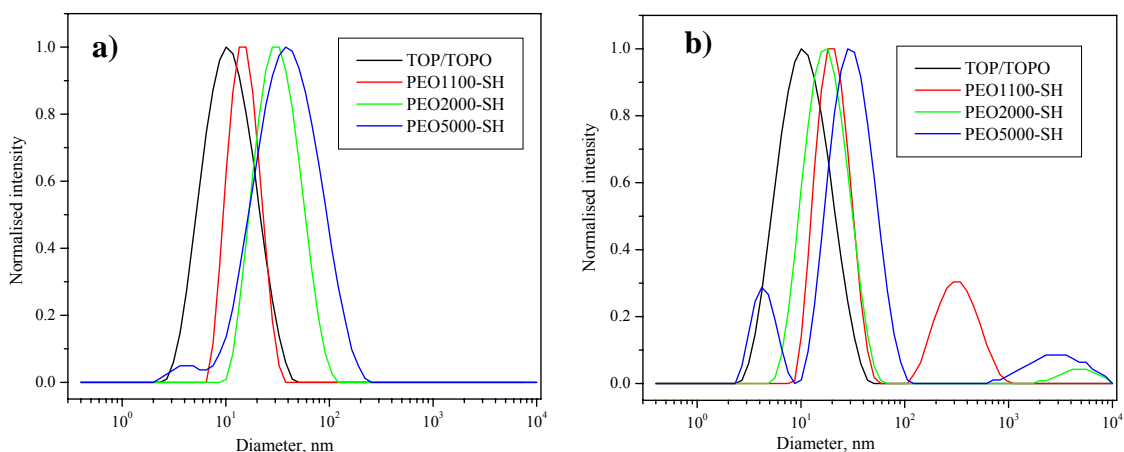


Figure 3.4.4. Size distribution of the CdSe/CdS nanoparticles before and after ligand exchange dispersed in a) chloroform and b) water

As stated in section 3.3.4, the values of the hydrodynamic radii observed in these measurements cannot be taken as absolute, however trends are clearly observed. After the ligand exchange had been performed and the nanoparticles re-dispersed in chloroform (Figure 3.4.4 a), an increase in the hydrodynamic radii was observed, which follows the trend of increasing molecular weight of the ligands. This indicates that successful ligand exchange by polymeric ligands had occurred. When the nanoparticles were dispersed in water, peaks appearing at higher values in the DLS plot for the nanoparticles stabilised with PEO5000-SH, indicate some agglomeration. However, they are not the dominating structures present in the solution, as judged by the number distribution (not presented).

Interestingly, the hydrodynamic radii measured in water were lower compared to the values obtained in chloroform, except for the nanoparticles covered with PEO1100-SH, where an increase in the hydrodynamic radii was observed. At this moment, it is not clear what the origin of these differences is and whether they can be attributed to the somewhat different preparation of the samples in chloroform and in water. The aqueous solutions had to be centrifuged for a long time before the measurements in order to remove traces of agglomerates present in the solution, since the DLS measurements are extremely sensitive to any traces of larger size agglomerates. The most important information that can be extracted from these measurements is, however, that the hydrodynamic radii of a nanoparticle-polymer conjugate should not exceed 15 nm (the value for the nanoparticle-[PEO5000-SH]), which determines the possible future use of the obtained conjugates in biological experiments.

The observation that the nanoparticles stabilised with mono-SH-PEO were stable for months, while the nanoparticles stabilised with mono-amino-PEO precipitated within a day is a consequence of the stronger thiol-Cd than amino-Cd bonding. However, the strong hydrogen bonding which can be formed between the amino group and the water molecules should not be excluded as a factor leading to the less stable bonding between mono-amino-PEO and the nanoparticles. In order to compare the stability of the two types of nanoparticle-PEO conjugates, the luminescence was followed with time for both conjugates. Long-term experiments with dilute and concentrated aqueous solutions of nanoparticles covered with different ligands were performed (Figure 3.4.5.).

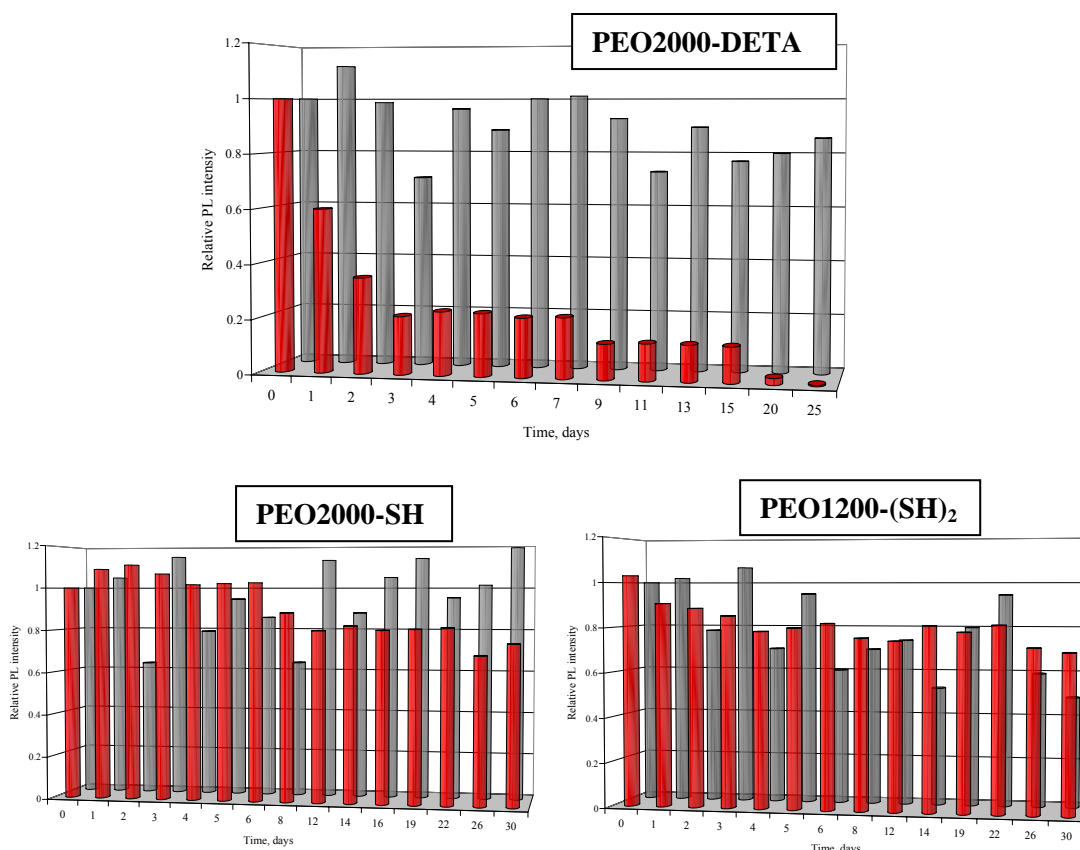


Figure 3.4.5. Relative PL intensities changes with time of CdSe/CdS nanoparticles stabilised with different polymeric ligands in dilute (■) and in concentrated (■) aqueous solutions

In the case of amino-functionalised polymer, a continuous decrease in the luminescence was observed for the nanoparticles in dilute solution. The gradual loss of ligands via desorption in the dilute solution is the probable cause of the loss of luminescence. Only in the case of this polymer was a shift to higher transition energies in the absorption spectra with time observed (not presented), indicating a deterioration of the nanoparticles with the loss of ligand.<sup>140</sup> On the other hand the luminescence of the nanoparticles in concentrated solution, although with some variation, was not strongly affected in the time frame of 25 days. In the case of nanoparticles stabilised with mercapto-functionalised polymers, the luminescence changed in the same manner independently of the storage conditions. A drastic decrease in the luminescence and change in the absorption features for dilute solution were not observed within 30 days. All the samples of the water-soluble

nanoparticles were prepared with the same polymer/nanoparticle ratio, leading to the conclusion that the observed difference between nanoparticles stabilised with mercapto- or amino-functionalised polymers are a consequence of the stronger binding of the mercapto groups compared to the amino groups. The reason for such a difference between these two ligands can also be interaction with the solvent. Thus, while amino groups associate readily by hydrogen bonding and form a hydrogen bond with water as well, this is not the case for the thiol group, which shows little tendency to associate by hydrogen bonding. It would be expected, if the only factor affecting the luminescence is the desorption of polymeric ligands, that the polymer bearing two SH groups should show improved stability compared to the monodendate polymer having only one binding group. However, the luminescence changes for the nanoparticles stabilised with PEO1200-(SH)<sub>2</sub> were comparable or slightly worse compared to the nanoparticles stabilised with PEO2000-SH. The fact that the luminescence changed in the same manner for both the concentrated and dilute solutions indicates that some other processes other than desorption of the ligand are responsible for the changes in the luminescence of the nanoparticles with PEO1200-(SH)<sub>2</sub>.

It may be concluded that, while both types of nanoparticle-polymer conjugates (amino- and mercapto-stabilised) are stable in concentrated solutions, the nanoparticles stabilised with mercapto-functionalised PEOs are more robust and less sensitive to concentration changes.

Although thiols are very widely used to stabilise nanoparticles in water, thiol-capped nanoparticles show very low photochemical stability in solution. In a study of the photochemical instability of thiol-stabilised nanoparticles, it was found that the deterioration process of thiol-stabilised CdSe nanoparticles proceeds in three steps: photocatalytic oxidation of the thiol ligands (which is the main reason for the poor stability of thiol-stabilised nanoparticles), photooxidation of the nanocrystals and the precipitation of the nanocrystals as a result of the first two processes.<sup>59</sup> The diffusion of oxygen through the organic coating of the nanoparticles was found to be the rate-determining step in the photooxidation of the nanocrystal-ligand complexes, since nanoparticles coated with longer carbon chain ligands show improved stability.

Following this line of argumentation, polymer-coated nanoparticles should be more stable than nanoparticles stabilised with small molecule thiols, such as mercaptopropionic acid. Photooxidation experiments were performed on the nanoparticles stabilised with different ligands by illuminating the solution of colloids and following the changes in the absorption characteristics of the nanoparticles. Upon exposure to light, the nanocrystals become smaller due to their degradation and a blue shift in the size-dependent absorption spectrum was observed. Simultaneously, the absorbance (optical density, OD) at the maximum of the first absorption peak decreased, also due to the decrease in the size of the nanoparticles. As an example of the changes in the absorption characteristics with illumination time, the absorption spectra of the nanoparticles covered with PEO1100-SH are presented in Figure 3.4.6.

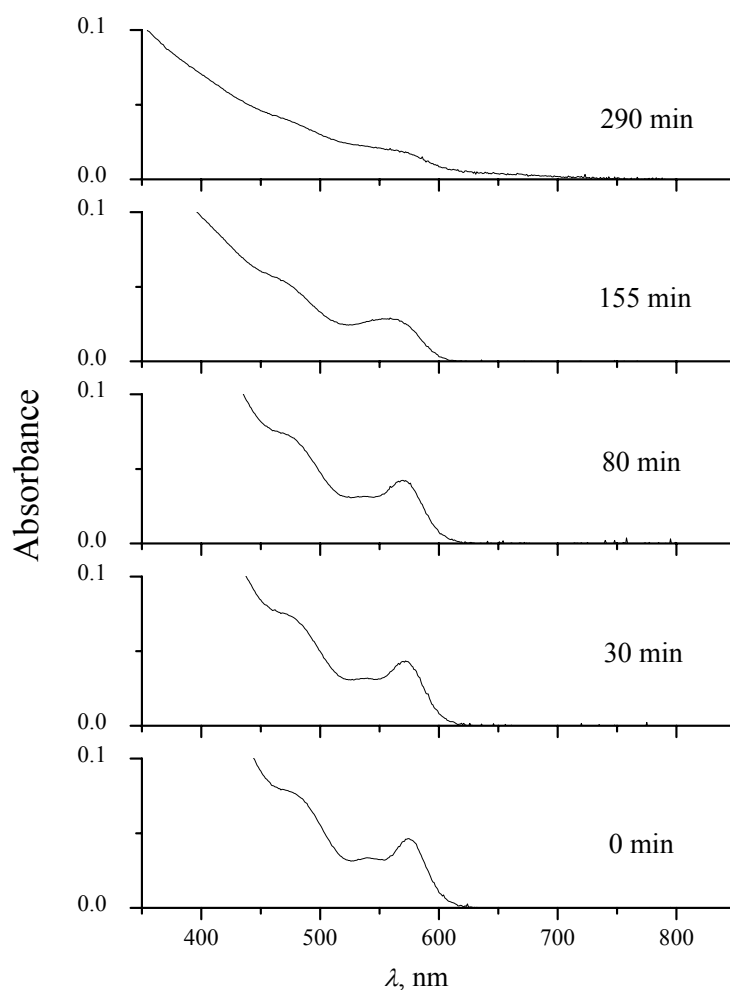


Figure 3.4.6. Temporal changes of the absorption spectra of PEO1100-SH stabilised CdSe/CdS nanoparticles in water upon illumination

The temporal evolution of optical density was followed for different nanoparticle-polymer conjugates up to the point of precipitation (in the case where it occurred), which can be seen as the non-zero base line (upper spectrum in Figure 3.4.6.). The temporal evolution of the optical density at the maximum of the first absorption peak of nanoparticles covered with different ligands is illustrated in Figure 3.4.7. Nanoparticles covered with long polymeric ligands were compared with nanoparticles stabilised with mercaptopropionic acid (MPA). It was found that the stability of the nanoparticles increased with increasing excess of the thiol ligands present in the solution, since the first oxidation step involves the oxidation of the ligands themselves.<sup>59</sup> The sample of nanoparticles in water stabilised with MPA containing free MPA was also included in the study (sample: MPA+extra MPA in Figure 3.4.7). The amount of added excess MPA, expressed as the ligand/nanoparticle ratio, was ten times higher in this case than the polymer/nanoparticle ratio used in the ligand exchange procedure.

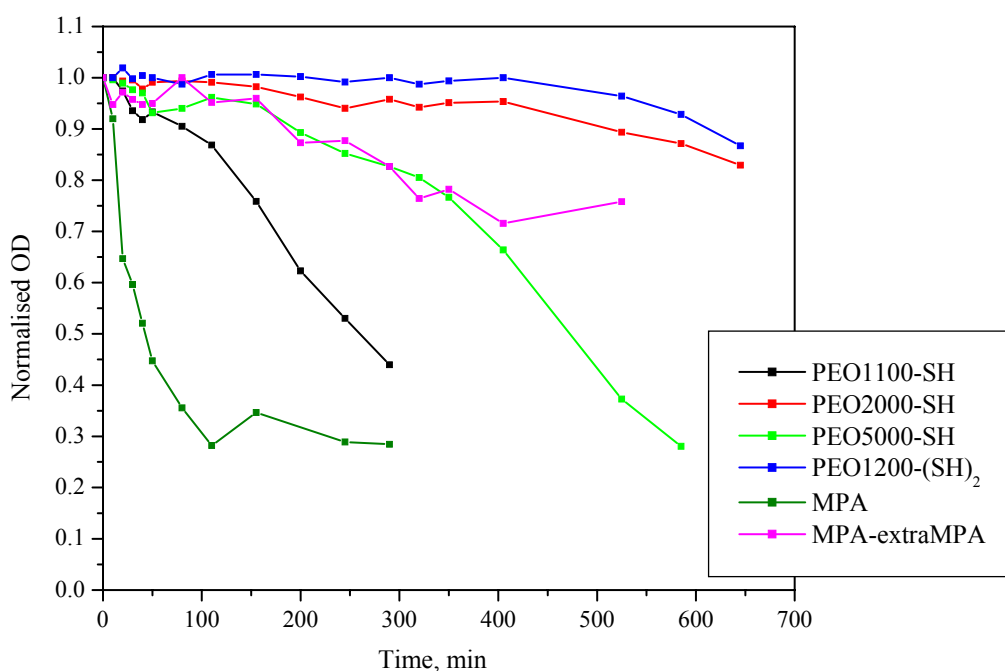


Figure 3.4.7. Temporal decrease of the OD at the first absorption maximum of CdSe/CdS nanoparticles stabilised with different ligands upon illumination

Nanoparticles covered with MPA are the least stable of all the investigated samples. With the addition of free MPA, as expected, the stability improved. The initiation period, the time before which no degradation of the nanoparticles was observed due to the degradation of the thiol ligands alone, increased with increasing amount of free ligands available in the solution, which replace the ones that have formed disulfides in the first degradation step.

Of all the samples stabilised with polymeric ligand, the least stable was the one with the polymer of the lowest molecular weight. This result corresponds to the findings that by increasing the length of the ligand chain, the stability is improved, due to the hindered diffusion of oxygen to the surface of the nanoparticle, where the photooxidation processes occur. In this respect, the most stable nanoparticle-polymer conjugates should be the ones covered with PEO5000-SH. However, although more stable than the nanoparticles covered with PEO1100-SH, the nanoparticles covered with this ligand start to decompose earlier than nanoparticles covered with PEO2000-SH. According to the proposed mechanism, the nanoparticles commence to degrade when there is no longer free ligand available in the solution to replace the transformed ones. When high molecular weight ligands are used, the dynamics of the exchange of the ligands on the nanoparticle surface also become an important factor in the determination of the overall dynamics of the photooxidation. A reasonable assumption is that the exchange of ligands which have undergone degradation and new ones from the solution is hindered in the case of the PEO5000-SH ligand, and the nanoparticles themselves start to degrade earlier, although at a lower rate than when they are covered with PEO1100-SH, due to the slower diffusion of oxygen.

Contrary to previous findings for low molecular weight thiols, i.e., that nanoparticles covered with dithiols are less stable than those covered with monothiols, nanoparticles covered with polymers of a similar molecular weight were more stable when the ligand possessed two binding thiol groups. The proposed explanation that dithiols cannot pack as densely as monothiols does not hold for polymeric ligands. It can be assumed that the packing density is determined by the size of the polymer chain rather than the steric hindrance imposed by the binding part of the molecule, which is the determining factor in the packing of small molecules. Thus, for polymers of similar molecular weight

PEO1100-SH and PEO1200-(SH)<sub>2</sub> the packing density should be similar, resulting in a higher concentration of -SH groups connected to, or in the vicinity, of Cd sites on the surface of the nanoparticle, in the latter case. The observed difference in the photooxidation dynamics between the two nanoparticle-polymer conjugates can, thus, be the consequence of a higher local concentration of thiol groups next to the surface of the nanoparticle, which undergo photooxidation to disulfide before the degradation of the nanoparticles themselves commences.

In order to gain further understanding and to prove the above-stated hypothesis concerning the different behaviour of the nanoparticle-polymer conjugates, a more thorough investigation of their photo stability is necessary. However, from the results presented above, it can be concluded that, as expected, due to the thicker organic shell, nanoparticles covered with polymeric ligands are more stable than those capped with low molecular weight thiols. Since the amount of free ligand available in the solution plays a dominant role in determining the stability of nanoparticles stabilised with small molecules, the influence of the amount of polymer employed in the ligand exchange was investigated. The temporal evolution curves of the OD at the first absorption maximum during the illumination of nanoparticles with different contents of polymeric ligand are presented in Figure 3.4.8.

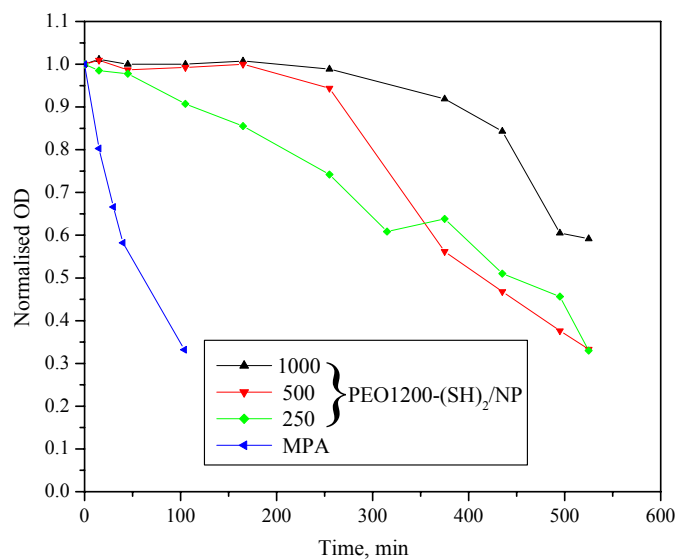


Figure 3.4.8. Temporal decrease of the OD at the first absorption maximum of water-soluble CdSe/CdS nanoparticles obtained with different PEO1200-(SH)<sub>2</sub>/nanoparticle ratios during the ligand exchange and MPA-coated nanoparticles

With decreasing polymer/nanoparticle ratio during the ligand exchange, the stability of the nanoparticles deteriorated. Assuming that there was no free MPA in the solution and a full coverage of nanocrystals of 3.0 nm diameter, the total amount of MPA per nanoparticle should be no more than 300, which is comparable with the lowest amount of polymeric ligand per nanoparticle employed in the ligand exchange. Even for this lowest ligand/nanoparticle ratio, the nanoparticles coated with polymeric ligand are more stable (longer initiation period and slower degradation of nanoparticles) than those coated with MPA.

### 3.4.2 Ligand exchange with branched mercapto-functionalised poly(ethylene oxide)

In the further development of ligands which could effectively stabilise nanoparticles in water, PEO-based molecules with SH binding groups and an additional hydroxyl functionality at the other molecule end were synthesised. The hydroxyl functionality at the outer shell of the nanoparticle could serve for a further functionalisation and the

choice of the end product is versatile. Recently, a successful transformation of the OH terminal group at gold nanoparticle surface to ester, carbamate, carboxylic acid, nitrite and aldehyde groups in high yield and without any deleterious effects on the nanoparticles themselves was demonstrated.<sup>130</sup>

The synthesised ligands differ in the number of SH binding groups and the number of PEO chains per molecule (Figure 3.4.9).

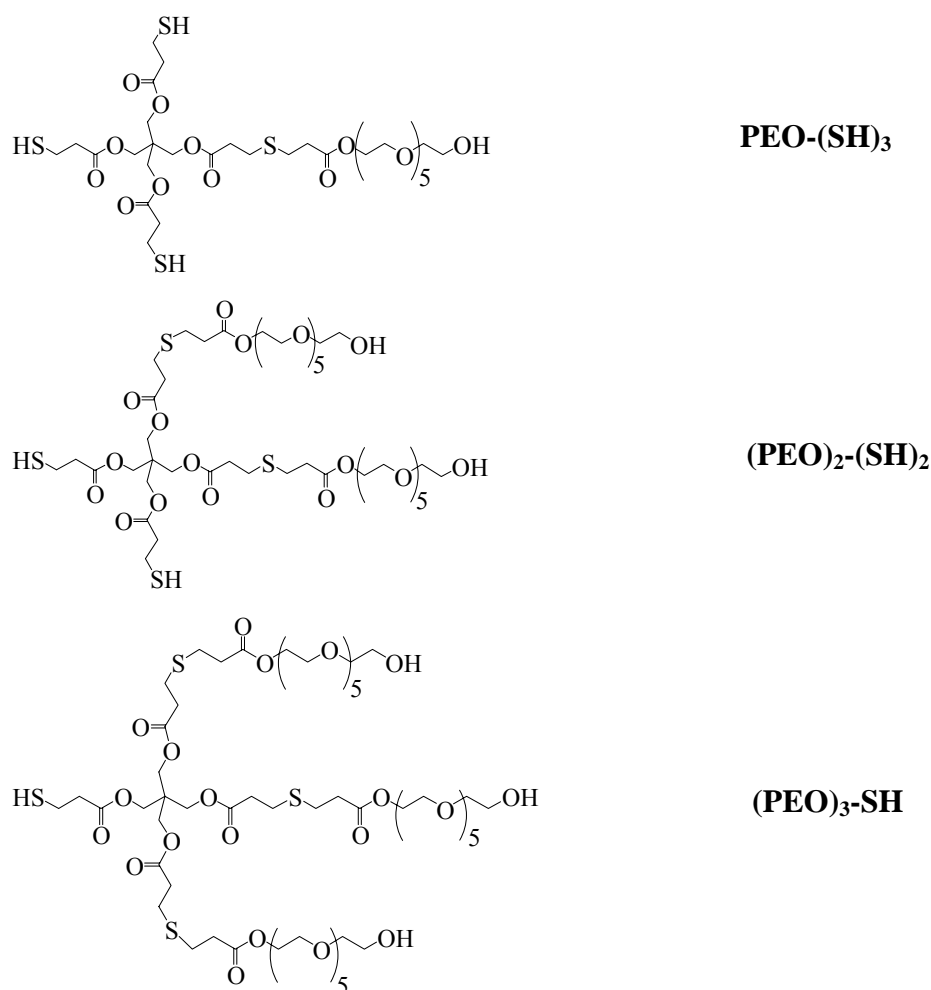


Figure 3.4.9. Structural formulas of mercapto-functionalised PEOs with a branched structure

The solubility properties of the synthesised ligands in water depend on the structure of the ligand, i.e., the balance of hydrophilicity/hydrophobicity. Aqueous solutions of these ligands exhibit a lower critical solution temperature (LCST) transition at different

temperatures depending on the structure of the molecule; above this temperature, the solubility of the ligand is reduced and the solution undergoes phase separation. Aqueous poly(ethylene oxide) solutions alone are known to exhibit such a behaviour with a LCST generally in the range 100-200 °C, with the position of the LCST shifting to higher values with decreasing molecular weight, and completely disappearing for PEO oligomers.<sup>141</sup> As far as the room temperature solubility of the present ligands is concerned, the ligand containing only one PEO chain per molecule is not soluble in water at room temperature, but its solubility is improved by lowering the temperature. The ligand with two PEO chains is completely soluble in water at slightly lower temperatures than room temperature, while the ligand with three PEO branches is completely soluble in water at room temperature. Thus, the structure and behaviour of the ligands resemble those of non-ionic surfactants, such as poly(ethylene oxide)alkyl ethers,  $\text{CH}_3(\text{CH}_2)_m(\text{OCH}_2\text{CH}_2)_n\text{OH}$ . They also exhibit a LCST behaviour in water with a phase diagram very similar to that of the PEO-water system, only with lower values of the LCST, in the range 0-100 °C.<sup>142,143</sup> The LCST values for non-ionic surfactants, similar to here, increase with increasing contribution of the hydrophilic part.

The same method for the ligand exchange and transfer into the water used for all the polymeric ligands was also applied for these ligands. The solubility of the ligand determined the solubility of the nanoparticles. However, in the case of the ligand with two PEO branches,  $(\text{PEO})_2\text{-(SH)}_2$ , which was insoluble in water at room or elevated temperatures, the nanoparticles covered with this ligand were completely soluble independent of the temperature (Figure 3.4.10). This behaviour will be discussed later with the results of the dynamic light scattering (DLS) measurements



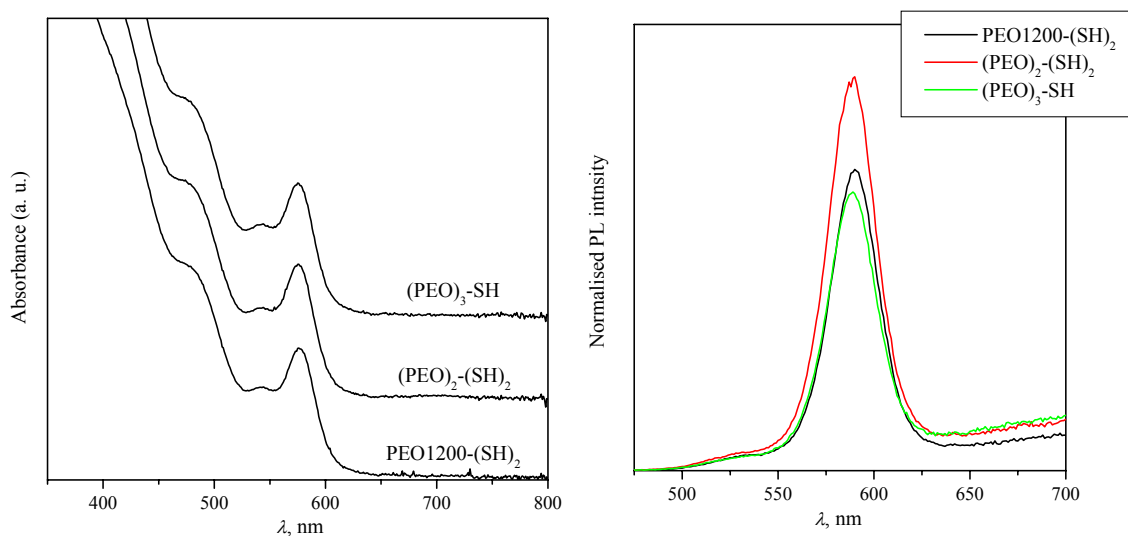


Figure 3.4.11. Absorption and luminescence spectra of water-soluble CdSe/CdS nanoparticles covered with different mercapto-functionalised PEOs

Due to the binding through the mercapto group, as expected, the luminescence intensities are of the same order of magnitude as those observed for linear mercapto-functionalised PEOs.

The size of the nanoparticle-polymer conjugate is much smaller compared to other nanoparticle-polymer conjugates investigated so far. This is to be expected since the polymer coating is thinner in the case of the branched mercapto-functionalised ligands.

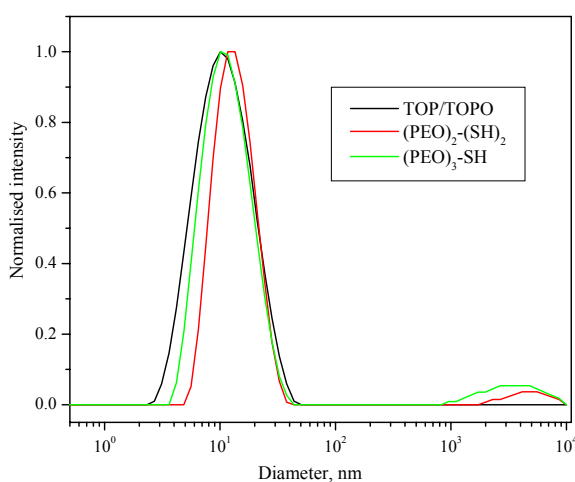


Figure 3.4.12. Size distribution of CdSe/CdS nanoparticles in chloroform (TOP/TOPO) and in water after ligand exchange with branched mercapto-functionalised PEOs

As can be seen in Figure 3.4.12, the hydrodynamic radii do not change much after ligand exchange, and are below 10 nm. However, as previously stated, the values obtained should not be taken as absolute values. With an increasing number of branches, the hydrodynamic radii do not increase further, rather a ‘shrinking’ is observed, for which there is no apparent explanation. The presence of large diameter species is almost certainly the consequence of dust in the aqueous solutions. It is well known that polar solvents, especially water, are much more difficult to obtain dust-free than non-polar solvents such as chloroform.

The aqueous solutions of nanoparticles covered with  $(\text{PEO})_2\text{-(SH)}_2$  and of the ligand alone were subjected to DLS measurements at different temperatures (Figure 3.4.13). The amounts of water used for the preparation of the solutions were chosen such that the amount of  $(\text{PEO})_2\text{-(SH)}_2$  in both solutions, with and without nanoparticles, should be the same, under the assumption that the loss of ligand through the ligand exchange process was negligible. The concentration of free  $(\text{PEO})_2\text{-(SH)}_2$  is, however, lower in the solution of the nanoparticle- $[(\text{PEO})_2\text{-(SH)}_2]$  conjugate. If loss of ligand occurred during the ligand exchange process, then the concentration of the free ligand would be even lower. The behaviour observed for the nanoparticle- $[(\text{PEO})_2\text{-(SH)}_2]$  conjugate solution is then inherent only to the conjugate.

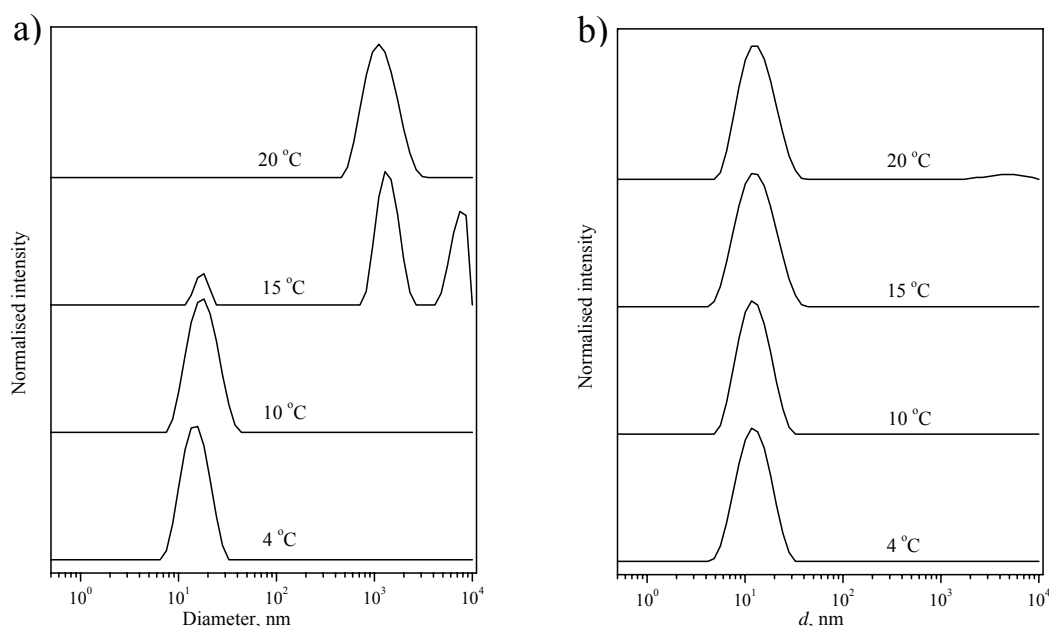


Figure 3.4.13. The changes in the size distribution with increasing temperature in aqueous solutions of a)  $(\text{PEO})_2\text{-(SH)}_2$  ligand and b) CdSe/CdS nanoparticles covered with this ligand

Contrary to that observed for the ligand alone, the sizes observed in the solution of nanoparticles did not change with increasing temperature (Figure 3.4.13). The aqueous solution of the ligand underwent a phase transition between 10-15 °C. Below this temperature, a single peak was observed at 11 nm. This value is too large to correspond to a single molecule of  $(\text{PEO})_2\text{-(SH)}_2$  and can be the consequence of an overestimation of the size by DLS, as was already observed for nanoparticles in chloroform, and has already been reported for the same technique and equipment in this size region.<sup>144</sup> On the other hand, it can be speculated that the  $(\text{PEO})_2\text{-(SH)}_2$  forms micelles below the LCST, where the hydrophobic part of the molecule interacts to form a core, as is the case for alkyl PEO non-ionic surfactants. With increasing temperature, the hydrophobic interaction becomes dominant, which leads to increasing size of the micelle and ultimately aggregate formation.<sup>145</sup> In the case of the nanoparticle-ligand conjugate, the ligands are tightly bound to the nanoparticle. The contribution of the core (nanoparticle with the hydrophobic part of the ligand) to the hydrophobic interaction is thus hindered and the nanoparticle-polymer conjugate behaviour is mainly determined by the

interaction of the PEO shell. In the case of the nanoparticle-[PEO-(SH)<sub>3</sub>] conjugate, a clear solution at room temperature was not obtained (Figure 3.4.10.). The nature of the aggregates formed at room temperature in this solution is not clear. A more detailed investigation would be necessary to reveal the behaviour of the nanoparticle-[PEO-(SH)<sub>3</sub>] conjugate.

Since the thickness of the organic coating influences the dynamics of the photooxidation processes to which nanoparticles covered with a mercapto-ligand are prone, a photochemical investigation was also performed on nanoparticles stabilised with branched mercapto-functionalised PEOs. The photochemical stability of nanoparticles stabilised with branched mercapto-functionalised PEOs was compared in a parallel experiment with the stability of nanoparticles covered with the linear PEO with two SH binding groups, as well as with MPA stabilised nanoparticles (Figure 3.4.14)

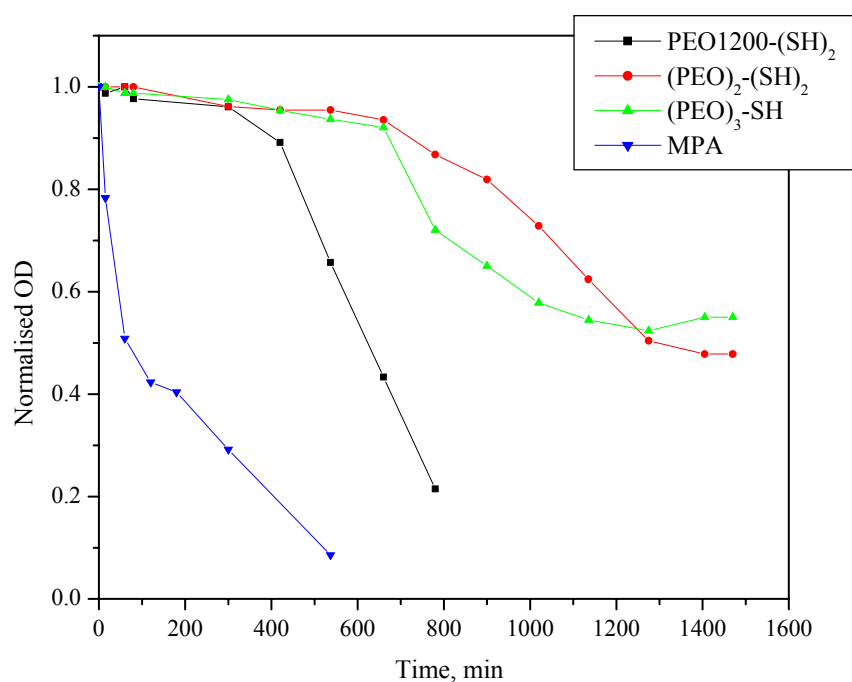


Figure 3.4.14. Temporal evolution of the OD at the first absorption maximum of CdSe/CdS nanoparticles stabilised with different mercapto-ligands

Although the molecular weights of the PEO part of the branched ligands are much smaller than that of the PEO part of the linear ligand, the stabilities of nanoparticles covered with branched ligands were slightly better. The branched structure and cone shape of these ligands can lead to better packing densities compared to the linear one, thus improving the diffusion barrier to oxygen. All the investigated nanoparticle-conjugates showed improved stability compared to the MPA coated nanoparticles.

The small size of the nanoparticles covered with branched ligands, improved stability compared to the MPA-coated nanoparticles, stronger binding of the ligand compared to the amino-functionalised PEOs and the existence of a suitable functionality at the outer organic shell highly recommends these nanoparticle-polymer conjugates for biomedical experiments.

## 4. Conclusion

The main focus of this work was the phase transfer of nanoparticles from non-polar organic solvents into water. The method chosen to achieve phase transfer was the exchange of the native capping ligands with water-soluble polymers. The employed polymers were based on highly water-soluble poly(ethylene oxide), PEO, which was functionalised so that it contained suitable functional groups which could bind to the nanoparticle. Amino and mercapto functionalities were used as binding groups.

This work deals mostly with the phase transfer of semiconductor nanoparticles based on CdSe. The CdSe nanoparticles were synthesised by the hot-injection technique in a “greener” chemical approach. The influence of the amount of phosphonic acid (tetradecylphosphonic acid, TDPA), employed as one of the coordinating ligands during the synthesis of CdSe, on the kinetics of the growth and properties of the CdSe nanoparticles was investigated. With decreasing amount of TDPA, the particle growth was faster, for very low amounts often uncontrollable, and the luminescence yields were lower. For all further syntheses of the CdSe nanoparticles used in this work, the highest investigated amount of TDPA investigated (0.9 wt%) was employed. The core CdSe nanoparticles were covered with an inorganic shell of CdS, a higher band gap material, to produce more robust CdSe/CdS nanoparticles. In addition, even more stable, CdSe/CdS/ZnS, core/shell/shell nanoparticles were synthesised using a one pot synthetic method. All the synthesised nanoparticles were characterised by absorption and luminescence spectroscopy, as well as XRD and TEM analysis.

To obtain poly(ethylene oxide) ligands possessing amino functional groups, two types of synthetic routes were utilised. In one, block copolymers poly(ethylene oxide)-*b*-(ethylene imine), PEO-*b*-PEI, were synthesised by the cationic ring opening polymerization of 2-ethyl-2-oxazoline, starting from tosyl-PEO as the macroinitiator. Three polymers with varying length of the PEI block (5, 10 and 20 PEI units) were synthesised. In the second approach, PEO was coupled with different amino group bearing molecules by the

diisocyanate coupling reaction. In the second approach, in addition to linear polymers, produced by coupling PEO and diethylenetriamine or pentaethylenehexamine, branched ones were also synthesized by coupling two PEOs to a small molecular weight PEI core. Ligands with mercapto groups as binding groups were also produced in two different ways. In the first approach, esterification of mercaptopropionic acid with PEO monomethyl ether was performed resulting in linear polymers of different length with a mercapto group at one end of the polymer chain. In this way, starting from PEO with two hydroxyl groups at one end of polymer chain, a ligand with two mercapto groups was also synthesised. PEO based ligands possessing more mercapto groups and with branched structures were prepared through the Michael type reaction between the acrylate end group of acrylate-functionalised PEO and the mercapto group of a molecule with four mercapto groups. Three types of ligands were produced with one two or three PEO branches possessing three, two or one mercapto group, respectively. The PEO ligands with mercapto and with amino functionalities were characterised by NMR spectroscopy and SEC, in order to confirm the desired structure.

Ligand exchange was achieved by exposure of the nanoparticles to a large excess of amino-functionalised PEO-based ligands. Subsequent addition of a non-solvent for the new capping groups enabled the nanoparticles covered with PEO to be separated from the native ligands. The obtained PEO covered nanoparticles were readily soluble in water, whereby all their properties were retained. The solutions of nanoparticles were stable for months and insensitive to a change in the ionic strength of the medium. In solutions of low pH values, the nanoparticles exhibited lower photoluminescence efficiencies due to the protonation of the amino groups, and such solutions were less stable than those of higher pH value. The luminescence efficiencies of nanoparticles transferred into water were generally lower compared to those of nanoparticles in chloroform. The efficiencies were not decreased only in the case of the ligand with a small binding part and with the lowest molecular weight PEO block, and were sometimes even higher than those measured for the nanoparticles in chloroform. Using the same method for ligand exchange, in addition to semiconductors, magnetic  $\text{Fe}_3\text{O}_4$  and  $\text{CoPt}_3$  nanoparticles could also be made water-soluble with the amino-functionalised PEOs.

Depending on the [amino-functionalised polymer]/nanoparticle ratio employed during the ligand exchange, which dictates the number of attached polymers to the nanoparticles, the structure of the nanoparticle-polymer conjugate can be directed. For low ratios, worm-like, while for the high ratios spherical conjugates were present in the respective aqueous solutions. The type of the structure can also be varied by changing the type of the employed ligand. The formation of worm-like conjugates is promoted when the binding amino part of the PEO ligand is small. All the observed changes could be qualitatively described by the packing parameter theory.

In an attempt to further increase the stability of the polymer-nanoparticle conjugate, the crosslinking reaction of the PEO2000-PEI-branched around the nanoparticles with hexamethylenediisocyanate was investigated. Although the reaction, which was followed by IR spectroscopy, was successfully performed without any deleterious effect on the nanoparticles, the stability, as judged from chemical and long-term stability experiments, was not improved. Further optimization of the ligand architecture, as well as the use of a more suitable crosslinking agent is necessary for the nanoparticles with a crosslinked polymeric shell to show better characteristics.

The same method for ligand exchange was applied in the case of mercapto-functionalised PEO ligands. Aqueous solutions of nanoparticles covered with mono-mercapto-functionalised PEOs were more stable than those containing nanoparticles bearing mono-amino ligands. This behaviour is due to the stronger binding of the mercapto group and its more difficult dissociation from the nanoparticle surface, which are the result of the less pronounced hydrogen bonding of the mercapto group. The luminescence efficiencies were lower for the nanoparticles stabilised with mercapto-functionalised PEOs, however, they were still high enough for these nanoparticles to be employed in further experiments of interest. The size of the nanoparticle-polymer conjugates, measured by dynamic light scattering, increased with increasing polymer chain length. Nanoparticles covered with branched PEO ligands of the smallest molecular weight exhibited hydrodynamic radii in water which were insignificantly larger than the hydrodynamic radii of the native nanoparticles in chloroform.

The photochemical stability of the nanoparticles covered with mercapto-functionalised PEOs was investigated and compared to the properties of nanoparticles covered with

mercaptopropionic acid. In all cases, nanoparticles covered with a dense polymer coating were more stable than the nanoparticles stabilised with mercaptopropionic acid.

The attachment of PEO based ligands, different with respect to the binding group and the overall molecular architecture, to nanoparticles allows for the properties of the nanoparticle-polymer conjugate to be chosen as desired. The different ligand molecular architecture also allows the final structure of the conjugate to be predicted and dictated.

## 5. Zusammenfassung

Zentraler Punkt dieser Arbeit war der Phasentransfer von Nanopartikeln aus unpolaren Lösungsmitteln in wässrige Lösungen. Die zum Phasentransfer gewählte Methode tauscht die ursprünglichen Liganden gegen wasserlösliche Polymere aus. Die verwendeten Polymere basierten auf wasserlöslichem Poly(ethylene oxid), PEO, welches so funktionalisiert wurde, dass es geeignete funktionelle Gruppen zur Bindung an die Nanopartikeloberfläche bekam. Amino- und Mercapto-funktionelle Gruppen wurden als bindende Gruppen verwendet.

Diese Arbeit beschäftigt sich hauptsächlich mit dem Phasentransfer von auf CdSe basierenden Halbleiternanopartikeln. Die CdSe Nanopartikel werden durch die „hot-injection“-Technik mittels einer „grüneren“ Methode synthetisiert. Der Einfluss des Anteils an Phosphonsäure (tetradecylphosphonic acid, TDPA), die bei der Synthese von CdSe als koordinierender Ligand wirkt, wurde in Hinblick auf die Kinetik des Wachstums und die Eigenschaften der CdSe Nanopartikel erforscht. Mit sinkendem TDPA Anteil konnte eine Beschleunigung des Partikelwachstums beobachtet werden (wobei ein sehr geringer TDPA Anteil zu einem unkontrollierten Reaktionsverlauf führt), während die Quantenausbeute abnahm. Für alle weiteren, im Rahmen dieser Arbeit angefertigten Synthesen wurde der höchste TDPA Anteil (0.9 Gew.-%) verwendet. Um robustere CdSe/CdS Nanopartikel herzustellen wurde der CdSe Kern der Nanopartikel mit einer anorganischen CdS Hülle, einem Material mit größerer Bandlücke, beschichtet. Außerdem wurden noch stabilere CdSe/CdS/ZnS core/shell/shell Nanopartikel über eine „one pot synthesis“ hergestellt. Alle synthetisierten Nanopartikel wurden über Absorptions- und Lumineszenzspektroskopie, XRD und TEM charakterisiert.

Zur Herstellung von Poly(ethyleneoxid) Liganden, die funktionelle Aminogruppen enthalten wurden zwei Synthesewege eingesetzt. Einerseits wurden die Blockcopolymere Poly(ethyleneoxid)-*b*-(ethyleneimin), PEO-*b*-PEI, durch kationische Ringöffnungspolymerisation von 2-Ethyl-2-oxazolin hergestellt, wobei Tosyl-PEO als

Makroinitiator wirkte. Drei verschiedene Polymere mit unterschiedlicher Länge des PEI Blocks (5, 10 und 20 PEI Einheiten) wurden synthetisiert. Andererseits wurde PEO durch eine Diisocyanat-Kupplungs-Reaktion mit verschiedene Aminogruppen enthaltenen Molekülen verbunden. Außerdem wurden, neben linearen Polymeren durch Kupplung von PEO an Diethylentriamin oder Pentaethylenhexamin, auch verzweigte, durch Kupplung von zwei PEOs an einen PEI-Kern mit kleinerem molekularem Gewicht, hergestellt.

Liganden mit Mercaptogruppen als bindende Gruppe wurden ebenfalls über zwei Methoden hergestellt. Bei dem ersten Ansatz wurde Mercaptopropionsäure an PEO-Monomethylether gebunden, was lineare Polymere unterschiedlicher Länge mit einer Mercaptogruppe an einem Ende der Polymerkette ergab. Auf diese Weise wurden auch Liganden mit zwei Mercaptogruppen hergestellt, wobei von PEO mit zwei Hydroxylgruppen an einem Ende der Polymerkette ausgegangen wurde. Auf PEO basierende Liganden mit mehreren Mercaptogruppen und verzweigter Struktur wurden über eine Michael-Reaktion zwischen der Acrylat-Endgruppe von Acrylat-funktionalisiertem PEO und der Mercaptogruppe eines Moleküls mit vier Mercaptogruppen hergestellt. Drei verschiedene Typen von Liganden mit ein, zwei oder drei PEO Verzweigungen, die entsprechend drei, zwei oder eine Mercaptogruppe enthielten wurden synthetisiert. Die Charakterisierung der PEO Liganden mit Mercapto- und Amionfunktionalisierung erfolgte über NMR Spektroskopie und GPC, um die gewünschte Struktur zu bestätigen.

Der Ligandenaustausch wurde bei einem hohen Überschuss an aminofunktionalisierten Liganden durchgeführt. Die Zugabe von Fällungsmittel für die neuen stabilisierenden Liganden ermöglichte eine Abtrennung der ursprünglichen Liganden. Die erhaltenen, mit PEO stabilisierten Nanopartikel sind gut in Wasser löslich, wobei alle ihre Eigenschaften erhalten bleiben. Die kolloidalen Nanopartikel Lösungen sind über Monate stabil und unempfindlich gegenüber der Ionenstärke der Lösung. In Lösungen mit einem niedrigen pH-Wert haben die Nanopartikel, bedingt durch Protonierung der Aminogruppen, geringere Photolumineszenzen, wodurch die Lösungen eine geringere Stabilität als bei höherem pH-Wert besitzen. Die Photolumineszenz der in Wasser transferierten Nanopartikel sind generell geringer im Vergleich zu denen von Nanopartikeln in

Chloroform. Nur im Falle von Liganden mit kleinerem Bindungsblock und kurzen PEO Block wird die Photolumineszenz nicht gesenkt. Sie ist manchmal allerdings sogar höher als jene von in Chloroform gemessenen Partikeln. Die gleiche Methode für den Ligandenaustausch wurde neben Halbleitern auch bei magnetischen  $\text{Fe}_3\text{O}_4$  und  $\text{CoPt}_3$  Nanopartikeln angewendet um mittels aminofunktionalisierten PEOs wasserlösliche Partikel zu erhalten.

In Abhängigkeit von dem [Amino-funktionalisiertes Polymer]/Nanopartikel Verhältnis während des Ligandenaustausches, was die Anzahl von den an die Nanopartikel bindenden Polymeren angibt, kann die Struktur der Nanopartikel-Polymer Konjugate beeinflusst werden. Bei einem niedrigen Verhältnis bilden sich wurmförmliche, während bei einem hohen Anteil sphärische Konjugate in der wässrigen Lösung beobachtet werden. Die Struktur kann ebenfalls durch den verwendeten Liganden-Typ gesteuert werden. Die Ausbildung von wurmförmlichen Konjugaten wird gefördert, wenn der bindende Aminoblock klein ist. Alle beobachteten Änderungen können qualitativ durch das Packungsparameter Modell beschrieben werden.

Für eine weitere Steigerung der Stabilität von Polymer-Nanopartikel Konjugaten wurde eine vernetzende Reaktion zwischen den die Nanopartikel umgebenden verzweigten PEO2000-PEI Einheiten mit Hexamethylendiisocyanat untersucht. Obwohl die Reaktion, die durch IR-Spektroskopie charakterisiert wurde, erfolgreich verlief ohne Beeinträchtigung der Nanopartikel, konnte die Stabilität, wie nach chemischen und Langzeitstabilitätstests beurteilt werden konnte, nicht gesteigert werden. Eine weitere Optimierung der Ligandenarchitektur und der Einsatz eines geeigneten Vernetzungsmittels sind erforderlich um bessere Charakteristiken von Nanopartikeln mit vernetzter organischer Hülle zu erhalten.

Die gleiche Ligandenaustausch Methode wurde im Fall der Mercapto funktionalisierten PEO Liganden eingesetzt. Wässrige Lösungen von Nanopartikeln, die mit Mono-Mercapto-funktionalisiertem PEO umgeben werden, erwiesen sich als stabiler als die mit Mono-Amino Liganden stabilisierte Nanopartikel. Dieses Verhalten resultiert aus der stärkeren Bindung von Mercaptogruppen und die dadurch schwierigere Dissoziation von der Nanopartikeloberfläche, was ein Resultat der weniger starken Wasserstoffbrückenbindungen von Mercaptogruppen ist. Die Lumineszenz ist geringer

für Nanopartikel, die mit Merkupto-funktionalisiertem PEO stabilisiert wurden. Trotzdem ist sie auch in diesem Fall für Nanopartikel noch hoch genug, um sie für weitere interessante Experimente einzusetzen. Die Größe der Nanopartikel-Polymer-Konjugate wurde durch dynamische Lichtstreuung ermittelt und steigt bei längerer Polymerkette. Nanopartikel, stabilisiert mit verzweigten PEO Liganden eines niedrigeren molekularen Gewichtes, weisen in Wasser unwesentlich größere hydrodynamische Radien auf, als in Chloroform gelöste Nanopartikel mit den ursprünglichen Liganden.

Die Photostabilität der Nanopartikel, die mit Merkupto-funktionalisiertem PEO stabilisiert sind wurde untersucht und mit den Eigenschaften von Nanopartikeln, beschichtet mit Mercaptopropionsäure, verglichen. In allen Fällen erwiesen sich Nanopartikel mit einer dichten Polymerhülle als stabiler im Vergleich zu den mit Mercaptopropionsäure stabilisierten Nanopartikeln.

Die Anlagerung von auf PEO basierenden Liganden, welche sich sowohl in Hinblick auf die Bindungsgruppe, als auch durch die Molekulare-Architektur unterscheiden, an Nanopartikel ermöglicht eine Einstellung der Eigenschaften von Nanopartikel-Polymer-Konjugaten. Die unterschiedliche Ligandenarchitektur ermöglicht ebenfalls eine Voraussage und Steuerung der finalen Struktur der Konjugate.

## 6. Experimental part

### 6.1 Synthesis procedures and methods

All chemicals used were of analytical grade or of the highest purity available. If not otherwise stated, all chemicals were used without further purification. All synthesis procedures were performed under an inert atmosphere using the Schlenk technique. The tosyl-terminated PEO, used as macroinitiator in the synthesis of block copolymers, was synthesized and kindly provided by Ute Liprand<sup>84</sup>. The mono-amino PEOs were not synthesised within the frame of this study. PEO500-NH<sub>2</sub> (Pluriol<sup>®</sup> A 520 A) is a commercial polymer from the BASF. PEO2400-NH<sub>2</sub> and PEO3200-NH<sub>2</sub> were synthesised and kindly provided by Michael Stoltzenburg<sup>146</sup>. Magnetic nanoparticles were synthesised and kindly provided by Maren Krack (Fe<sub>3</sub>O<sub>4</sub>)<sup>147</sup> and Vesna Aleksandrovic (CoPt<sub>3</sub>)<sup>148</sup>. Core/shell CdSe/ZnS nanoparticles were kindly provided by Dimitri Talapin.

#### 6.1.1 Synthesis of CdSe/CdS nanoparticles

Semiconductor CdSe/CdS nanoparticles were synthesized using the “greener” approach developed by Mekis<sup>64</sup>. In the first step, CdSe core nanoparticles were prepared. For this purpose, selenium and cadmium stock solutions were prepared and stored in a glove box. Selenium stock solution was prepared by dissolving 1.58 g of selenium (99.999%, ChemPur) in 20 ml of distilled tri-*n*-octylphosphine (TOP, 90%, Fluka) and the stock solution of cadmium-acetate was prepared by dissolving 0.80 g of cadmium-acetate (99.99 %, ChemPur) in 20 ml of TOP. In a typical procedure, 8 g of tri-*n*-octylphosphine oxide (TOPO, > 98%, Merck) were dried and degassed under vacuum at 180 °C for 1 h in a 50 ml three-necked flash. Then, TOPO was cooled to 100 °C, 5 g of hexadecylamine (HDA, > 92%, Merck) and 0.15 g of *n*-tetradecylphosphonic acid (TDPA, 99% Alfa

Aesar) were added. The drying procedure was continued at 120 °C under vacuum for 20 min. Selenium stock solution (2 ml) was added and the reaction mixture was heated to 300 °C. After reaching the nucleation temperature, 3 ml of the cadmium ion stock solution were injected under vigorous stirring. After the nucleation step, the reaction temperature was lowered to the growth temperature of 260 °C. Depending on the size of the nanoparticles required, the reaction time was varied.

A CdS shell was grown around CdSe by injection of H<sub>2</sub>S gas. The reaction mixture containing the freshly prepared CdSe nanocrystals was set to 140 °C. After the nitrogen flow was stopped, H<sub>2</sub>S gas was injected in 2 ml portions (1 injection every 15 min) through a septum into the stirred solution. Typically, a total amount of 8 ml was injected. After the H<sub>2</sub>S addition, the reaction mixture was stirred for a further 30 min. Then the nitrogen flow was recommenced, the temperature decreased to 100 °C and the solution was stirred for one more hour. After cooling to the 50 °C, 15 ml of chloroform were added to the solution. The obtained nanocrystals were precipitated using methanol and re-dissolved in chloroform. The chloroform solution of nanocrystals was filtered through a PTFE 0.2- $\mu$ m membrane filter. After filtration, the precipitation procedure was repeated two more times. For further use, the nanoparticle stock solution was filtered once more and stored at room temperature.

### **6.1.2 Synthesis of CdSe/CdS/ZnS nanoparticles**

As for the CdSe/CdS nanoparticles, the synthesis of CdSe/CdS/ZnS nanoparticles was performed by the injection of H<sub>2</sub>S gas<sup>69</sup>. In a typical procedure, a mixture of 0.3 g of zinc-acetate (99.99 % Aldrich) and 3 g HDA were dried and degassed at 130 °C under vacuum for 1 h and then added into a solution of freshly prepared CdSe/CdS nanoparticles at 90 °C. The mixture was heated to 220 °C, the nitrogen flow was stopped and total of 8-10 ml of H<sub>2</sub>S gas were injected in 2 ml portions (1 injection every 15 min) through a septum. After the H<sub>2</sub>S addition, the reaction mixture was cooled to 90 °C and stirred one more hour under a nitrogen flow. Then the solution was cooled to 50 °C and 15 ml of chloroform were added. The purification procedure was the same as in the case of the CdSe/CdS nanoparticles.

### 6.1.3 Synthesis of poly(ethylene oxide)-*b*-(ethylene imine) block copolymers

Poly(ethylene oxide)-*b*-(ethylene imine) block copolymers were synthesised by the cationic polymerization of 2-ethyl-2-oxazoline and further hydrolysis of the obtained poly(ethylene oxide)-*b*-(2-ethyl-2-oxazoline). As the macroinitiator for the cationic polymerisation, tosylated poly(ethylene oxide) (PEO-Ts) of 6080 g/mol was employed. The PEO-Ts macroinitiator was obtained by termination of the anionic polymerisation of ethylene oxide using the chloride of toluenesulphonic acid.<sup>84</sup>

**Synthesis of poly(ethylene oxide)-*b*-(2-ethyl-2-oxazoline), PEO-POxz.** In a 250 ml two-necked flask, 4 g of the PEO-Ts macroinitiator were lyophilised two times using benzene and finally dissolved in 20 ml of acetonitrile (freshly distilled over CaH<sub>2</sub>). To this solution, the amount required for the desired block length of freshly distilled 2-ethyl-2-oxazoline was added. The reaction mixture was stirred for 4 days at 80 °C. To terminate the reaction, 1.2 equivalents of piperidine were added and the reaction mixture was stirred for two more hours at 80 °C. The obtained polymer was precipitated using cold diethyl ether (– 40 °C) and dried at 40 °C under vacuum.

**Synthesis of poly(ethylene oxide)-*b*-(ethylene imine), PEO-PEI.** The obtained PEO-POxz was dissolved in 30 ml of water in a 250 ml round bottom flask. To this solution, 2 mol excess of concentrated hydrochloric acid was added and the reaction mixture was refluxed over night. The solution was neutralised using an anionic ion exchange resin (Lewatit 500, Bayer) at 60 °C. The final pH of the polymer solution after passing over the resin was 7-8. The polymer was freeze-dried and stored at room temperature before further use.

### 6.1.4 Synthesis of amino-functionalized poly(ethylene oxide) via the diisocyanate coupling reaction

**Synthesis of isocyanate terminated poly(ethylene oxide), PEO-NCO.** As an example, the synthesis of PEO-NCO using poly(ethylene oxide) monomethyl ether (Fluka) of 2000 g/mol molecular weight will be presented. In a two-necked flask equipped with a reflux condenser 2.22 g of freeze-dried PEO2000 were dissolved in 20 ml of chloroform. The chloroform had previously been treated with hexamethylenediisocyanate (HMDI,

Aldrich) for 4 h at 60 °C prior to distillation, in order to remove any traces of water and ethanol. To this chloroform solution, 4.50 ml (25 mol excess) of HMDI were added and the reaction mixture was refluxed for 24 h. After cooling to room temperature and concentration of the solution, the obtained PEO2000-NCO was precipitated twice in a 20-fold excess of cold diethyl ether. PEO2000-NCO was dried under vacuum at room temperature. In the case of PEO molecular weight of 5000 g/mol, the mol excess of HMDI was 50.

***Coupling of poly(ethylene oxide) with diethylenetriamine, PEO-DETA.*** The PEO-NCO obtained in the first step was further reacted with diethylenetriamine (DETA, >98 % Aldrich) to obtain two amino groups at one end of the polymer chain. Briefly, 2.0 g of PEO2000-NCO were dissolved in 20 ml of chloroform. To this solution, a solution of 9.44 ml DETA in 20 ml of chloroform was added stepwise over two hours at room temperature. The reaction mixture was kept at 40 °C for 2 h. The obtained PEO2000-DETA was precipitated twice from chloroform solution into a 20-fold excess of diethyl ether to remove unreacted DETA. For all other PEO-NCOs, the same reaction conditions were applied.

***Coupling of poly(ethylene oxide) with pentaethylenhexamine, PEO-PEHA.*** The procedure to obtain PEO-PEHA was the same as in the case of PEO-DETA. The mol excess of pentaethylenhexamine (PEHA, technical grade, Aldrich) was 100, as in the case of the shorter amine DETA.

***Coupling of poly(ethylene oxide) to branched poly(ethylene imine), PEO-PEI-branched.*** In a two-necked flask equipped with a reflux condenser, 1.6 g of PEO2000-NCO was dissolved in 20 ml of chloroform. To this solution, a solution of 0.159 g of poly(ethylene imine) (PEI 400 g/mol, Aldrich) in 20 ml of chloroform were added. The ratio of PEO to PEI was chosen to produce a polymer with two branches of PEO on one PEI core. The reaction mixture was stirred over night at 60 °C. After completion of the reaction, the PEO2000-PEI-branched was precipitated from chloroform into diethyl ether. For all other PEO-PEI-branched ligands, the same reaction conditions were applied.

### 6.1.5 Synthesis of poly(ethylene oxide)s with a mercapto end group

**Synthesis of PEOs with mercapto groups by esterification with mercaptopropionic acid, PEO-SHs.** To obtain PEO-SHs of different molecular weight, the OH end group of PEO was esterified using mercaptopropionic acid. The same procedure was applied for all PEOs, with different ratios of acid to PEOs for different molecular weight PEOs. As an example, the synthesis of PEO-SH of 2000 g/mol will be presented. In a 50 ml three-necked flask, 6.114 g of PEO2000 and 1.59 ml (6 mol excess) of 3-mercaptopropionic acid (MPA, Aldrich) were mixed. The reaction mixture was heated to 160 °C and stirred overnight at this temperature. After cooling to 60 °C, 5 ml of chloroform were added and the obtained PEO2000-SH was precipitated into a 50-fold excess of diethyl ether. The obtained white powder was dried under vacuum. For PEO of 1100 g/mol and 1200 g/mol (TEGOMER<sup>®</sup> D 3403, Degussa), a 3 mol excess and for PEO of 5000 g/mol, a 12 mol excess of MPA were used.

**Synthesis of PEOs with mercapto end groups via the Michael addition reaction, (PEO)<sub>x</sub>-(SH)<sub>y</sub>.** The Michael type reaction between the acrylate end group of poly(ethylene oxide) monoacrylate (Bisomer<sup>®</sup> PEA6, Laporte Performance Chemicals), PEO-Acrylate, and the SH groups of pentaerythritol tetrakis(3-mercaptopropionate) (Aldrich) was used to obtain molecules with different numbers of SH groups. The reaction was performed in bulk in the dark with pyridine as the catalyst. The chosen ratio of reactants determined the final molecular structure of the (PEO)<sub>x</sub>-(SH)<sub>y</sub>. In a typical procedure to about 2 g of PEO-Acrylate, the chosen amount of pentaerythritol tetrakis(3-mercaptopropionate) was added in a 25 ml three-necked flask. Pyridine was added in a predetermined amount and the reaction mixture was stirred under an inert nitrogen atmosphere for 24 h. After completion of the reaction, the pyridine was removed under reduced pressure. The obtained liquid polymers were stored in the dark before further use.

### 6.1.6 Ligand exchange procedures

**Ligand exchange with pyridine.** The solvent was removed under a nitrogen flow from 2 ml of concentrated nanoparticle solution in a 25 ml three-necked flask. To the obtained

solid, 5 ml of pyridine were added. The mixture was heated to 65 °C and stirred at this temperature for 2 h. After cooling to room temperature, hexane was added to precipitate the nanoparticles. After centrifugation, the supernatant was removed and the nanoparticle pellet was re-dissolved in 5 ml of pyridine and heated again. The procedure was repeated five times in order to remove as much as possible of the original TOP/TOPO ligands.

***Ligand exchange with mercaptopropionic acid.*** Mercaptopropionic acid stock solution was prepared by dissolving 50 mg of MPA in 15 ml of methanol. The pH value of the stock solution was adjusted to 10.6 by addition of trimethylammonium hydroxide. To 9.5 mg of the nanoparticle powder in a 25 ml three-necked flask, 10 ml of MPA stock solution were added under a nitrogen flow. The dispersed solid gradually dissolved in the reaction medium. In the dark, the reaction mixture was heated at 65 °C for 6 h, and further stirred at room temperature over night. The nanoparticles were precipitated out from the chloroform solution once with ethyl acetate and twice with diethyl ether. The final nanoparticle powder was dissolved in 2 ml of methanol and stored in the dark before further use. The obtained nanoparticles covered with MPA were readily soluble in polar organic solvents, such as alcohols and water.

***Ligand exchange with functionalized PEOs.***

*a) Exchange with pyridine covered nanoparticles as an intermediate step.* Pyridine capped nanoparticles were placed in a reaction vial and a chloroform solution of the polymeric ligands containing the desired amount of new capping groups were added. The chloroform and pyridine were evaporated under a nitrogen flow. The solid was re-dissolved in chloroform and the solvent was again removed. This cycle was repeated five times. Without the addition of new capping groups, the nanoparticles lose their solubility in chloroform after the first evaporation of the solvent, indicating the successful removal of pyridine by evaporation even from the surface of the nanoparticles.

*b) Direct exchange.* Nanoparticles dissolved in chloroform are mixed with chloroform solution of polymers containing the desired amount of new ligands. After short mixing, a non-solvent for the new capping groups (PEO based ligands), i.e., hexane or cyclohexane, was added. The nanoparticles covered with the polymer, insoluble in the aliphatic solvents, agglomerated and could be easily separated by centrifugation. Most of the original TOP/TOPO ligands remained dispersed in the supernatant.

### 6.1.7 Crosslinking of PEO2000-PEI-branched shell

The ligand exchange was performed with PEO2000-PEI-branched using a ratio polymer/nanoparticle of 250. To the so-obtained nanoparticles dissolved in chloroform (with a concentration of nanoparticles of  $3\text{-}7\cdot 10^{-5}$  mol dm<sup>-3</sup>), a chloroform solution containing the predetermined amount of HMDI was added. The solution was heated at 60 °C under stirring and the reaction was followed by IR spectroscopy, through the disappearance of the band characteristic for the isocyanate group. After the completion of the reaction, the mixture was cooled and the nanoparticles were washed by precipitation with hexane. Finally the nanoparticles were dissolved in water and stored for further chemical stability experiments.

**Chemical stability of nanoparticles.** In a typical HCl etching experiment, aqueous solutions of nanoparticles were placed in cuvettes and the optical density at the first absorption maximum was adjusted to be equal (around 0.02-0.05) for all samples (uncrosslinked and crosslinked). Then a solution of HCl was added (300-1000  $\mu$ l, 0.1 M) and the changes in the absorption were followed by recording the UV-vis spectra at certain time intervals. In a similar experiment, to investigate the oxidation of nanoparticles, instead of HCl, a solution of hydrogen-peroxide (250  $\mu$ l, 3 wt% in water) was added to the aqueous solution of different samples of nanoparticles (first absorption maximum around 0.05), i.e., uncrosslinked and crosslinked. The absorption spectra were recorded at certain time intervals.

### 6.1.8 Photochemical investigations

Solutions of nanoparticles with different surface capping groups were prepared for the photochemical investigations and placed in standard quartz cuvettes. For each experiment, the optical density at the first absorption maximum of the solution was set to the same value around 0.05. The cuvettes containing the samples were placed in front of a 450W output power Xenon lamp equipped with water filter to cut off NIR irradiation. During the irradiation at chosen time intervals, the absorption spectrum of the samples was recorded, in order to follow the degradation of the nanoparticles.

## 6.2 Characterisation

### 6.2.1 Nuclear Magnetic Resonance Spectroscopy (NMR)

$^1\text{H}$ -NMR and  $^{13}\text{C}$ -NMR spectra were recorded in  $\text{CDCl}_3$  using tetramethylsilane as the internal standard or in  $\text{D}_2\text{O}$  using the solvent peak as the internal standard. An AMX400 Bruker spectrometer (400 MHz) was used. The spectra were evaluated using the MestRe-C program.

### 6.2.2 Size Exclusion Chromatography (SEC)

Molecular weights ( $M_w$  and  $M_n$ ) and molecular weight distribution (polydispersity index,  $PI$ ) of all the polymers were determined by SEC. Four columns (300x8 mm, SDplus, 5 $\mu\text{m}$ ) ( $10^5$ ,  $10^3$ , 500, 100 Å) from the company MZ, thermostated at 70 °C were used. The pump was from Thermo Separation Product (P1000) and degasser from Uniflows (DG1210). The polymers were detected using a UV detector (Spectra Series UV1000) and an RI detector (Shodex 71). The eluent was dimethylformamide at a flow rate of 1.0 ml/min. The polymer concentrations were in the range of 1.5 – 3.0 g/l and 20  $\mu\text{l}$  were injected for each run. The calibration was performed with PEO standards from the company PSS. For the evaluation of  $M_w$ ,  $M_n$  and  $PI$ , HSNTeqGPC, Version 5.1.5 software was used.

### 6.2.3 Fourier Transformed Infrared Spectroscopy (FTIR)

FTIR spectroscopy was carried out on a Bruker FT-Infrared spectrometer type Equinox 55, using the geometry for attenuated total reflectance measurements (ATR). A solution of the sample was dropped onto the crystal surface and allowed to dry before the measurement.

#### **6.2.4 Optical Characterisation**

The absorption spectra were recorded on Cary 50, Cary 100 or Cary 500 spectrometers (Varian). The data obtained from the absorption spectra were used to calculate the size and extinction coefficients of nanoparticles using published calibration curves<sup>77</sup>.

The luminescence measurements were performed on a FluoroMax-2 or a FluoroLog-3 spectrometer (Instruments SA) or an Eclipse spectrometer (Varian). Except for the quantum yield measurements, the fluorescence spectra were recorded between 470 and 800 nm at room temperature using an excitation wavelength of 450 nm. Estimates of quantum yield were obtained by comparing the integrated emission from Rhodamine 6G in ethanol with that of the nanoparticles. The sample and Rhodamine 6G were excited at the wavelength obtained at the cross-over of the absorption spectra of both samples. Literature data for the luminescence efficiency of the dye was used. The obtained values for the quantum yield were not corrected for the refractive indices of the solvents. However, the error was smaller than 5 %.

#### **6.2.5 Transmission electron microscopy (TEM)**

A Philips CM-300 microscope operating at 300 kV was used for the TEM measurements. Samples were prepared by placing a drop of a dilute chloroform or water solution on a carbon-coated copper grid. The excess solution was removed with filter paper and the grids were dried in air.

#### **6.2.6 Cryo-Transmission electron microscopy (Cryo-TEM)**

Cryo-TEM was carried out on a TEM LEO912 (Zeiss) electron microscope at the Pharmaceutical Institute, Albert-Ludwigs-University Freiburg.

### **6.2.7 Powder X-ray diffraction measurements (XRD)**

XRD measurements were performed on a Philips X'Pert diffractometer (Cu K $\alpha$ -radiation, variable entrance slit). The samples for these measurements were prepared by dropping a toluene solution of the nanoparticles on a standard single crystal Si support and evaporating the solvent.

### **6.2.8 Dynamic light scattering**

Dynamic light scattering analysis was performed on a Malvern Zetasizer Nano ZS system equipped with a single angle 173 $^{\circ}$  backscatter system using He-Ne laser illumination at 633 nm. For each measurement, the autocorrelation function was the average of three runs of 30 s, and for each sample three measurements were performed. All the solutions were filtered through 0.2  $\mu$ m PTFE membrane filter. The hydrodynamic radii were obtained using Dispersion Technology Software (DTS) Version 4.00 (Malvern Instruments).

## 7. Literature

1. W. J. Parak, L. Manna, F. C. Simmel, D. Gerion, P. Alivisatos, *Quantum dots in Nanoparticles from Theory to Application* (Ed.: Gunter Schmid) Wiley-VCH Weinheim, **2004**
2. A. P. Alivisatos, *J. Phys. Chem.*, **1996**, *100*, 13226
3. L. E. Brus, *J. Chem. Phys.*, **1984**, *80*, 4403
4. M. G. Bawendi, M. L. Steigerwald, L. E. Brus, *Ann. Rev. Phys. Chem.*, **1990**, *41*, 477
5. C. B. Murray, D. J. Norris, M. G. Bawendi, *J. Am. Chem. Soc.*, **1993**, *115*, 8706
6. E. V. Shevchenko, D. V. Talapin, A. L. Rogach, A. Kornowski, M. Haase, H. Weller, *J. Am. Chem. Soc.*, **2002**, *124*, 11480
7. T. Hyeon, S. S. Lee, J. Park, Y. Chung, H. B. Na, *J. Am. Chem. Soc.*, **2001**, *123*, 12798
8. M. J. Murcia, C. A. Naumann, *Biofunctionalisation of fluorescent nanoparticles in Nanotechnologies for the life sciences Vol 1*. (Ed.: C. S. S. R. Kumar) Wiley-VCH Weinheim, **2005**
9. F. Wang, W. B. Tan, Y. Zhang, X. Fan, M. Wang, *Nanotechnology*, **2006**, *17*, 1
10. P. Alivisatos, *Nat. Biotechnol.*, **2004**, *22*, 47
11. W. C. W. Chan, S. Nie, *Science*, **1998**, *281*, 2016
12. M. Bruchez, M. Moronne, P. Gin, S. Weiss, A. P. Alivisatos, *Science*, **1998**, *281*, 2013
13. W. J. Parak, D. Gerion, T. Pellegrino, D. Zanchet, C. Micheel, S. C. Williams, R. Boudreau, M. A. Le Gros, C. A. Larabell, P. A. Alivisatos, *Nanotechnology*, **2003**, *14*, 15
14. T. Pellegrino, S. Kudera, T. Liedl, A. Muñoz Javier, L. Manna, W. J. Parak, *Small*, **2005**, *1*, 48
15. I. L. Medintz, H. T. Uyeda, E. R. Goldman, H. Mattoussi, *Nat. Mater.*, **2005**, *4*, 435

16. R. E. Bailey, A. M. Smith, S. Nie, *Physica E*, **2004**, *25*, 1
17. J. M. Klostranec, W. C. W. Chan, *Adv. Mater.*, **2006**, *18*, 1953
18. W. W. Yu, E. Chang, R. Drezek, V. L. Colvin, *Biochem. Biophys. Res. Commun.*, **2006**, *348*, 781
19. W. Parak, T. Pellegrino, C. Plank, *Nanotechnology*, **2005**, *16*, 9
20. X. Michalet, F. Pinaud, T. D. Lacoste, M. Dahan, M. P. Bruchez, A. P. Alivisatos, S. Weiss, *Single Mol.*, **2001**, *2*, 261
21. W. C. W. Chan, D. J. Maxwell, X. Gao, R. E. Bailey, M. Han, S. Nie, *Curr. Opin. Biotechnol.*, **2002**, *13*, 40
22. X. Michalet, F. F. Pinaud, L. A. Bentolila, J. M. Tsay, S. Doose, J. J. Li, G. Sundaresan, A. M. Wu, S. S. Gambhir, S. Weiss, *Science*, **2005**, *307*, 538
23. X. Gao, L. Yang, J. A. Petros, F. F. Marshall, J. W. Simons, S. Nie, *Curr. Opin. Biotechnol.*, **2005**, *16*, 63
24. M. E. Akerman, W. C. W. Chan, P. Laakkonen, S. N. Bhatia, E. Ruoslati, *Appl. Biol. Sci.*, **2002**, *99*, 12617
25. A. M. Derfus, W. C. W. Chan, S. N. Bhatia, *Adv. Mater.*, **2004**, *16*, 961
26. S. F. Wuister, I. Swart, F. Van Driel, S. G. Hickey, C. de Mello Donegá, *Nano Lett.*, **2003**, *3*, 503
27. S. Ravindran, S. Kim, R. Martin, E. M. Lord, C. S. Ozkan, *Nanotechnology*, **2005**, *16*, 1
28. G. P. Mitchell, C. A. Mirkin, R. L. Letsinger, *J. Am. Chem. Soc.*, **1999**, *121*, 8122
29. K. Hanaki, A. Momo, T. Oku, A. Komoto, S. Maenosono, Y. Yamaguchi, K. Yamamoto, *Biochem. Biophys. Res. Commun.*, **2003**, *302*, 496
30. C.-C. Chen, C.-P. Yet, H.-N. Wang, C.-Y. Chao, *Langmuir*, **1999**, *15*, 6845
31. R. Gill, I. Willner, I. Shweky, U. Banin, *J. Phys. Chem. B*, **2005**, *109*, 23715
32. D. Gerion, F. Pinaud, S. C. Williams, S. Weiss, A. P. Alivisatos, *J. Phys. Chem. B*, **2001**, *105*, 8861
33. A. Schroedter, R. Eritja, W. E. Ford, J. M. Wesseis, H. Weller, *Nano Lett.*, **2002**, *2*, 1363
34. W. Jiang, S. Mardyani, H. Fischer, W. C. W. Chan, *Chem. Mater.*, **2006**, *18*, 872

35. H. Mattoussi, J. M. Mauro, E. R. Goldman, G. P. Anderson, V. C. Sundar, F. V. Mikulec, M. G. Bawendi, *J. Am. Chem. Soc.*, **2000**, *122*, 12142
36. S. Kim, M. G. Bawendi, *J. Am. Chem. Soc.*, **2003**, *125*, 14652
37. S.-W. Kim, S. Kim, J. B. Tracy, A. Jasanoff, M. G. Bawendi, *J. Am. Chem. Soc.*, **2005**, *127*, 4556
38. T. Nann, *Chem. Commun.*, **2005**, *13*, 1735
39. Y. Liu, M. Kim, Y. Wang, Y. A. Wang, X. Peng, *Langmuir*, **2006**, *22*, 6341
40. S. Pathak, S.-K. Choi, N. Arnheim, M. E. Thompson, *J. Am. Chem. Soc.*, **2001**, *123*, 4103
41. T. Uyeda, I. L. Medintz, J. K. Jaiswal, S. M. Simon, H. Mattoussi, *J. Am. Chem. Soc.*, **2005**, *127*, 3870
42. Y. A. Wang, J. J. Li, H. Chen, X. Peng, *J. Am. Chem. Soc.*, **2002**, *124*, 2293
43. B. Dubertret, P. Skourides, D. J. Norris, V. Noireaux, A. H. Brivanlou, A. Libchaber, *Science*, **2002**, *298*, 1759
44. X. Wu, H. Liu, J. Liu, K. N. Haley, J. A. Treadway, J. P. Larson, N. Ge, F. Peale, M. P. Bruchez, *Nat. Biotechnol.*, **2003**, *21*, 41
45. T. Pellegrino, L. Manna, S. Kudera, T. Liedl, D. Koktysh, A. L. Rogach, S. Keller, J. Rädler, G. Natile, W. J. Parak, *Nano Lett.*, **2004**, *4*, 703
46. X. Gao, Y. Cui, R. M. Levenson, L. W. K. Chung, S. Nie, *Nat. Biotechnol.*, **2004**, *22*, 969
47. L. Feng, X. Kong, K. Chao, Y. Sun, Q. Zeng, Y. Zhang, *Mater. Chem. Phys.*, **2005**, *93*, 310
48. Q. A. Pankhurst, J. Connolly, S. K. Jones, J. Dobson, *J. Phys. D: Appl. Phys.*, **2003**, *36*, 167
49. W. W. Yu, E. Chang, C. M. Sayes, R. Drezek, V. L. Colvin, *Nanotechnology*, **2006**, *17*, 4483
50. S. G. Grancharov, H. Zeng, S. Sun, S. X. Wang, S. O'Brien, C. B. Murray, J. R. Kirtley, G. A. Held, *J. Phys. Chem. B*, **2005**, *109*, 13030
51. Y. Jun, Y.-M. Huh, J. Choi, J.-H. Lee, H.-T. Song, S. Kim, S. Yoon, K.-S. Kim, J.-S. Shin, J.-S. Suh, J. Cheon, *J. Am. Chem. Soc.*, **2005**, *127*, 5732
52. H.-T. Song, J. Choi, Y.-M. Huh, S. Kim, Y. Jun, J.-S. Suh, J. Cheon, *J. Am. Chem. Soc.*, **2005**, *127*, 9992

53. A. M. Smith, H. Duan, M. N. Rhyner, G. Ruan, S. Nie, *Phys. Chem. Chem. Phys.*, **2006**, *8*, 3895
54. T. Pons, H. T. Uyeda, I. L. Medinz, H. Mattoussi, *J. Phys. Chem. B*, **2006**, *110*, 20308
55. E. L. Bentzen, I. D. Tomlinson, J. Mason, P. Gresch, M. R. Warnement, D. Wright, E. Sandrs-Bush, R. Blakely, S. J. Rosenthal, *Bioconjugate Chem.*, **2005**, *16*, 1488
56. C. Kirchner, T. Liedl, S. Kudera, T. Pellegrino, A. Muñoz Javier, H. E. Gaub, S. Stölze, N. Fertig, W. J. Parak, *Nano Lett.*, **2005**, *5*, 331
57. A. M. Derfus, W. C. W. Chan, S. N. Bhatia, *Nano Lett.*, **2004**, *4*, 11
58. R. Hardman, *Environ. Health Persp.*, **2006**, *114*, 165
59. J. Aldana, Y. A. Wang, X. Peng, *J. Am. Chem. Soc.*, **2001**, *123*, 8844
60. A. L. Rogach, A. Kornowski, M. Gao, A. Eychmüller, H. Weller, *J. Phys. Chem. B*, **1999**, *103*, 3065
61. A. L. Rogach, D. Nagesha, J. W. Ostrander, M. Giersig, N. A. Kotov, *Chem. Mater.*, **2000**, *12*, 2676
62. D.-W. Deng, J.-S. Yu, Y. Pan, *J. Colloid. Interf. Sci.*, **2006**, *299*, 225
63. C. de Mello Donegá, P. Liljeroth, D. Vanmaekelbergh, *Small*, **2005**, *1*, 1152
64. I. Mekis, D. V. Talapin, A. Kornowski, M. Haase, H. Weller, *J. Phys. Chem. B*, **2003**, *107*, 7454
65. L. Qu, Z. A. Peng, X. Peng, *Nano Lett.*, **2001**, *1*, 333
66. J. E.-B. Katari, V. L. Colvin, A. P. Alivisatos, *J. Phys. Chem.*, **1994**, *98*, 4109
67. X. Peng, M. C. Schlamp, A. V. Kadavanich, A. P. Alivisatos, *J. Am. Chem. Soc.*, **1997**, *119*, 7019
68. R. Xie, U. Kolb, J. Li, T. Basché, A. Mews, *J. Am. Chem. Soc.*, **2005**, *127*, 7480
69. D. V. Talapin, I. Mekis, S. Götzinger, A. Kornowski, O. Benson, H. Weller, *J. Phys. Chem. B*, **2004**, *108*, 18826
70. M. B. Mohamed, D. Tonti, A. Al-Salman, A. Chemseddine, M. Chergui, *J. Phys. Chem. B*, **2005**, *109*, 10533
71. D. V. Talapin, A. L. Rogach, A. Kornowski, M. Haase, H. Weller, *Nano Lett.*, **2001**, *1*, 207
72. K. Yu, S. Singh, N. Patrito, V. Chu, *Langmuir*, **2004**, *20*, 11161

73. E. E. Foos, J. Wilkinson, A. J. Mäkinen, N. J. Watkins, Z. H. Kafafi, J. P. Long, *Chem. Mater.*, **2006**, *18*, 2886
74. Z. A. Peng, X. Peng, *J. Am. Chem. Soc.*, **2001**, *123*, 1389
75. W. W. Yu, Y. A. Wang, X. Peng, *Chem. Mater.*, **2003**, *15*, 4300
76. A. G. Kanaras, C. Sönnichsen, H. Liu, A. P. Alivisatos, *Nano Lett.*, **2005**, *5*, 2164
77. W. W. Yu, L. Qu, W. Guo, X. Peng, *Chem. Mater.*, **2003**, *15*, 2854
78. Z. A. Peng, X. Peng, *J. Am. Chem. Soc.*, **2001**, *123*, 183
79. C. R. Bullen, P. Mulvaney, *Nano Lett.*, **2004**, *4*, 2303
80. T. Saegusa, H. Ikeda, H. Fujii, *Macromolecules*, **1972**, *5*, 108
81. K. Aoi, M. Okada, *Prog. Polym. Sci.*, **1996**, *21*, 151
82. S. C. Lee, H. S. Choi, T. Ooya, N. Yui, *Macromolecules*, **2004**, *37*, 7464
83. Y. Akiyama, A. Harada, Y. Nagasaki, K. Kataoka, *Macromolecules*, **2000**, *33*, 5841
84. U. Lipprandt, *Ph.D. Thesis*, Universität Hamburg, **2004**
85. M. J. Roberts, M. D. Bently, J. M. Harris, *Adv. Drug Deliver. Rev.*, **2002**, *54*, 459
86. M. Sedláč, H. Cölfen, *Macromol. Chem. Phys.*, **2001**, *202*, 247
87. H. Petersen, P. M. Fechner, D. Fischer, T. Kissel, *Macromolecules*, **2002**, *35*, 6867
88. M. Sedláč, M. Antonietti, H. Cölfen, *Macromol. Chem. Phys.*, **1998**, *199*, 247
89. S. N. Sidrov, L. M. Bronstein, P. M. Valetsky, J. Hartmann, H. Cölfen, H. Schnablegger, M. Antonietti, *J. Colloid. Interf. Sci.*, **1999**, *212*, 197
90. L. Qi, H. Cölfen, M. Antonietti, *Nano Lett.*, **2001**, *1*, 61
91. H. Cölfen, *Macromol. Rapid. Commun.*, **2001**, *22*, 219
92. M. Glodde, S. R. Sirsi, G. J. Lutz, *Biomacromolecules*, **2006**, *7*, 347
93. S. Luo, J. Xu, Y. Zhang, S. Liu, C. Wu, *J. Phys. Chem. B*, **2005**, *109*, 22159
94. A. H. Latham, M. E. Williams, *Langmuir*, **2006**, *22*, 4319
95. M. P. Lutolf, N. Tirelli, S. Cerritelli, L. Cavalli, J. A. Hubbell, *Bioconjugate Chem.*, **2001**, *12*, 1051

96. A. E. Rydholm, S. K. Reddy, K. S. Anseth, C. N. Bowman, *Biomacromolecules*, **2006**, *7*, 2827
97. A. E. Rydholm, N. L. Held, C. N. Bowman, K. S. Anseth, *Macromolecules*, **2006**, *39*, 7882
98. J. Rieger, K. Van Butsele, P. Lecomte, C. Detrembleur, R. Jérôme, C. Jérôme, *Chem. Commun.*, **2005**, *2*, 274
99. M. Heggli, N. Tirelli, A. Zisch, J. A. Hubbell, *Bioconjugate Chem.*, **2003**, *14*, 967
100. M. G. Berrettini, G. Braun, J. G. Hu, G. F. Strouse, *J. Am. Chem. Soc.*, **2004**, *126*, 7063
101. D. V. Talapin, A. L. Rogach, I. Mekis, S. Haubold, A. Kornowski, M. Haase, H. Weller, *Colloids Surf. A*, **2002**, *202*, 145
102. J.-G. Liang, S.-S. Zhang, X.-P. Ai, X.-H. Ji, Z.-K. He, *Spectrochim. Acta A*, **2004**, *61*, 2974
103. C. Zhang, S. O'Brien, L. Balogh, *J. Phys. Chem. B*, **2002**, *106*, 10316
104. M. Kuno, J. K. Lee, B. O. Dabbousi, F. V. Mikulec, M. G. Bawendi, *J. Phys. Chem.*, **1997**, *106*, 9869
105. C. Bullen, P. Mulvaney, *Langmuir*, **2006**, *22*, 3007
106. R. Comparelli, F. Zezza, M. Striccoli, M. L. Curri, R. Tommasi, A. Agostiano, *Mater. Sci. Eng. C*, **2003**, *23*, 1083
107. G. Kalyuzhny, R. W. Murray, *J. Phys. Chem. B*, **2005**, *109*, 7012
108. C. F. Landes, M. Braun, M. A. El-Sayed, *J. Phys. Chem. B* **2001**, *105*, 10554
109. C. Landes, C. Burda, M. Braun, M. A. El-Sayed, *J. Phys. Chem. B.*, **2001**, *105*, 2981
110. S. N. Sharma, Z. S. Pillai, P. V. Kamat, *J. Phys. Chem. B.*, **2003**, *107*, 10088
111. C. Landes, M. Braun, C. Burda, M. A. El-Sayed, *Nano Lett.* **2001**, *1*, 667
112. C. Landes, M. A. El-Sayed, *J. Phys. Chem. A*, **2002**, *106*, 7621
113. M. A. El-Sayed, *Acc. Chem. Res.*, **2004**, *37*, 326
114. R. Li, J. Lee, B. Yang, D. N. Horspool, M. Aindow, F. Papadimitrakopoulos, *J. Am. Chem. Soc* **2005**, *127*, 2524
115. M. Wang, J. K. Oh, T. E. Dykstra, X. Lou, G. D. Scholes, M. A. Winnik, *Macromolecules*, **2006**, *39*, 3664

116. F. Seker, A. B. Ellis, *Macromolecules*, **2000**, *33*, 582
117. J. Lal, I. F. Hakem, *Eur. Phys. J. E*, **2004**, *15*, 217
118. I. F. Hakem, J. Lal, *Europhys. Lett.*, **2003**, *64*, 204
119. M. Zhang, M. Drechsler, A. H. E. Möller, *Chem. Mater.*, **2004**, *16*, 537
120. D. Wyrwa, N. Beyer, G. Schmid, *Nano Lett.*, **2002**, *2*, 419
121. N. Duxin, F. Liu, H. Vali, A. Eisenberg, *J. Am. Chem. Soc.*, **2005**, *127*, 10063
122. J. C. M. van Hest, D. A. P. Delnoye, M. W. P. L. Baars, M. H. P. Van Genderen, E. W. Meijer, *Science*, **1995**, *268*, 1592
123. J. N. Israelachvili, D. J. Mitchell, B. W. Ninham, *J. Chem. Soc., Faraday Trans. 2*, **1976**, *72*, 1525
124. J. Mitchell, B. W. Ninham, *J. Chem. Soc., Faraday Trans. 2*, **1981**, *77*, 601
125. L. Zhang, A. Eisenberg, *J. Am. Chem. Soc.*, **1996**, *118*, 3168
126. S. Förster, T. Plantenberg, *Angw. Chem. Int. Ed.*, **2002**, *41*, 688
127. S. Förster, M. Zisenis, E. Wenz, M. Antonietti, *J. Chem. Phys.*, **1996** *104*, 9956
128. W. Guo, J. J. Li, Y. A. Wang, X. Peng, *Chem. Mater.*, **2003**, *15*, 312
129. W. Guo, J. J. Li, Y. A. Wang, X. Peng, *J. Am. Chem. Sci.*, **2003**, *125*, 3901
130. H. Tan, T. Zhan, W. Y. Fan, *J. Phys. Chem. B*, **2006**, *110*, 21690
131. G. H. Woehrle, L. O. Brown, J. E. Hutchison, *J. Am. Chem. Soc.*, **2005**, *127*, 2172
132. W. Shi, Y. Sahoo, M. T. Swihart, *Colloids Surf. A*, **2004**, *246*, 109
133. A. H. Latham, M. E. Williams, *Langmuir*, **2006**, *22*, 4319
134. T. Prozorov, A. Gedanken, *Adv. Mater.*, **1998**, *10*, 532
135. S. F. Wuister, C. de Mello Donegá, A. Meijerink, *J. Phys. Chem. B*, **2004**, *108*, 17393
136. S. Hohng, T. Ha, *J. Am. Chem. Soc.*, **2004**, *126*, 1324
137. S. Jeong, M. Achermann, J. Nanda, S. Ivanov, V. I. Klimov, J. A. Hollingsworth, *J. Am. Chem. Soc.*, **2005**, *127*, 10126
138. H. Mattoussi, J. M. Mauro, E. R. Goldman, G. P. Anderson, V. C. Sundar, F. V. Mikulec, M. G. Bawendi, *J. Am. Chem. Soc.*, **2000**, *122*, 12142
139. J. A. Kloepfer, S. E. Bradforth, J. L. Nadeau, *J. Phys. Chem. B*, **2005**, *109*, 9996

140. H. Düllefeld, K. Hoppe, J. Kolny, K. Schilling, H. Weller, A. Eychmüller, *Phys. Chem. Chem. Phys.*, **2002**, 4, 4747
141. G. N. Malcolm, J. S. Rowlinson, *Trans. Faraday Soc.*, **1957**, 53, 921
142. R. Kjellander, *J. Chem. Soc., Faraday Trans. 2*, **1982**, 78, 2025
143. M. Corti, C. Minero, V. Degiorgio, *J. Phys. Chem.*, **1984**, 88, 309
144. R. Plummer, D. J. T. Hill, A. K. Whittaker, *Macromolecules*, **2006**, 39, 8379
145. P.-G. Nilsson, H. Wennerström, B. Lindman, *J. Phys. Chem.*, **1983**, 87, 1377
146. M. Stoltzenburg, *Diploma Thesis*, Universität Hamburg, **2004**
147. M. Krack, *Ph.D. Thesis*, Universität Hamburg, **2006**
148. V. Aleksandrovic, *Ph.D. Thesis*, Universität Hamburg, **2006**
149. G. M. Lukovkin, V. S. Pshezhetsky, G. A. Murtazeva, *Eur. Polym. J.*, **1973**, 9, 559

## Appendix 1

### Calculation of the number of different amino groups in the branched poly(ethylene imine)

The  $^{13}\text{C}$ -NMR spectrum of the branched poly(ethylene imine), PEI-branched, was used to prove the branched structure of the polymer and to calculate the ratio of primary, secondary and tertiary amino groups in the molecule. The spectrum of PEI-branched with the assignment<sup>147</sup> of the signals to the corresponding carbon atoms is presented in Figure App.1.1.

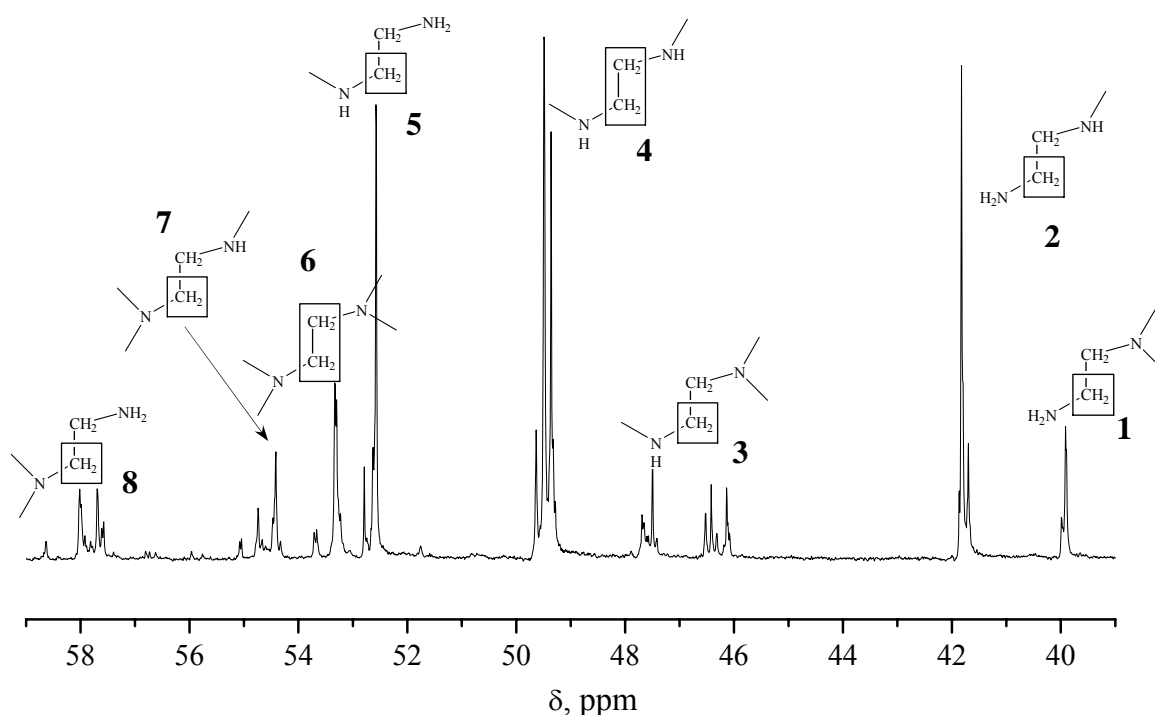


Figure App.1.1.  $^{13}\text{C}$  NMR spectrum of PEI-branched in  $\text{CDCl}_3$

The ratio of the different amino groups can be calculated from the intensities of the signals belonging to carbon atoms next to the different amino groups using the formula:

$$1^{\circ} : 2^{\circ} : 3^{\circ} = (I_1 + I_2) : (I_3 + I_4 + I_5) : (I_6 + I_7 + I_8)$$

The obtained ratio of different amino groups was calculated to be 35 % primary, 47 % secondary and 18 % tertiary groups. For PEI of 423 g/mol molecular weight, this means that the molecule contained on average, 3 primary, 5 secondary and 2 tertiary amino groups.

## Appendix 2

### Calculation of the number of polymer chains per nanoparticle from the average distance between the nanoparticles on a TEM grid

The average number of polymer chains per nanoparticle was calculated from the averaged distance between the nanoparticles obtained from TEM images. TEM images from which the distance was determined together with the corresponding autocorrelation function images are given Figure App.2.1 and Figure App.2.2. The numbers below each image indicate the polymer/nanoparticle ratio used during the ligand exchange, which influenced the number of polymeric chains attached to a nanoparticle and, consequently, the distance between nanoparticles.

#### PEO2000-DETA

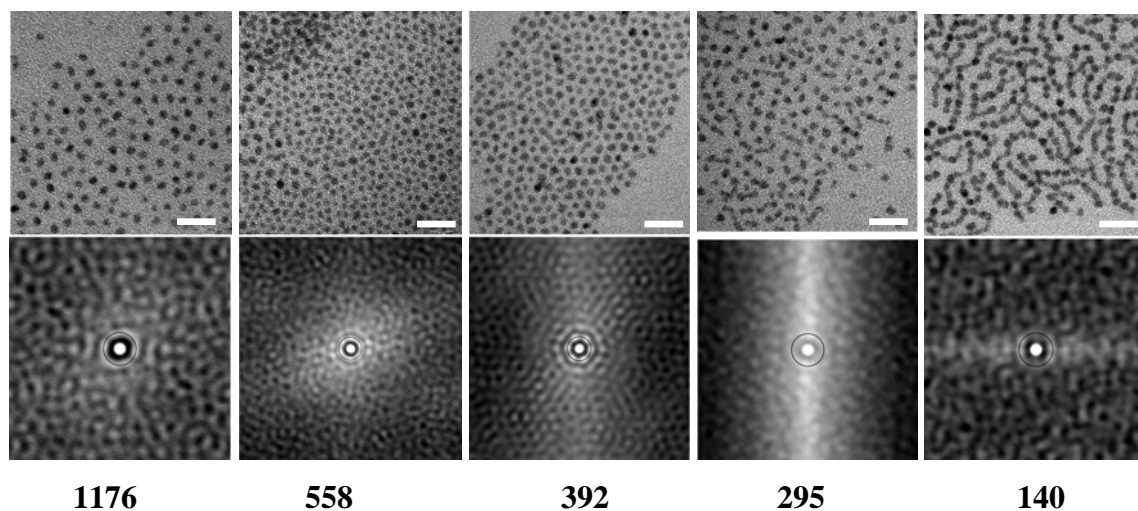


Figure App.2.1. TEM-images (scale bar 20 nm) and the corresponding autocorrelation function the samples of water-soluble CdSe/CdS nanoparticles obtained with different [PEO2000-DETA]/nanoparticle ratios during the ligand exchange

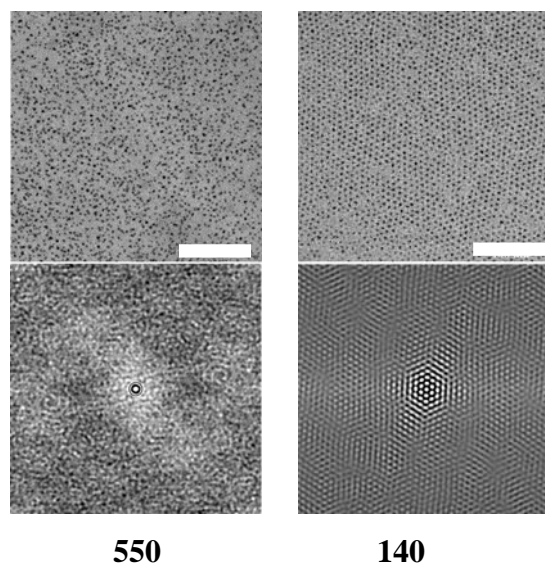
**PEO2000-PEO-branched**

Figure App.2.2. TEM-images (scale bar 100 nm) and the corresponding autocorrelation function for samples of water-soluble CdSe/CdS nanoparticles obtained with different [PEO2000-PEI-branched]/nanoparticle ratios during the ligand exchange

For hexagonal packing of nanoparticles with a base length  $a$  (distance between neighbouring nanoparticles) and height  $a \frac{\sqrt{3}}{2}$ , the volume of the unit cell is:

$$V_{\text{cell}} = \frac{3}{4} a^3$$

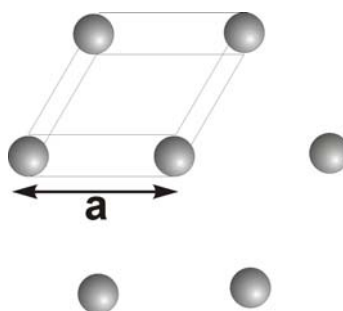


Figure App.2.3. Schematic representation of the hexagonal packing model used for the calculation of the distance between nanoparticles

The volume occupied by the polymer was calculated as the difference between the volume of the unit cell and the volume of a nanoparticle of radius  $R$ , under the assumption that there is one nanoparticle per unit cell:

$$V_{\text{poly}} = V_{\text{cell}} - V_{\text{nano}} = \frac{3}{4}a^3 - \frac{4\pi}{3}R^3$$

The number of polymer chains per nanoparticle can be calculated using the expression:

$$N_{\text{poly}} = \frac{V_{\text{poly}}}{N_{\text{PEO}}V_{\text{PEO}}}$$

where  $N_{\text{PEO}}$  is the degree of polymerisation of the PEO in the employed polymeric ligand.  $V_{\text{PEO}}$  is the volume occupied by a PEO monomer unit:

$$V_{\text{PEO}} = \frac{M_{\text{PEO}}}{N_L \rho_{\text{PEO}}}$$

where  $M_{\text{PEO}}$  is the monomer molar mass, i.e., 44.05 g/mol,  $\rho_{\text{PEO}}$  the bulk density of PEO of 1.13 g/cm<sup>3</sup> and  $N_L$  the Avogadro's number.

The area of the nanoparticle surface per polymeric chain is then:

$$a_{\text{poly}} = \frac{A_{\text{nano}}}{N_{\text{poly}}}$$

where  $A_{\text{nano}} = 4\pi R^2$  is the surface area of a nanoparticle of radius  $R$ .

The results obtained for the number of polymer chains per nanoparticle included in this study with a of diameter 3.4 nm) and the surface area per polymeric ligand for the two employed ligands are summarised in Tabele App.2.1.

Tabela App.2.1. Calculated number of polymeric ligands per nanoparticle and surface area of nanoparticle per polymeric ligand

| Polymeric ligand     | Ratio <sup>1)</sup> | $a$ , nm | $N_{\text{poly}}$ | $a_{\text{poly}}$ , nm <sup>2</sup> |
|----------------------|---------------------|----------|-------------------|-------------------------------------|
| PEO2000-DETA         | 1176                | 8.7      | 161               | 0.225                               |
|                      | 558                 | 6.0      | 48                | 0.754                               |
|                      | 392                 | 6.0      | 48                | 0.754                               |
|                      | 295 <sup>2)</sup>   | 8.7      | 161               | 0.225                               |
|                      | 148                 |          |                   |                                     |
| PEO2000-PEI-branched | 550                 | 9.4      | 102               | 0.335                               |
|                      | 140                 | 8.6      | 78                | 0.468                               |

1) Refers to the polymer/nanoparticle ratio used during the ligand exchange; 2) the formation of cylindrical micelle already occurred with this sample

## Appendix 3

### Used chemicals and their safety precaution information

| Substance                                      | R-phrases               | S-phrases            | Hazard signs |
|--|-------------------------|----------------------|--------------|
| 2-ethyl-2-oxazoline                            | 10-20/21/22             | 16-26-28-36/37/39    | Xn           |
| 3-mercaptopropionic acid                       | 25-34                   | 7-26-36/37/39-45     | T            |
| Acetonitrile                                   | 23/24/25                | 16/27/44             | F, T         |
| Benzene  | 45-11-48/23/24/25       | 53-45                | F, T         |
| Cadmium acetate                                | 20-22-50-53             | 60-61                | Xn, N        |
| Calcium hydride                                | 15                      | 7/8-24/25-43         | F            |
| Chloroform                                     | 22-38-40-48/20/22       | 36/37                | Xn           |
| Diethylenetriamine                             | 21/22-34-43             | 26-36/37/39-45       | C            |
| Diethylether                                   | 12-19                   | (2-)9-16-29-33       | F+           |
| Dimethylformamide                              | 61-20/21-36             | 53-45                | T            |
| Ethanol  | 11                      | 7-16                 | F            |
| Ethyl acetate                                  | 11-36-66-67             | 16-26-33             | F, Xi        |
| Hexadecylamine                                 | 34                      | 26-36/37/39-45       | C            |
| Hexamethylenediisocyanate                      | 23-36/37/38-42/43       | 26-28-38-45          | T            |
| Hexane   | 11-48/20                | 9-16-24/25-29-51     | F, Xn, N     |
| Hydrochloric acid                              | 34-37                   | 26-45                | C, Xi        |
| Hydrogen sulfide                               | 12-26-50                | 9-16-28-36/37-45-61  | F+, T+, N    |
| Lewatit 500                                    | 36                      | 26-36                | -            |
| Methanol                                       | 11-23/24/25-39/23/24/25 | 7-16-36/37-45        | F, T         |
| Pentaerythritol tetrakis(3-mercaptopropionate) | 36/37/38                | 26-36                | Xi           |
| Pentaethylenhexamine                           | 34-43-50/53             | 26-36/37/39-45-60-61 | C, N         |
| Poly(ethylene oxide)                           | -                       | -                    | -            |
| Poly(ethyleneimine)                            | -                       | -                    | -            |
| Pyridine                                       | 11-20/21/22             | 26-28                | F, Xn        |
| Selenium                                       | 23/25-33                | 20/21-28-45          | T            |
| Sodium hydroxide                               | 35                      | 26-37/39-45          | C            |
| Tetrabutylammonium hydroxide                   | 34                      | 26-36/37/39-45       | C            |
| Tetradecylphosphonic acid                      | -                       | -                    | Xi           |
| Toluene  | 11-20                   | 16-25-29-33          | F, Xn        |
| Trioctylphosphine                              | 36/37/38                | 26-36                | Xi           |
| Trioctylphosphine oxide                        | 34-50/53                | 26-36/37/39-45-60-61 | C, Xi        |
| Zinc acetate                                   | 22-36-50/53             | 26-60-61             | Xn, N        |

**Risk (R-) and safety precaution (S-) phrases used in the classification, packaging, labelling and provision of information on dangerous substances****Risk phrases (R-Phrases)**

- R1: Explosive when dry
- R2: Risk of explosion by shock, friction fire or other sources of ignition
- R3: Extreme risk of explosion by shock friction, fire or other sources of ignition
- R4: Forms very sensitive explosive metallic compounds
- R5: Heating may cause an explosion
- R6: Explosive with or without contact with air
- R7: May cause fire
- R8: Contact with combustible material may cause fire
- R9: Explosive when mixed with combustible material
- R10: Flammable
- R11: Highly flammable
- R12: Extremely flammable
- R13: Extremely flammable liquefied gas
- R14: Reacts violently with water
- R15: Contact with water liberates highly flammable gases
- R16: Explosive when mixed with oxidising substances
- R17: Spontaneously flammable in air
- R18: In use, may form flammable/explosive vapour-air mixture
- R19: May form explosive peroxides
- R20: Harmful by inhalation
- R21: Harmful in contact with skin
- R22: Harmful if swallowed
- R23: Toxic by inhalation
- R24: Toxic in contact with skin
- R25: Toxic if swallowed
- R26: Very toxic by inhalation
- R27: Very toxic in contact with skin
- R28: Very toxic if swallowed
- R29: Contact with water liberates toxic gas
- R30: Can become highly flammable in use
- R31: Contact with acids liberates toxic gas
- R32: Contact with acids liberates very toxic gas
- R33: Danger of cumulative effects
- R34: Causes burns
- R35: Causes severe burns
- R36: Irritating to eyes
- R37: Irritating to respiratory system
- R38: Irritating to skin
- R39: Danger of very serious irreversible effects
- R40: Possible risk of irreversible effects
- R41: Risk of serious damage to eyes
- R42: May cause sensitisation by inhalation
- R43: May cause sensitisation by skin contact
- R44: Risk of explosion if heated under confinement
- R45: May cause cancer
- R46: May cause heritable genetic damage
- R47: May cause birth defects

- R48: Danger of serious damage to health by prolonged exposure
- R49: May cause cancer by inhalation
- R50: Very toxic to aquatic organisms
- R51: Toxic to aquatic organisms
- R52: Harmful to aquatic organisms
- R53: May cause long-term adverse effects in the aquatic environment
- R54: Toxic to flora
- R55: Toxic to fauna
- R56: Toxic to soil organisms
- R57: Toxic to bees
- R58: May cause long-term adverse effects in the environment
- R59: Dangerous to the ozone layer
- R60: May impair fertility
- R61: May cause harm to the unborn child
- R62: Possible risk of impaired fertility
- R63: Possible risk of harm to the unborn child
- R64: May cause harm to breastfed babies

**Combination of risks**

- R14/15: Reacts violently with water, liberating highly flammable gases
- R15/29: Contact with water liberates toxic, highly flammable gas
- R20/21: Harmful by inhalation and in contact with skin
- R20/21/22: Harmful by inhalation, in contact with skin and if swallowed
- R20/22: Harmful by inhalation and if swallowed
- R21/22: Harmful in contact with skin and if swallowed
- R23/24: Toxic by inhalation and in contact with skin
- R23/24/25: Toxic by inhalation, in contact with skin and if swallowed
- R23/25: Toxic by inhalation and if swallowed
- R24/25: Toxic in contact with skin and if swallowed
- R26/27: Very toxic by inhalation and in contact with skin
- R26/27/28: Very toxic by inhalation, in contact with skin and if swallowed
- R26/28: Very toxic by inhalation and if swallowed
- R27/28: Very toxic in contact with skin and if swallowed
- R36/37: Irritating to eyes and respiratory system
- R36/37/38: Irritating to eyes, respiratory system and skin
- R36/38: Irritating to eyes and skin
- R37/38: Irritating to respiratory system and skin
- R42/43: May cause sensitization by inhalation and skin contact
- R48/20: Harmful: danger of serious damage to health by prolonged exposure
- R48/20/21: Harmful: danger of serious damage to health by prolonged exposure through inhalation and in contact with the skin
- R48/20/21/22: Harmful: danger of serious damage to health by prolonged exposure through inhalation, in contact with skin and if swallowed
- R48/20/22: Harmful: danger of serious damage to health by prolonged exposure through inhalation, and if swallowed
- R48/21: Harmful: danger of serious damage to health by prolonged exposure in contact with skin
- R48/21/22: Harmful: danger of serious damage to health by prolonged exposure in contact with skin and if swallowed
- R48/22: Harmful: danger of serious damage to health by prolonged exposure if swallowed

- R48/23: Toxic: danger of serious damage to health by prolonged exposure through inhalation
- R48/23/24: Toxic: danger of serious damage to health by prolonged exposure through inhalation and in contact with skin
- R48/23/24/25: Toxic: danger of serious damage to health by prolonged exposure through inhalation, in contact with skin and if swallowed
- R48/23/25: Toxic: danger of serious damage to health by prolonged exposure through inhalation and if swallowed
- R48/24: Toxic: danger of serious damage to health by prolonged exposure in contact with skin
- R48/24/25: Toxic: danger of serious damage to health by prolonged exposure in contact with skin and if swallowed
- R48/25: Toxic: danger of serious damage to health by prolonged exposure if swallowed
- R50/53: Very toxic to aquatic organisms, may cause long term adverse effects in the aquatic environment
- R51/53: Toxic to aquatic organisms, may cause long term adverse effects in the aquatic environment
- R52/53: Harmful to aquatic organisms, may cause long-term adverse effects in the aquatic environment

**Safety precaution phrases (S-Phrases)**

- S1: Keep locked up
- S2: Keep out of reach of children
- S3: Keep in a cool place
- S4: Keep away from living quarters
- S5: Keep contents under ... (appropriate liquid to be specified by the manufacturer)
- S6: Keep under ... (inert gas to be specified by the manufacturer)
- S7: Keep container tightly closed
- S8: Keep container dry
- S9: Keep container in a well ventilated place
- S12: Do not keep the container sealed
- S13: Keep away from food, drink and animal feeding stuffs
- S14: Keep away from ... (incompatible materials to be indicated by the manufacturer)
- S15: Keep away from heat
- S16: Keep away from sources of ignition-No Smoking
- S17: Keep away from combustible material
- S18: Handle and open container with care
- S20: When using do not eat or drink
- S21: When using, do not smoke
- S22: Do not breathe dust
- S23: Do not breathe gas/fumes/vapour/spray (appropriate wording to be specified by manufacturer)
- S24: Avoid contact with skin
- S25: Avoid contact with eyes
- S26: In case of contact with eyes, rinse immediately with plenty of water and seek medical advice
- S27: Take off immediately all contaminated clothing
- S28: After contact with skin, wash immediately with plenty of ... (to be specified by the manufacturer)
- S29: Do not empty into drains
- S30: Never add water to this product

- S33: Take precautionary measures against static discharges  
S34: Avoid shock and friction  
S35: This material and its container must be disposed of in a safe way  
S36: Wear suitable protective clothing  
S37: Wear suitable gloves  
S38: In case of insufficient ventilation, wear suitable respiratory equipment  
S39: Wear eye/face protection  
S40: To clean the floor and all objects contaminated by this material use (to be specified by the manufacturer)  
S41: In case of fire and/or explosion do not breath fumes  
S42: During fumigation/spraying wear suitable respiratory equipment (appropriate wording to be specified by the manufacturer)  
S43: In case of fire, use ... (indicate in the space the precise type of fire fighting equipment. If water increases the risk, add "never use water")  
S44: If you feel unwell, seek medical advice (show the label where possible)  
S45: In case of accident or if you feel unwell, seek medical advice immediately (show the label where possible)  
S46: If swallowed, seek medical advice immediately and show the container or label  
S47: Keep at temperature not exceeding ... °C (to be specified by the manufacturer)  
S48: Keep wetted with ... (appropriate material to be specified by the manufacturer)  
S49: Keep only in the original container  
S50: Do not mix with ... (to be specified by the manufacturer)  
S51: Use only in well-ventilated areas  
S52: Not recommended for interior use on large surface areas  
S53: Avoid exposure - obtain special instructions before use  
S54: Obtain the consent of pollution control authorities before discharging to waste-water treatment plants  
S55: Treat using the best available techniques before discharge into drains or the aquatic environment  
S56: Do not discharge into drains or the environment, dispose to an authorised waste collection point  
S57: Use appropriate containment to avoid environmental contamination  
S58: To be disposed of as hazardous waste  
S59: Refer to manufacturer/supplier for information on recovery/recycling  
S60: This material and/or its container must be disposed of as hazardous waste  
S61: Avoid release to the environment. Refer to special instructions / safety data sheet  
S62: If swallowed, do not induce vomiting: seek medical advice immediately and show the container label

**Combined safety phrases**

- S1/2: Keep locked up and out of reach of children  
S3/9: Keep in a cool, well ventilated place  
S3/7/9: Keep container tightly closed in a cool, well ventilated place  
S3/14: Keep in a cool place away from ... (incompatible materials to be indicated by the manufacturer)  
S3/9/14: Keep in a cool, well-ventilated place away from ... (incompatible materials to be indicated by the manufacturer)  
S3/9/49: Keep only in the original container in a cool, well ventilated place  
S3/9/14/49: Keep only in the original container in a cool, well-ventilated place away from (incompatible materials to be indicated by the manufacturer)  
S3/9/49: Keep only in the original container in a cool, well ventilated place

- 
- S3/14: Keep in a cool place away from ... (incompatible materials to be indicated by the manufacturer)
- S7/8: Keep container tightly closed and dry
- S7/9: Keep container tightly closed and in a well ventilated place
- S7/47: Keep container tightly closed and at a temperature not exceeding...°C (to be specified by manufacturer)
- S20/21: When using do not eat, drink or smoke
- S24/25: Avoid contact with skin and eyes
- S29/56: Do not empty into drains, dispose of this material and its container to hazardous or special waste collection point
- S36/37: Wear suitable protective clothing and gloves
- S36/37/39: Wear suitable protective clothing, gloves and eye/face protection
- S36/39: Wear suitable protective clothing, and eye/face protection
- S37/39: Wear suitable gloves and eye/face protection
- S47/49: Keep only in the original container at temperature not exceeding ...°C (to be specified by the manufacturer)

## CURRICULUM VITAE

### PERSONAL DATA

**First name:** Marija  
**Last name:** Nikolic  
**Date of birth:** September 10, 1973.  
**City of birth:** Smederevo, Serbia

### EDUCATION:

**since 01.04.2004** Experimental work on the PhD Thesis in the group of Prof. Dr. Horst Weller, Institute for Physical Chemistry, University of Hamburg

**1998-2002** MSc., Faculty of Technology and Metallurgy, University of Belgrade; Thesis title: "Synthesis and characterization of biodegradable aliphatic polyesters"

**1992-1998** Study at the Faculty of Technology and Metallurgy, Belgrade, University of Belgrade; Division profile: Organic Chemical Technology and Polymeric Engineering

**1998** Diploma work in Polymer Engineering, at the Faculty of Technology and Metallurgy, University of Belgrade; Thesis title: "Synthesis and characterization of biodegradable polyesters"

**1988-1992** High School of Sciences and Mathematics Gymnasium "Jovan Skerlic", Vladicin Han

### WORK EXPERIENCE:

**2004-2006** Practical experiments supervision in Physical Chemistry (Flash Photolysis experiment), University of Hamburg

**1998-2004** Teaching Assistant in General Chemistry at the Faculty of Technology and Metallurgy, University of Belgrade

**2002/03** Teaching assistant in Polymer Synthesis for foreign graduate students organised in English, at the Faculty of Technology and Metallurgy, University of Belgrade

**1999** Technical training at the Department of Chemical and Process Engineering, University of Newcastle upon Tyne, England

**1996** Technical training at the State University Lvivska Polytechnika, Lviv, Ukraine

## **PARTICIPATION IN PROJECTS:**

- 2002-2004** “Synthesis, Modification and Characterization of Synthetic and Natural polymeric Materials“, Financed by the Ministry of Science and Technology of the Republic of Serbia.
- 2002-2004** “Synthesis, Characterization and Application of Hyperbranched Polyesters“, Coatings and Paint Factory “Duga Nova“, Belgrade

## **PUBLICATIONS:**

1. M. S. Nikolic, J. Djonlagic, “Synthesis and Characterization of Biodegradable Poly(butylene succinate-co-butylene adipate)s”, *Polymer Degradation and Stability*, **2001**, 74, 263-270
2. M. S. Nikolic, D. Poleti, J. Djonlagic, “Synthesis and Characterization of Biodegradable Poly(butylene succinate-co-butylene fumarate)s”, *European Polymer Journal*, **2003**, 39, 2183-2192
3. D. Jovanovic, M. Nikolic, J. Djonlagic, “Synthesis and Characterization of Biodegradable Aliphatic Copolyesters with Hydrophilic Soft Segments“, *Journal of the Serbian Chemical Society*, **2004**, 69, 1013-1028
4. M. Kalagasidis-Krusic, D. Dankovic, M. Nikolic, J. Filipovic, “Poly(acrylamide-co-itaconic acid) and semi-IPNS with Poly(ethylene glycol): Preparation and Characterization”, *Macromolecular Chemistry and Physics*, **2004**, 205, 2214-2220
5. M. S. Nikolic, M. Krack, V. Aleksandrovic, S. Foerster, H. Weller, “Tailor-Made Ligands for Biocompatible Nanoparticles”, *Angewandte Chemie*, **2006**, 45, 6577-6580

## Declaration

The research presented within, was carried out by the author at the University of Hamburg. It is the author's original work and all sources of information as well as the results obtained in collaboration with other people are pointed out.

The dissertation has not been submitted in whole or in part for a degree at any other university.

Hamburg, March 2007

Marija Nikolic